Revised: August 1, 1998

CAR-TR-711 July 1, 1994

The Maryland Revolving-Field Monitor: Theory of the Instrument and Processing Its Data

Mark Edwards, Zygmunt Pizlo, Casper J. Erkelens,
Han Collewijn, Julie Epelboim, Eileen Kowler,
Michael R. Stepanov, Robert M. Steinman

CENTER FOR AUTOMATION RESEARCH

Laboratory for Basic Research in Sensory Systems

UNIVERSITY OF MARYLAND
COLLEGE PARK, MARYLAND
20742-4411

Revised: August 1, 1998

CAR-TR-711 July 1, 1994

The Maryland Revolving-Field Monitor: Theory of the Instrument and Processing Its Data

Mark Edwards[1], Zygmunt Pizlo[2], Casper J. Erkelens[3], Han Collewijn[4], Julie Epelboim[1], Eileen Kowler[5], Michael R. Stepanov[1], Robert M. Steinman[1]

[1]Psychology, University of Maryland, College Park, MD
[2]Psychological Sciences, Purdue University, West Lafayette, IN
[3]Biophysics, University of Utrecht, The Netherlands
[4]Physiology, Erasmus University Rotterdam, The Netherlands
[5]Psychology, Rutgers University, New Brunswick, NJ

Abstract

This report contains a complete description of the method for processing the data from Table Experiments collected by the Maryland Revolving-Field Monitor (RFM). The apparatus used in these experiments included magnetic-field-sensor coils worn on each of the subject's eyes (sensor-coils), two non-coplanar coils attached to the subject's forehead (head-coil device), and a sparker device attached to the subject's head (head-sparker). The raw data recorded from this apparatus included horizontal and vertical eye angles for both eyes, horizontal, vertical, and torsional head angles, and distances from the head sparker to each of four microphones all in real time.

All of the above raw data are processed to produce quantities that can be used to analyze the eye-movement behavior of subjects who participated in the Table Experiments. Such quantities include the real-time lines-of-sight of the subject, horizontal and vertical gaze-errors relative to a given target, table gaze-positions, and target and ocular vergence. All of these analysis quantities can be determined once the real-time positions of the sighting-centers of both eyes are known

The body of this work contains a description of the RFM apparatus, descriptions of various calibration activities performed during the Table Experiments, derivations of the equations relating the subject's real-time sighting-center positions to the raw data colected by the RFM, and derivations of the equations that relate the sighting-center positions to the analysis quantities mentioned above. The report concludes with three appendixes that contain Table Experiment calibration details, introductory material regarding vectors and matrices, and a derivation of the basic equation used to determine the elements of the matrix describing an arbitrary rotation.

Support provided by AFOSR Grants 91-0124, FA9620-92-J0260 and F49620-94-1-0333

Contents

List of Figures

Chapter 1

Introduction

This document contains a detailed description of the method for converting the raw data collected in Table Experiments into data suitable for analysis. Its purpose is to provide derivations of the mathematical equations contained in the method from first principles. Its further purpose is to provide a sufficiently detailed description so that the method can be implemented in a computer program. The target audience includes those who are mathematically sophisticated and those who are not. Appendixes B and C at the end of this document contain reviews of the relevant mathematics for the latter type of reader.

The raw data include horizontal and vertical eye-angles for each eye, horizontal, vertical, and torsional head-angles at each RFM burst during a given trial, and the distance from the head-sparker to each of four microphones for each strobe of the sparker during a given trial. The processed data include the direction of lines-of-sight, horizontal and vertical gaze-errors relative to a given target, table gaze-positions, and target and ocular vergence on each RFM burst during a given trial.

The fundamental quantities needed for determination of these processed data are the **sighting-centers of the subject's eyes at each RFM burst of a given trial**. Once these quantities are calculated, the various processed data can be easily determined

This document begins with a description of the Maryland Revolving-Field Monitor (RFM) apparatus (chapter 2). This chapter describes the main components of the RFM, the physical meanings of the data that can be collected with the apparatus, and the coordinate systems relevant to the data-processing method described in later chapters. Chapter 3 presents the major activities performed in Table Experiments both for calibration and for the collection of raw data. Chapter 4 presents a complete derivation of the

mathematical equations relating the raw data to the real-time sighting-center positions of the subject. Chapter 5 presents a summary of processing the raw data into sighting-center positions in algorithmic form suitable for encoding in a computer program.

Chapters 6 through 8 contain derivations of the equations that relate the sighting-center positions to the various quantities required for fruitful analysis of the eye-movement behavior of participants in the Table Experiments. Chapter 6 covers the definition and computation of the line-of-sight direction of the subject. In Chapter 7, table gaze positions and gaze errors of a single eye relative to a given target are related to the sighting-center position of the eye. And finally, Chapter 8 contains a description of how the Helmholtz coordinate system axes are determined in terms of sighting-center positions and how ocular vergence angles are obtained using these axes.

The document concludes with three appendixes. Appendix A describes the method whereby the sighting-center of the subject's eye is obtained while his head is supported on the biteboard. Some details supporting the description of the transformation of a point in sparker coordinates to those in table coordinates are also provided. Appendix B focuses on the elementary mathematical properties of vectors and matrices. Appendix C contains the derivation of the rotation formula. This formula defines the elements of the matrix that describes an arbitrary rotation. The reader unfamiliar with vectors and matrices should read appendixes B and C first as they provide the mathematical background needed for understanding the derivations presented in Chapters 4 through 8.

Chapter 2

The Maryland Revolving-Field Monitor (RFM)

The RFM apparatus contains two major systems for the tracking of head and eye movements. The first of these is the revolving-magnetic-field monitor (RMFM) and the second is the sparker tracking system (STS). The RMFM has the capability of tracking the orientation in space of a magnetic-field sensor coil in real-time. The STS tracks the position in space of a sparker device in real-time. Each of these systems will be described in more detail below. These two devices have commensurate, but different, data-sampling rates. In what follows, each time-point at which the RMFM collects data will be termed a "burst". Each time-point at which the STS collects data will be called a "strobe".

2.1 Revolving-Magnetic-Field Monitor System (RMFM)

The RMFM system consists of two major parts: (1) a machine that produces three, mutually perpendicular, magnetic fields that revolve at different frequencies within a certain volume (magnetic-field volume) inside the RFM chamber, and (2) a sensor-coil device that, when placed inside this volume, carries an induced current that is dependent on its spatial orientation. A bank of electronics reads and processes this induced current and also controls the revolving fields.

Each revolving field is produced by two sets of ac-current-carrying coils mounted on a cubical frame[1] (each set is wound in a "cube-surface coil" arrangement). Each set of coils consists of five square coils lying in parallel

planes. These coils produce a magnetic field which oscillates along a fixed line. The two lines corresponding to the pair of sets of coils are perpendicular and are 90° out-of-phase causing the superposition of these magnetic fields to revolve in the plane that contains both lines. The magnetic field produced by this arrangement is spatially homogeneous throughout a large fraction of the volume contained inside the cubical frame. See figure 2.1.

There are three such pairs of sets of coils, each pair produces a magnetic field that revolves parallel to a particular plane at all points in the magnetic-field volume. The three planes are mutually perpendicular and consist of two vertical planes and one horizontal plane. The fields in the different planes revolve at different frequencies (976, 1952, and 3904 Hz) so that the orientation of the sensor-coil relative to each plane may be determined separately. The different relative orientations are computed by the electronics in real-time. In order to maintain the direction of the fields and their frequency of revolution, three mutually perpendicular reference coils are mounted inside the RFM chamber and the currents induced in them are measured by the electronics. The measured reference currents drive servo mechanisms that vary the current in the coils (and thereby the revolving fields) so that these reference currents remain strictly a superposition of three sinusoids having the above three frequencies.

The orientation of a sensor-coil relative to the planes in which the magnetic fields rotate is determined by comparing the phase of a particular harmonic component of the ac-current induced in the sensor-coil with that induced in the reference coil at the corresponding frequency associated with the magnetic field[2]. The total magnetic field generated in the RFM chamber volume is the superposition of the three revolving fields. The total ac-current induced in a sensor-coil immersed in this field will be a superposition of three sinusoids each having a different frequency. The electronics record this current, separate out the components of different frequencies, and then compute the phase difference between a particular component and that of the corresponding component of induced ac-current in the appropriate reference coil. The phase difference between corresponding frequency components of the currents in the sensor coil and reference coil equals the angle (expressed in radians) between the orthographic projections ov the unit normal vectors of the two coils onto the plane which contains the magnetic field revolving at that frequency. The phase difference is then converted by the electronics to a 16-bit number that is proportional to this angle in minutes of arc which

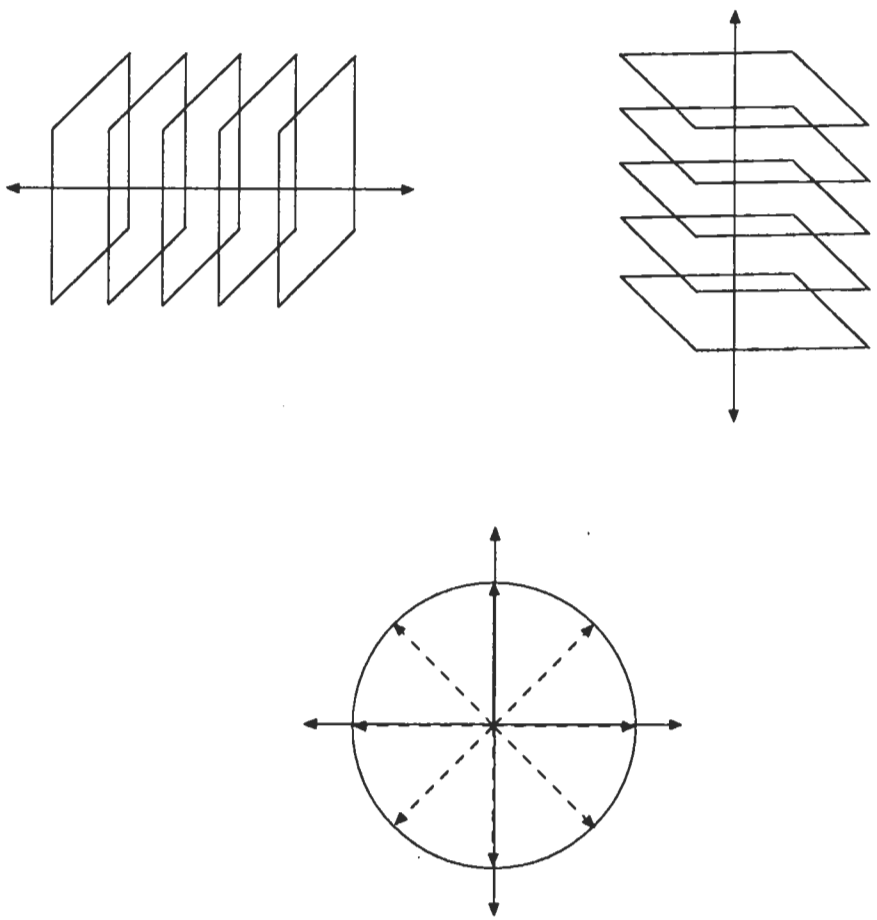

Figure 2.1: A single revolving magnetic field

is then read by computer. The precision of the angle measurement in minutes of arc ranges between 0.5 to 2 parts in 10^5 depending on the meridian. Each measured angle is stored as a 16-bit number. The sample rate of angles output by the RFM for Table Experiments is 488 Hz producing an effective bandwidth for head- and eye-angle measurements of 244 Hz.

The orientation of the planes that contain the revolving magnetic fields relative to the RFM chamber are shown schematically in fig. 2.2. There are two vertical planes and one horizontal plane. By convention, one defines a direction called "magnetic north". A coil whose normal (perpendicular) vector points toward magnetic north registers an angle of 225° or 13,500 minarc (minutes of arc) relative to what will be called in this document the "horizontal plane". This may be somewhat confusing as the plane is actually vertical but the rationale for the term lies in the fact that the angle records a rotation of the eye when the subject looks horizontally while facing magnetic north. The absolute values of the angles measured relative to a plane are unimportant. Only differences in angles matter. Thus the conventional reference position for this plane in this document will be magnetic north.

The plane that is perpendicular to the "horizontal plane" and is oriented roughly parallel to the floor will be called the "vertical plane". The angle between the sensor-coil plane and this plane (called the "vertical angle") changes when a subject (facing magnetic north) looks up (or vertically) even though the plane itself is horizontal. When the normal vector of a sensor-coil points toward magnetic north, the vertical angle registers 135° or 8100 minarc. By convention in this document, the reference position of this plane will again be magnetic north. The third plane is rarely used for collecting eye-angle data in Table Experiments because the subject sits roughly facing magnetic north while manipulating objects on the table. This causes the third signal to be very weak and thus detecting phase in this plane can be unreliable. As this angle would roughly record a rotation of the eye around the line-of-sight (torsion), this plane will be called the "torsional plane". Special coils can be used to record such eye torsions but they have not been used to date in the Table Experiments and no further discussion of them will be presented here. This plane is used extensively, however, for recording torsional *head* movements as will be described later.

The RMFM system is the only instrument in the world that taps the advantages of measuring orientation with the phase-detecting principle in any direction in three-dimensional space. The cube-surface coil arrangement,

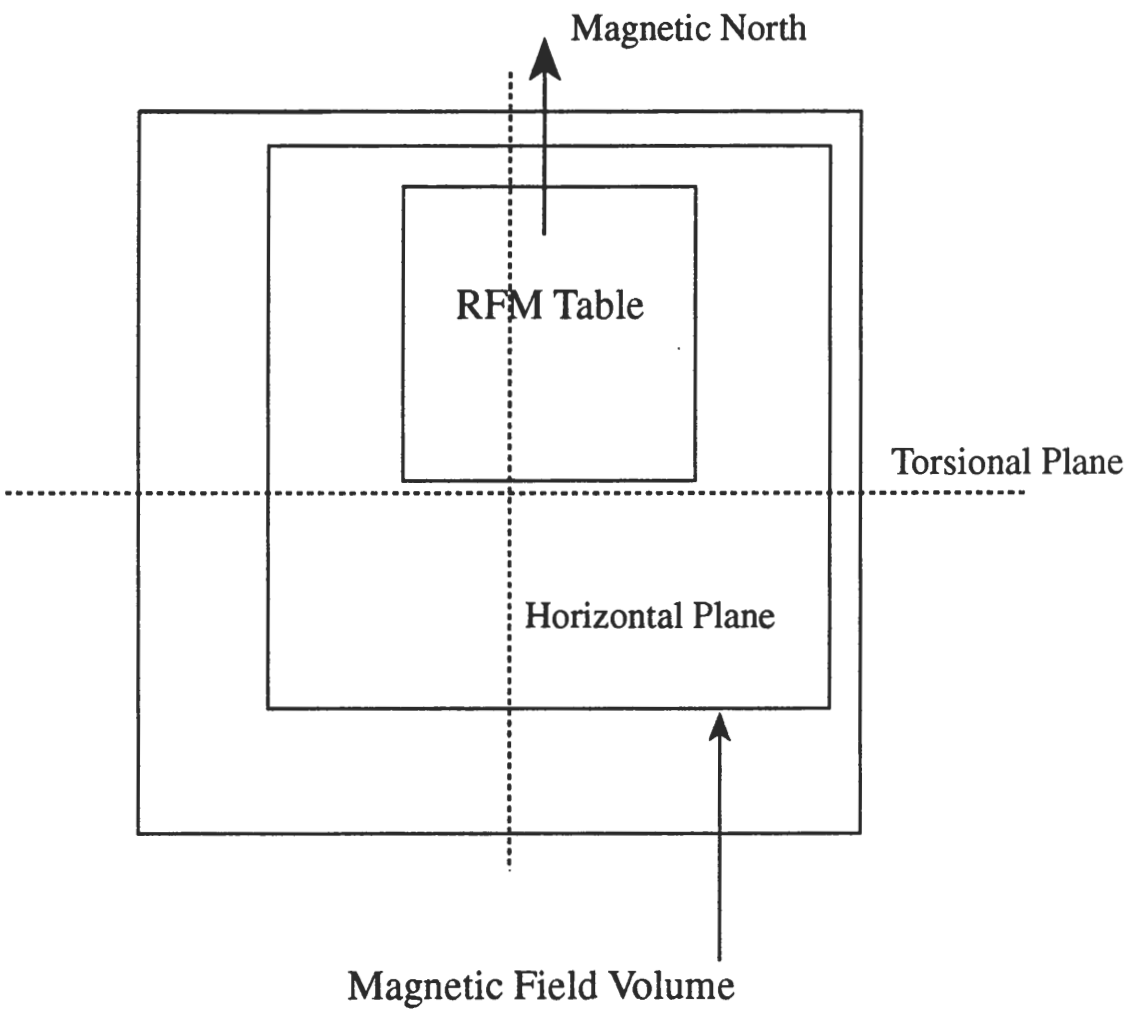

Figure 2.2: Schematic drawing of the RFM chamber (top view)

which is in use in at least one other laboratory, makes it possible to achieve a homogeneous revolving magnetic field in a volume large relative to the space needed to perform the Table Experiments. This is not the case with other systems, which employ pairs of Helmholtz-coils to produce the magnetic field. Phase detection on all three meridians (north-south and east-west vertical meridians as well as the horizontal meridian) allows absolute calibration of the orientation of the sensor-coil with respect to a reference frame fixed in the laboratory.

2.2 Sparker Tracking System (STS)

The sparker tracking system also contains two major parts (1) a set of four microphones mounted on a rectangular frame which is situated above the cubical frame that surrounds the magnetic field volume, and (2) devices called "sparkers" which are rods that have electrodes at one end separated by a tiny air gap. At the rate of 61 times per second (sparker strobe rate), a large potential difference is placed across these electrodes causing a spark to jump across. Each time this happens, a sharp, high-pitched (60 kHz on the leading edge) sound is emitted due to the heat from the spark. The sound travels to each of the microphones and is detected by each. The detected sound is fed into the STS circuitry. Since this circuitry also controls the sparker, it can determine the delay between the time the voltage was applied and the time the sound was detected by the microphones. These delays are output as distances (since the distance is proportional to the time delay via the speed of sound). Each microphone is labeled with a letter (i.e. A, B, C, D) and figure 2.3 shows the placement of the microphones around the RFM chamber. Note that the z-axis points down in this figure.

The position of a sparker can be determined by using the distances from any three of the four microphones. If the coordinates of the microphones are known in some system, then three distances determine the coordinates of two candidate points for the position of the sparker. The fact that the sparker must be inside the magnetic field volume uniquely determines the sparker position. The details of the method for determining the sparker position will be presented in chapter 4.

2.3 RFM Worktable

In addition to the RMFM and the STS, one further major piece of apparatus is used in Table Experiments. This is the RFM Worktable. This device is a flat surface on which there is a 14×11 rectangular grid of holes. Various rods that have either LED's or sparkers mounted on them can be placed in these holes. When a subject depresses one of these (LED) rods, a button at the bottom of the hole is activated and the event is output to a computer via circuitry connected to the table. In addition, there are small red lights mounted on the table adjacent to each hole which are used to indicate the setup for different trials during an experimental session. Finally there are infra-red photo-sensors just on either side of each hole which can be used to detect a subject touching the hole itself with his finger tip or to detect a rod entering or leaving each hole. These last photo-sensors have not yet been used in Table Experiments. See fig. 2.4.

The holes in the table are precisely machined such that their centers are 45 millimeters (mm) apart along both rows and columns. When a subject is seated in the RFM chamber and is facing magnetic north (his normal working position), the grid of holes appears as 11 rows and 14 columns. The farthest holes are just within arm's reach as the subject sits and moves naturally. As will be seen in the next section, these holes, in part, define the table coordinate system. All derived quantities are ultimately expressed in terms of this coordinate system.

2.4 RFM Coordinate Systems

There are three main coordinate systems that are defined for the RFM. They are (1) the Sparker Coordinate System (SCS), (2) the RFM Coordinate System (RFMCS), and (3) the Table Coordinate System (TCS). The planes in which the different magnetic fields revolve define the RFMCS and they are assumed parallel to the planes that define the TCS. The RFM Worktable has been placed so that this assumption is valid to within an experimental error of less than 10 minarc on every meridian. Thus only the SCS and the TCS will be described below.

A Cartesian coordinate system may be uniquely specified in the following way. First, specify the position of the origin relative to some landmark. Next,

choose two other points (noncollinear with the origin) which, along with the origin determine a plane. Lines from the origin to each of these points determines a pair of axes. These lines are not necessarily perpendicular but such axes can be determined from these by using the Gram-Schmidt orthogonalization procedure. Next, define the third perpendicular axis by taking the cross product of the orthogonal unit vectors that define the axes in the plane. Finally, assign positive directions along these axes.

2.4.1 The Sparker Coordinate System (SCS)

The origin of the Sparker Coordinate System is taken to be just inside the front of microphone A and the xy-plane is defined by similar points in microphones B and D (see fig. 2.3). The x-axis lies along a line from microphone A to microphone D. Since the microphones are mounted on an approximately rectangular frame, the y-axis could be taken to be along the line from microphone A to microphone B and the assumption made that these axes are perpendicular. However, this is not necessary because the straight-line distance from D to B can be measured. Therefore the y-axis is defined to lie along the line lying in the plane and to pass through the origin at A such that it is perpendicular to the x-axis already defined. The z-axis is determined by the cross product of the y-axis with the x-axis. This axis points downward. Hence points inside the magnetic field volume (in particular, sparker positions) have a positive z-coordinate. This coordinate system is shown schematically in fig. 2.3.

2.4.2 The Table Coordinate System (TCS)

The TCS is the fundamental coordinate system used in the method for processing of the raw data. All quantities that are dependent on a coordinate system (e.g. sighting-centers and table gaze positions) will ultimately be expressed in terms of this system. One reason for this is that it is in this coordinate system that target coordinates are most conveniently determined.

The TCS is defined in terms of landmarks that are attached to the RFM Worktable. For a subject facing magnetic north inside the magnetic field volume, the holes form a rectangular grid having eleven rows with each row containing fourteen holes. A system for labeling these holes has been standardized and is as follows. Each hole is labeled by its row number and column

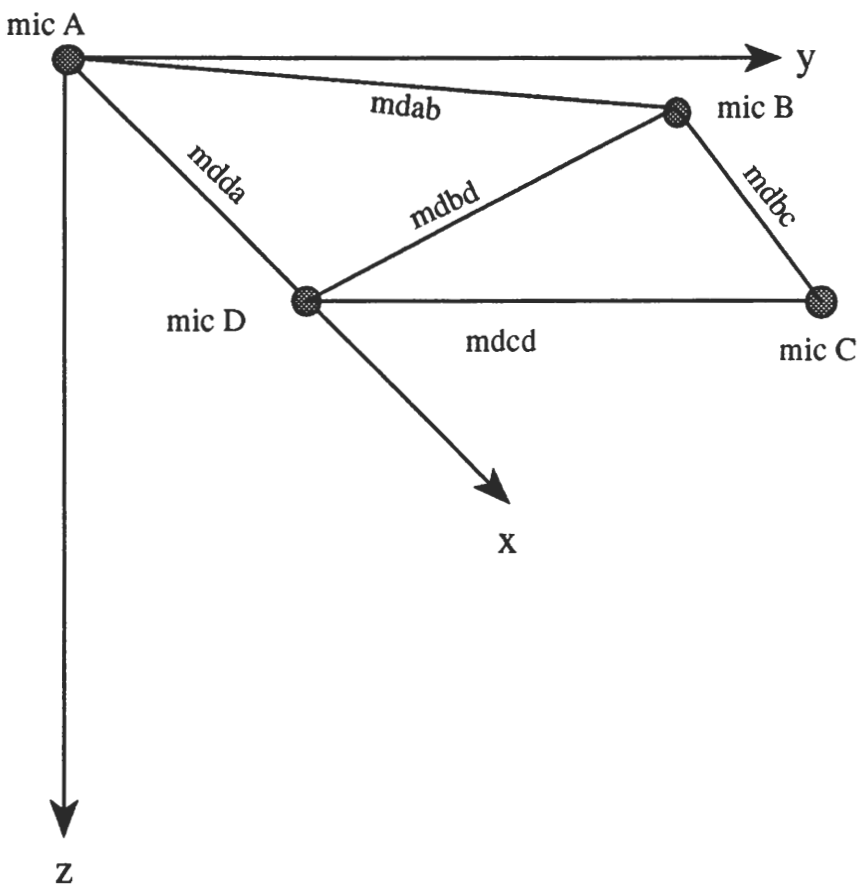

Figure 2.3: The Sparker Coordinate System (SCS)

number. For a subject in the orientation described above, the hole at the lower left is labeled row one and column one. Row numbers increase away from the subject towards magnetic north and column numbers increase to the right. A top view of the RFM Worktable is shown in fig. 2.4 below.

The origin of the TCS is defined to be above the center of the hole in the first row and the seventh column at the height of the low sparker. The xy-plane contains this point and is parallel to the surface of the RFM Worktable which is assumed to be planar. The x-axis lies in this plane and runs above the centers of the holes in column seven on the table; the positive sense of this axis is toward magnetic north. The y-axis is perpendicular to the x-axis and runs above the centers of the holes in row one; the positive sense of the x-axis is in the same direction as increasing column number in row one. The z-axis is perpendicular to both of these axes and is defined by the cross product of a unit vector along the y-axis with a unit vector along the x-axis. Both the TCS and the SCS are left-handed coordinate systems.

2.5 Types of Measurements Collected in the Table Experiment

In Table Experiments, a subject is fitted with an eye coil in each eye, the head-coil apparatus, and a head-sparker. The reason for collecting these data is to determine where on the RFM Worktable the subject is looking while performing a series of tasks such as tapping various LED rods in a specified order. The types of measurements that are collected are horizontal and vertical eye-angles from each eye; horizontal, vertical, and torsional head-angles from the head-coil apparatus; and the distances from the head-sparker to each of the four microphones. Each of these types of measurements will be described below.

2.5.1 Horizontal and Vertical Eye-Angles

At the beginning of a Table Experiment session, the subject is fitted with a Skalar-Delft silicone annulus sensor-coil in each eye (eye-coil). Imbedded in the silicone annulus are 9 turns of very thin copper wire wound into a tight coil. The twisted leads to this coil in the annulus are connected to the RFM circuitry which detects the current induced in the coil. This allows

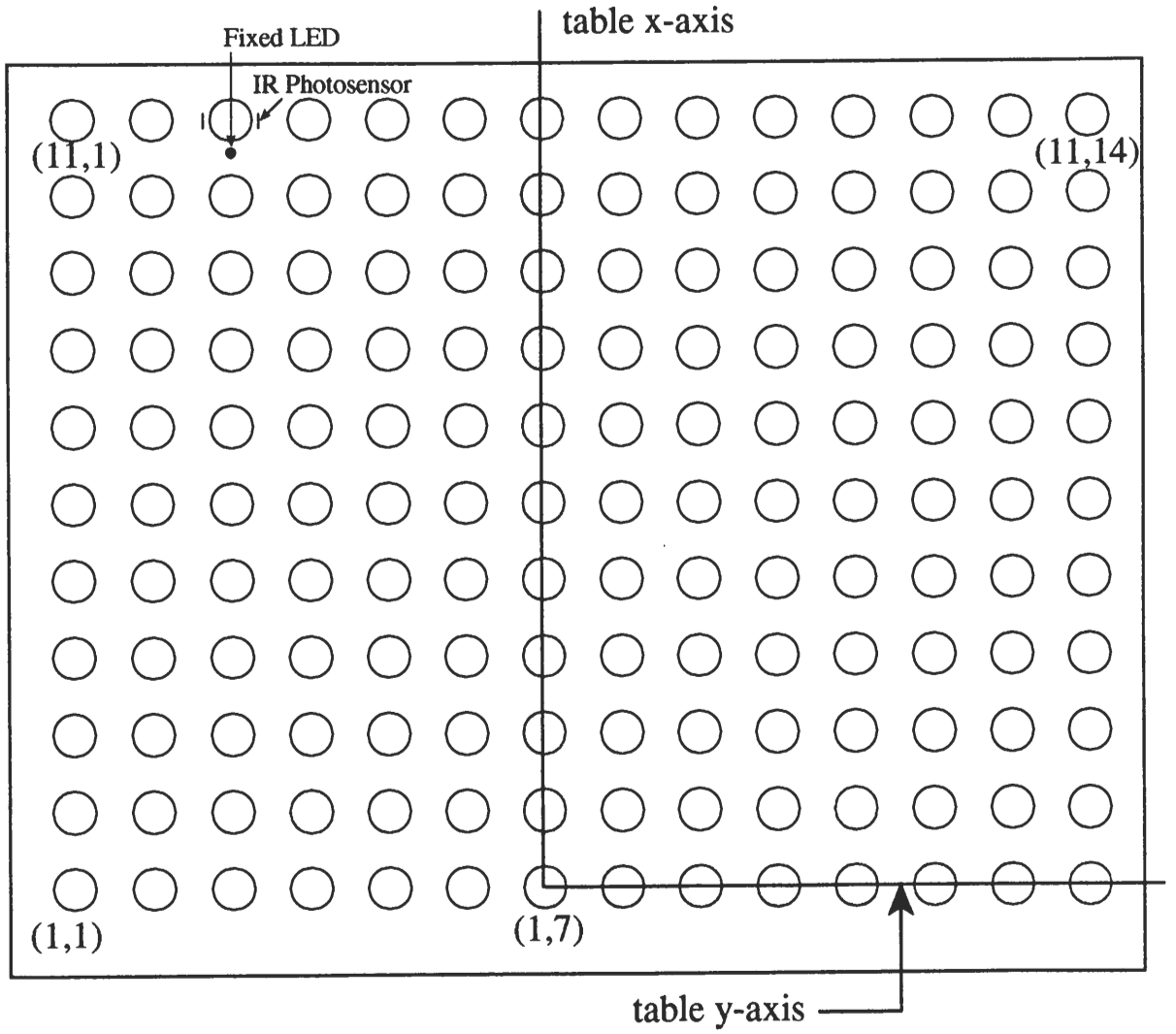

Figure 2.4: The top view of the RFM Worktable showing the TCS

the measurement of the horizontal and vertical eye-angles during each RFM burst in a trial.

To understand the physical meanings of these angles, one imagines the eye-coil to lie in a plane and then imagines a unit vector, perpendicular to this plane pointing away from the eye. If the eye-coil is perfectly centered on the subject's eyeball, then this unit vector will point directly along the subject's line-of-sight. This can never be known to be the case and the calibration techniques used to determine the correction for the angular offset between the sensor-coil's normal vector and the subject's line-of-sight will be described in chapter 3. The vertical eye-angle is the angle between the orthographic projection of this unit vector onto the TCS xz-plane and the TCS x-axis as shown in fig. 2.5. The horizontal eye-angle is the angle between the orthographic projection of the vector onto the TCS xy-plane and the TCS x-axis as shown in fig. 2.6.

For the vertical-angle case, one imagines a flashlight shined along the negative TCS y-axis. The unit vector perpendicular to the eye coil would then cast a shadow on the TCS xz-plane. The angle between this shadow and the TCS x-axis is the vertical angle. A similar paradigm can be constructed for the horizontal angle, a light is shined along the negative TCS z-axis and a shadow is cast onto the TCS xy-plane. The angle between this shadow and the TCS x-axis is the horizontal angle.

The vertical eye-angle is equivalent to a "first Helmholtz angle" (H_1) and gives the elevation of the plane of regard above the reference eye position if the TCS were fixed in the orbit of a subject's eye. The horizontal eye-angle is equivalent to a "first Fick angle" (F_1). Measurement of these two angles affords a unique determination of the spatial orientation of the subject's eye in space. From these angles a "second Helmholtz angle" and a "second Fick angle" can be determined. These mathematical relationships will be presented later.

2.5.2 Horizontal, Vertical, and Torsional Head-Angles

The RFM head-coil device consists of two sensor coils: a large coil and a smaller coil, which are mounted such that their planes are approximately perpendicular. When the device is fitted on the subject's forehead, the large coil lies roughly in the plane of the forehead and the smaller coil lies roughly in a vertical plane and perpendicular to the large head-coil when the subject's

head is positioned naturally. See fig. 2.7.

The horizontal and vertical head-angles are measured by reading the horizontal and vertical angles from the large head-coil, just as described above for the corresponding eye-angles. The torsional head-angle is the vertical angle of the smaller head-coil. The horizontal angle registers head movements when the subject shakes his head as in saying "no". The vertical angle registers head movements when the subject nods his head as in saying "yes". The torsional angle registers movements when the subject's head tilts toward either shoulder. These data types are the same as the eye-angles, namely, the angle between the projection of the unit vector perpendicular to the smaller head-coil onto the TCS yz-plane and the TCS y-axis.

It is important to collect here the precise definitions of the three head-angles measured by the RMFM because they will be used extensively in the mathematics developed in Chapter 4. The horizontal head-angle is the angle between the orthographic projection, onto the TCS xy-plane, of the unit vector normal to the large head-coil and the TCS x-axis. The vertical head-angle is the angle between the orthographic projection, onto the TCS xz-plane, of the unit vector normal to the large head-coil and the TCS x-axis. The torsion angle is the angle between the orthographic projection, onto the TCS yz-plane, of the unit vector normal to the smaller head-coil and the negative TCS y-axis. Figure 2.12 illustrates the torsion angle as measured by the RMFM.

2.5.3 Sparker Distances

The STS outputs the distance from the sparker to each of four microphones as is shown in figure 2.8 below. If the coordinates of the microphones are known in some coordinate system, then the coordinates of the sparker can be determined by triangulation on any three microphones. How this is done is presented in chapter 4.

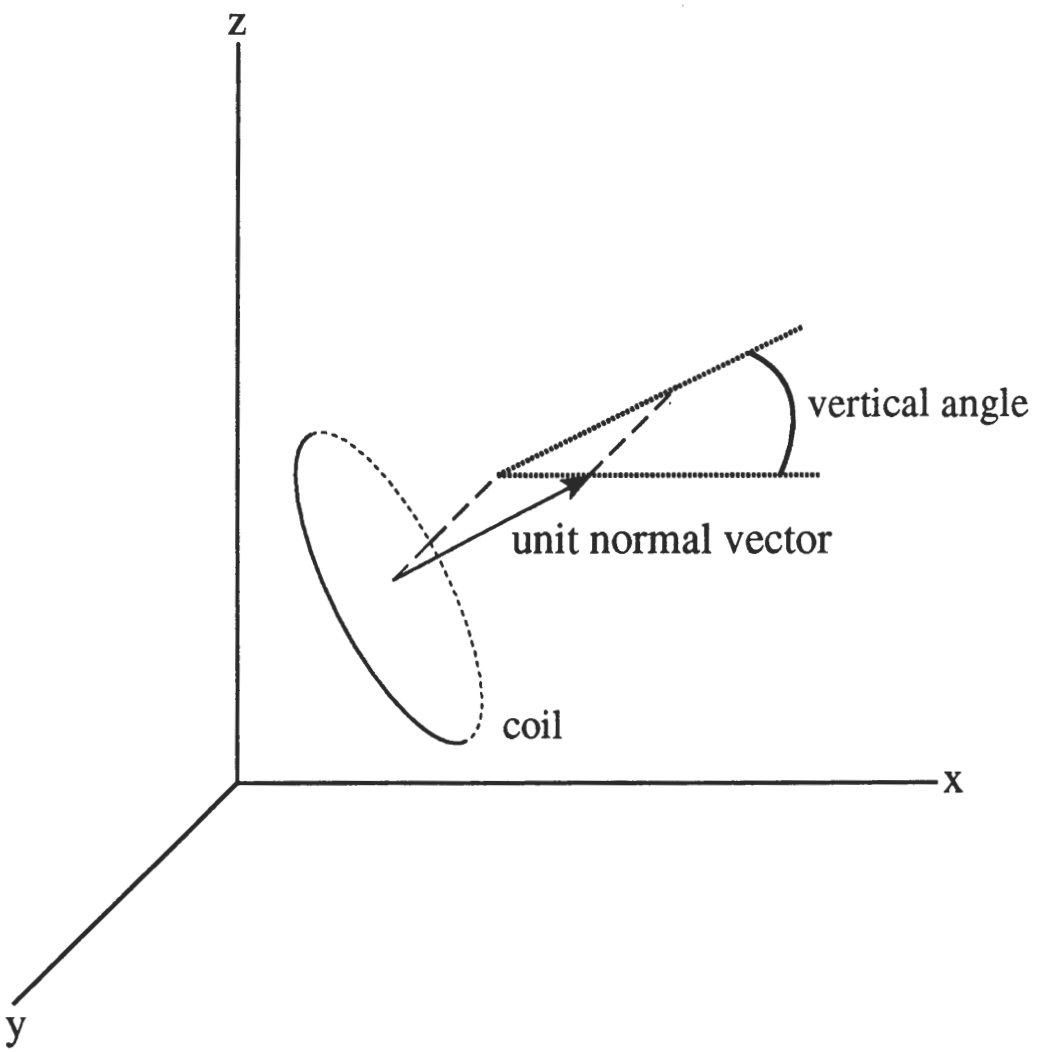

Figure 2.5: The vertical angle as measured by the RMFM

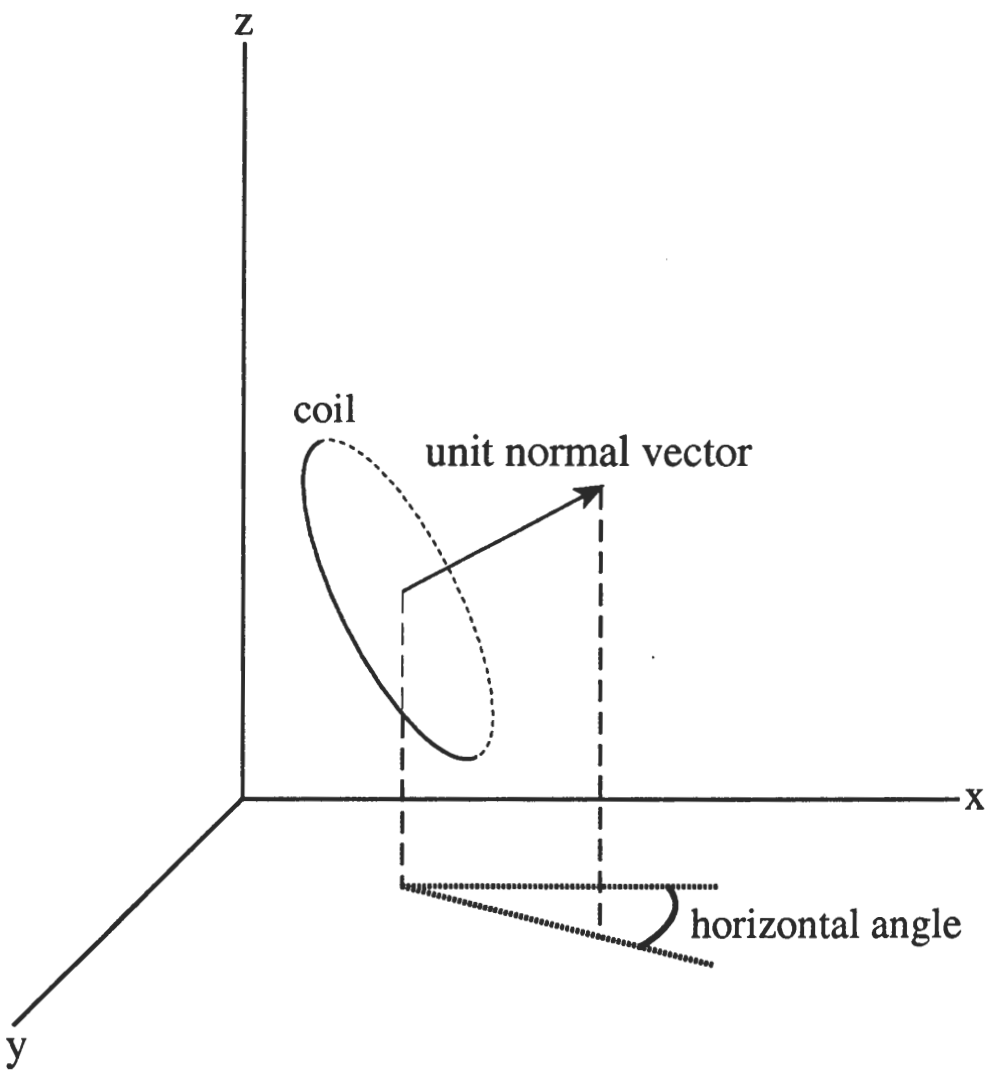

Figure 2.6: The horizontal angle as measured by the RMFM

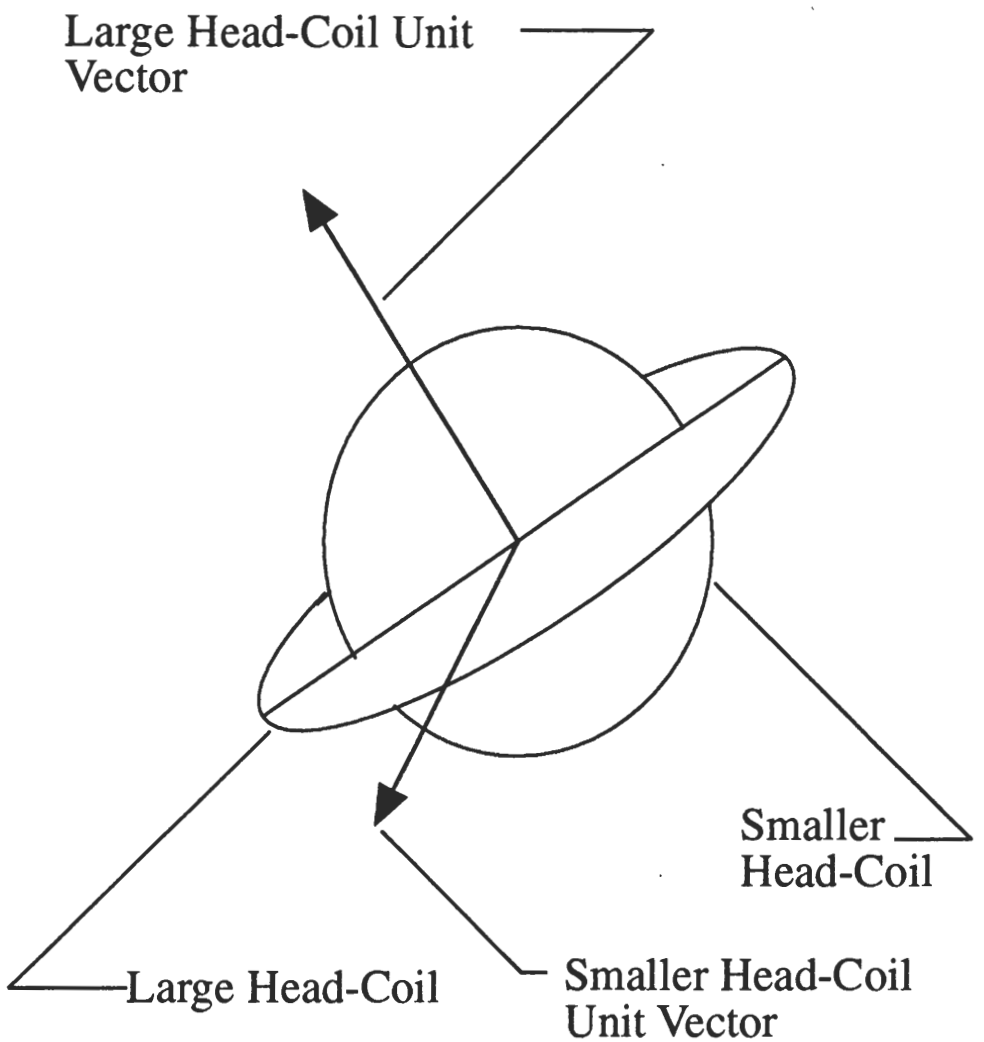

Figure 2.7: The head-coil device

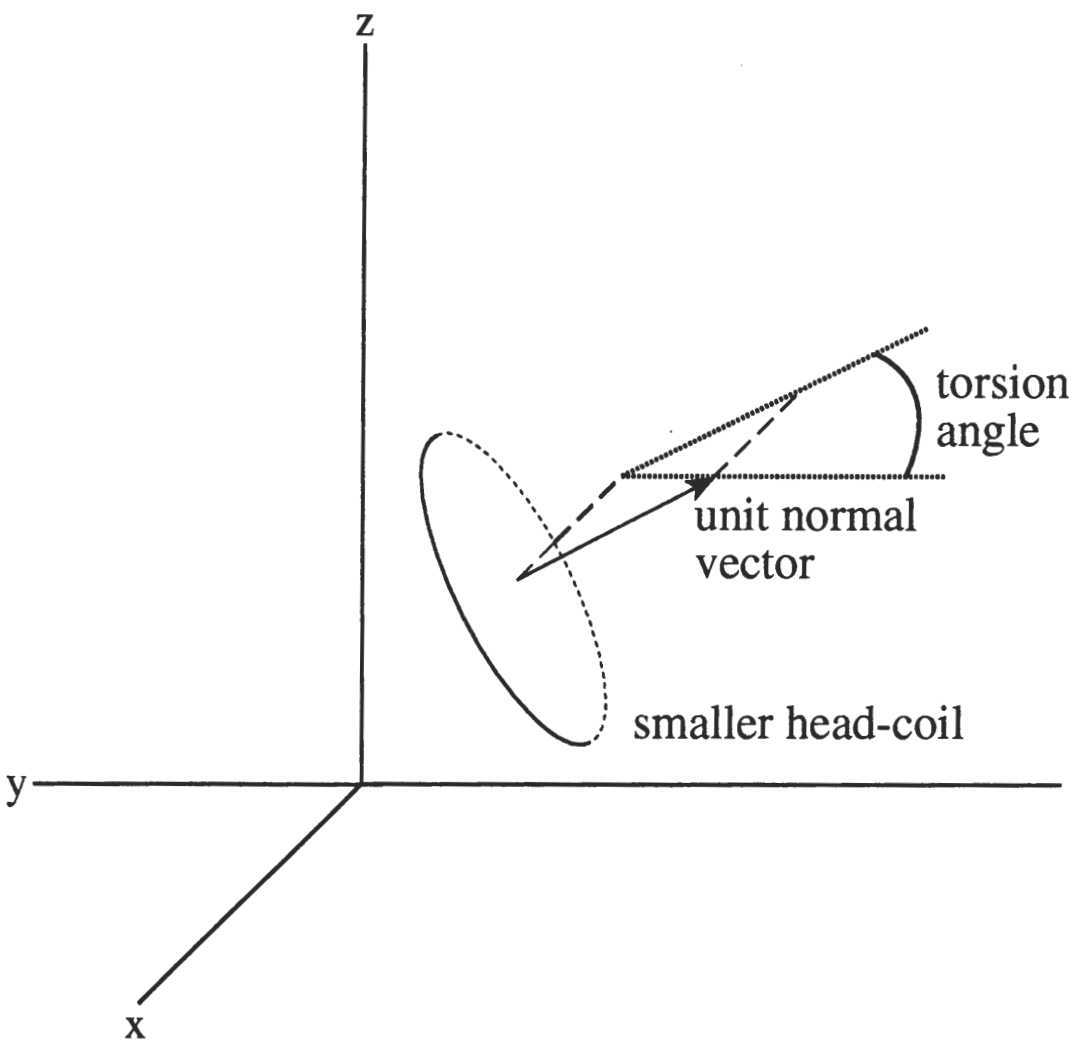

Figure 2.8: The torsion angle as measured by the RMFM

Chapter 3

Table Experiments

In this chapter, the major activities performed in Table Experiments will be described briefly. Most of the description will focus on the calibration procedures. Table Experiments performed to date actually consisted of two different sub-experiments. The first sub-experiment focused on the hand-eye coordination skills of the subject. The second sub-experiment was devoted to the investigation of eye movement behavior when a subject was perturbed during a saccade ("push experiments").

Four subjects participated in these experiments. Each subject was run in several sessions. The word "session" is defined to be an event during which a large amount of data was collected for a single subject. During a session a subject was fitted with eye-coils, head-coils, and head-sparker and performed activities that were repeated over many trials. The term "trial" will be used here to denote a short period during which eye-angle, head-angle, and head-sparker data were collected. The length of a trial ranged from 2 to 10 seconds and a session consisted of as many as 100 trials.

3.1 Calibration Measurements

There were three activities performed that will be called "calibration measurements" in this document. The first type of measurement was devoted to the calibration of the sparker measurements. The second measurement involved the determination of the offset of the eye-coil from the subject's line-of-sight when the coil was placed on the eye at the beginning of a session. The last type of measurement was performed for the purpose of determining the coordinates of the sighting-center for each of the subject's eyes when the subject's head was supported on the biteboard. The first and third of these

measurements were performed before the main sessions began. There were two methods used for the determination of the subject's sighting-center. A description of the method finally used will be presented in Appendix A. The other two measurements are described below.

3.1.1 Sparker Calibration

The main purpose of the sparker calibration measurements was to determine the conversion factor between the distance units output by the STS ("sparker units") and millimeters. All distance measurements are generally expressed in millimeters. This was done as follows.

A single sparker was placed in hole $(1, 7)$ of the RFM Worktable and the distances from this sparker to each microphone was measured using a vernier caliper. Sparker data were then collected. These data were then averaged over a trial which yielded distances from the sparker to each microphone in sparker units for that trial. The trial was replicated later and the same averages were computed to allow for modest ($< 2\ ^\circ F$) changes in room temperature during Table Experiments which usually lasted about $20 - 30$ minutes. The ratio of the distance to a microphone in millimeters to the same distance in sparker units then gave the scale factor (conversion factor) for that microphone. The two average scale factors for the trial were themselves averaged. These factors agreed to about three decimal places for each microphone. See fig. 2.8 above.

3.1.2 Eye-Coil and Head-Coil Offset Calibration

During each experimental session, eye-coil-offset calibration measurements (mirror trials) were performed. Generally, these measurements were performed only during the first two trials of a session, one trial for each eye. This was also done every time a new coil was placed on a subject's eye (occasionally a coil broke during a session and a new coil inserted so these measurements were sometimes performed more than once during a session).

A device containing a front-surface mirror was constructed so that it could be mounted such that the plane of the mirror was approximately parallel to the TCS yz-plane and such that the mirror surface faced the subject while his head was supported on a biteboard. Then, while on the biteboard and with one eye covered, the subject fixated the image of his pupil in the mirror.

In this situation, the line-of-sight of the uncovered eye of the subject was construed to be parallel to the TCS x-axis and horizontal and vertical eye-angle data were then collected. This procedure was repeated for the other eye. The readings were averaged over the trial to yield final offset values. See fig. 3.1; note that, in this figure, the offset of the eye-coil is exaggerated for clarity.

This determined the error of placement of the coil on the eye. If the coil had been placed perfectly, the horizontal reading would have been as close to 13,500 minarc as possible given the small error in aligning the TCS x-axis on the table with magnetic north and given the fixation error. Similarly the vertical reading would have been as close as possible to 8100 minarc. Offsets in both horizontal and vertical were generally smaller than a degree which means that the annuli were relatively well-centered on the eyeball - i.e. the unit vector normal to the annulus was nearly parallel to the line-of-sight. See [4] for the significance of this offset error for estimating the direction of the line-of-sight when the head is free to move about three axes.

It is essential for the computation of the subject's real-time sighting center to have head-angle readings for a case in which the sighting-center position is known. During these initial eye-coil calibration trials, head-angle readings were also collected. Every time a subject was fitted with the head-coil device, the placement of the device on the forehead, like the placement of the annulus on the eye, was slightly different. The head-angles collected at each RFM burst during these two calibration trials were averaged to yield initial head-angle readings. The use of these head-angle readings will be discussed in more detail in the next chapter.

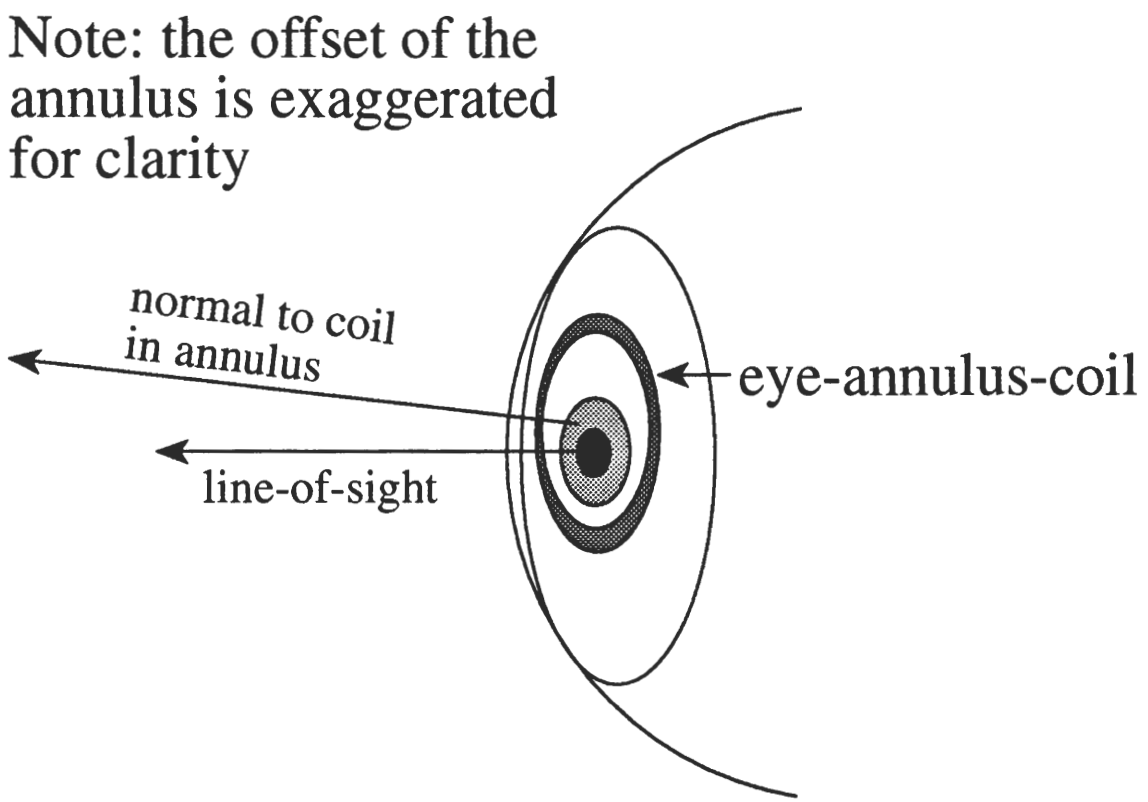

Figure 3.1: Eye-Coil offset

Chapter 4

Calculation of the Subject's Sighting-Center Position in Real-Time

To be able to calculate real-time quantities suitable for data analysis (e.g. table gaze positions or gaze errors relative to a given target), one must first compute the TCS position of the sighting-center of each subject's eye during each RFM burst on a trial. The data needed for such a calculation fall into two main categories: (A) static-head measurements and (B) free-head measurements. The first category of measurements are performed while the subject's head is supported on a biteboard. These static-head data include (1) the sighting-center position of each eye, (2) head-angle data, and (3) head-sparker data. Measurements in the free-head category include (4) head-angle data at each burst of the RFM during a given trial and (5) head-sparker data at each strobe of the sparker during the trial. Except for data type (1), all of the above are raw data and were collected in the experiments performed to date. The method for determining the first data type is the subject of Appendix A and will not be discussed here. All of what follows in this chapter refers to only one of the subject's eyes. The procedure is the same for the other eye.

The broad method for obtaining the subject's real-time sighting-center position is based on a simple idea. **If the subject's sighting-center position is known when the head-sparker position and head-coil orientation are also known**, as they are when measurements made while the subject's head is supported on a biteboard, **then**, since the head plus eye plus head-sparker are assumed not to move relative to each other, **a new head-sparker position and a new head-coil orientation together uniquely**

determine the new sighting-center position. See fig. 4.1. That is, there is a geometrical relationship among sighting-center position, head position, and head orientation due to the fact that the head-coil plus eye plus head-sparker is a rigid body. Note that this implies the assumption that the head-sparker and the head-coil devices do not appreciably wiggle or slip systematically while fixed to the subject's head. The head-sparker and head-coil devices were designed so that such wiggling and slippage is minimized. It is, therefore, the judgment of the experimenters that it is reasonable to make the rigid-body assumption.

The derivation of the geometrical relationship among the head-coil plus eye plus head-sparker is the core of this chapter. The plan of the chapter is as follows. First, the broad geometrical relationship mentioned above will be derived by separating it into a rotation of the head followed by a translation of the head. After this, the method for determining the TCS coordinates of the head-sparker given the head-sparker data will be derived (this is needed for the translation part of the preceding step. The rotation equations will be derived (the most critical derivation) by two independent methods. Two methods are used to derive the same final result as this result is rather complicated and one gains greater confidence in the answer by using two different derivations. Finally, the relationship between the angles contained in the final rotation matrix and the angles measured by the RFM is derived.

4.1 Finding the Sighting-Center Position

In this section, the fundamental equation for finding the TCS coordinates of the sighting-center of the eye in real-time will be derived in terms of measured quantities. The sections that follow will focus on the methods for obtaining the different terms in that equation.

As described earlier, the basic idea behind the method for obtaining the sighting-center position lies in treating the system of head-sparker plus head-coils plus eye as a rigid body. In this document, the **configuration** of this rigid body will be specified if both its **position** and its **orientation** are given.

The position of the body is specified if the coordinates of a point fixed in the body are given relative to some coordinate system. For

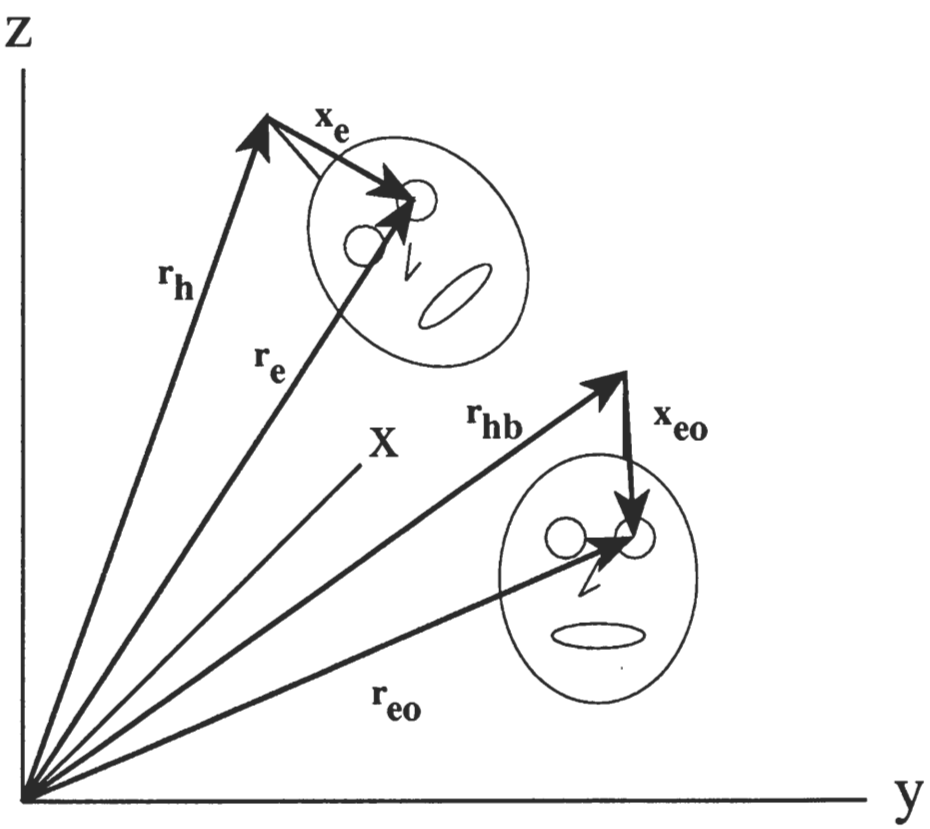

Figure 4.1: Change of configuration

the body of interest, this fixed point is the tip of the head-sparker and the coordinate system is the TCS.

The orientation of the body is specified if angles between two of the coordinate axes and a reference line fixed in the body are given and if the angle between a second body-fixed reference line, perpendicular to the first line, and one of the axes of the coordinate system is also given. For the case at hand, the first body-fixed reference line is defined to be that line perpendicular to the large head-coil and the two angles are those that its orthographic projections onto the TCS xy-, and xz-planes make with the positive TCS x-axis (these are the horizontal and vertical head-angles respectively). The second reference line is perpendicular to the smaller head-coil and the angle that must be specified is the angle that the line's projection onto the TCS yz-plane makes with the negative y-axis of the TCS (this is the torsional angle). Fixing these three angles uniquely specifies an orientation of the head-sparker plus head-coil plus eye rigid body (hereafter referred to as the "head").

Once the configuration of the head is specified, the transformation to any other configuration consists of a rotation and translation. By the term "transformation" is meant the mathematical equations that relate the position of a point fixed in the head (e.g. the sighting-center) when the head is in the initial configuration to the coordinates of the same head-fixed point when the head is in the final configuration. The word "translation" refers to a type of transformation that leaves the angles that specify the orientation of the body unchanged. The term "rotation" is another type of transformation in which the coordinates of the head-fixed reference point remain constant. These two transformations can be performed independently. That is, a rotation can be performed that leaves a given head-fixed reference point at the same physical position in space. Conversely, a translation can be performed that leaves unchanged the angles specifying the orientation of the head. See fig. 4.2.

Thus the transformation of the head from the initial configuration to the final configuration is performed in two steps: (1) The head is rotated about its reference point (i.e., the tip of the head-sparker) such that the angles defining its orientation have their correct values in the final head configuration, and (2) the head is translated so that the reference point is located at the coordinates of the final head configuration.

It is convenient to define a standard configuration and then to specify

all other configurations by transformations of the head from the standard configuration. The standard configuration will be as follows. The head-fixed reference point (i.e. head-sparker) is located at its position when the subject's head is supported on the biteboard and the head is oriented such that the large head-coil is perfectly aligned with the yz-plane of the TCS and the line formed by the intersection of the two head-coils is exactly parallel with the TCS z-axis. (See fig. 4.3)

4.1.1 Transformation of the Rigid Body

Let $\mathbf{r_{hb}}$ be the vector that locates the tip of the head-sparker when the subject's head is supported on the biteboard during the calibration trials of a session and let $\mathbf{r_{eb}}$ be the vector that locates the sighting-center position under the same circumstances. The second vector was determined prior to the beginning of the main sessions of the experiment and is assumed known here. How this was done is described in Appendix A. Thus the vector that points from the head-sparker to the sighting-center while the subject's head is supported on the biteboard is

$$\mathbf{x_{eb}} = \mathbf{r_{eb}} - \mathbf{r_{hb}}, \tag{4.1}$$

and the above equation can be rearranged to read:

$$\mathbf{r_{eb}} = \mathbf{r_{hb}} + \mathbf{x_{eb}}. \tag{4.2}$$

It is worth noting that the length of $\mathbf{x_{eb}}$ (which is the distance from head-sparker to sighting-center) cannot change because of the rigid body assumption. See fig. 4.4.

This is the fundamental formula, it applies not only here, but for any configuration of the head. In words it may be stated simply as follows: the vector from the origin to the sighting-center equals the vector from the origin to the sparker plus the vector from the sparker to the sighting-center. The statement of the above formula for an arbitrary burst of the RFM during a trial is

$$\boxed{\mathbf{r_e} = \mathbf{r_h} + \mathbf{x_e}.} \tag{4.3}$$

In the above formula, $\mathbf{r_e}$ is the vector from the origin of the TCS to the sighting-center, $\mathbf{r_h}$ is the vector from the origin to the head-sparker, and $\mathbf{x_e}$

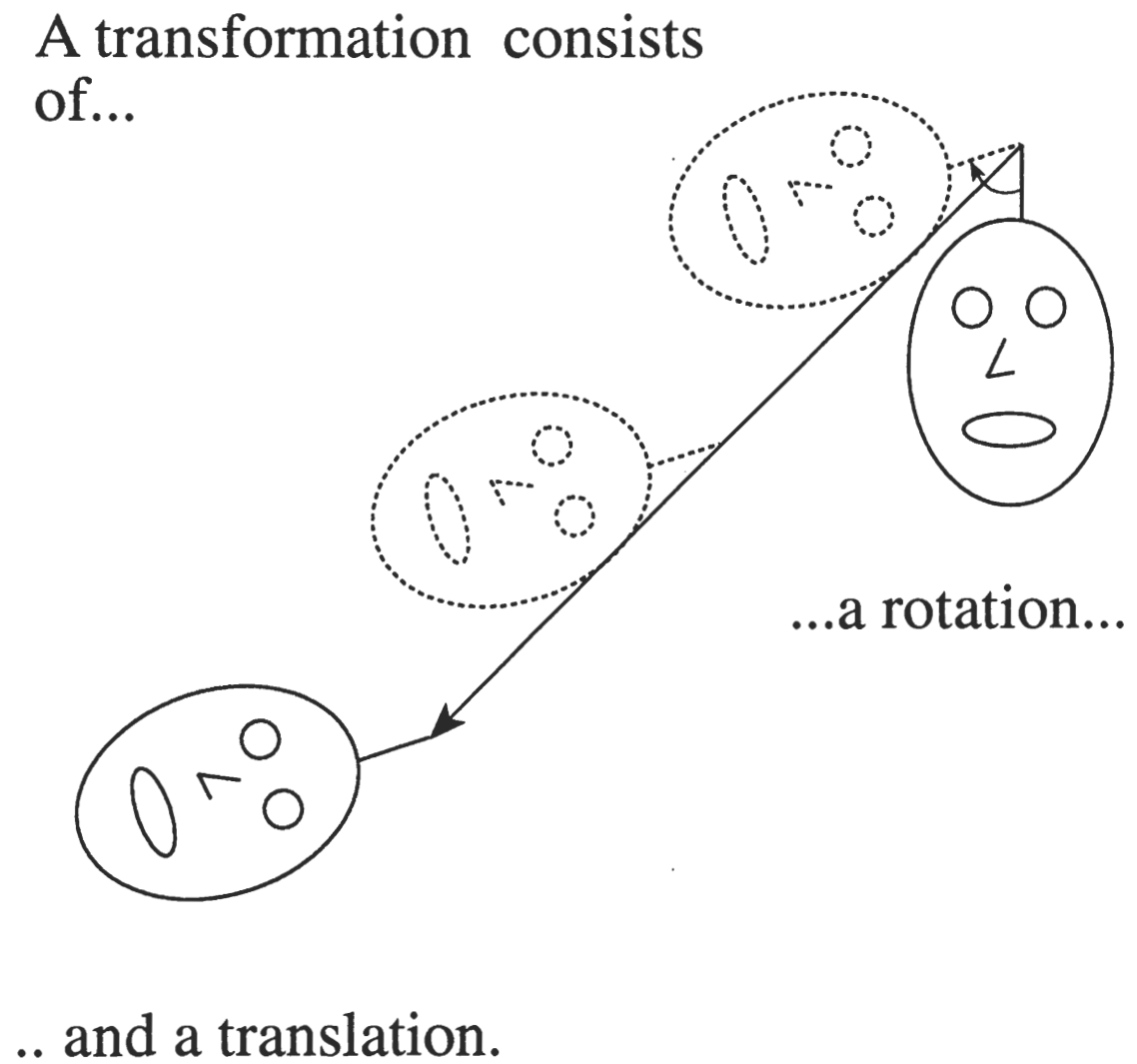

Figure 4.2: Transformation of the head

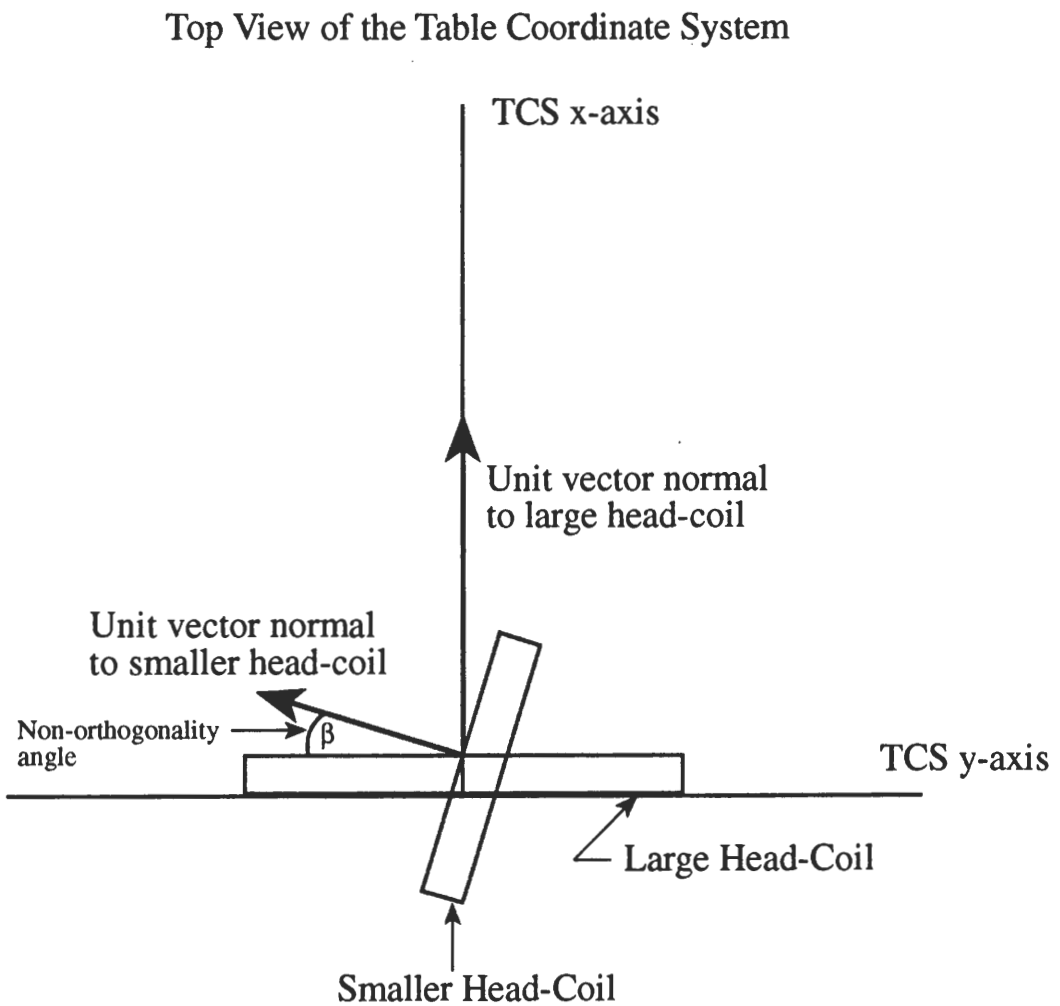

Figure 4.3: The standard configuration

is the vector from the head-sparker to the sighting-center. Both $\mathbf{r_e}$ and $\mathbf{x_e}$ are time-tagged at an arbitrary burst of the RFM during a trial and $\mathbf{r_h}$ is the vector described above time-tagged at the most recent strobe of the sparker at the time of the RFM burst (see fig. 4.4).

The transformation from the standard configuration of the head to another configuration can easily be described in terms of the above equation. In the standard configuration (labeled by 0), the above equation becomes

$$\mathbf{r_{e0}} = \mathbf{r_{hb}} + \mathbf{x_{e0}}, \tag{4.4}$$

where the b subscript in the first vector on the right-hand-side of the above equation refers to "biteboard" as the sparker position in the standard configuration is the biteboard position. And, in the final configuration, the formula is the same as Eq. 4.3 above

$$\mathbf{r_e} = \mathbf{r_h} + \mathbf{x_e}. \tag{4.5}$$

Now in the first step of the transformation described above, the head is rotated about the head-sparker point $\mathbf{r_{hb}}$. This leaves this vector unchanged and rotates $\mathbf{x_{e0}}$ into the vector $\mathbf{x_e}$. This may be represented by the equation.

$$\mathbf{x_e} = R(\theta_h, \theta_v, \theta_t)\mathbf{x_{e0}}, \tag{4.6}$$

where R is the 3×3 matrix that represents the rotation and depends only on the head-angle data. In the above equation, θ_h is the horizontal head-angle, θ_v is the vertical head-angle, and θ_t is the torsional head-angle all of which are measured in the final head configuration referenced to magnetic north and expressed in radians. The second step is a translation of the head to the new sparker position. This is represented by the equation

$$\mathbf{r_{h1}} = \mathbf{r_{hb}} + \mathbf{r_t}. \tag{4.7}$$

Where $\mathbf{r_t}$ is a vector from the standard sparker position to the new sparker position. Hence one can write

$$\mathbf{r_{e1}} = (\mathbf{r_{hb}} + \mathbf{r_t}) + R(\theta_h, \theta_v, \theta_t)\mathbf{x_{e0}}. \tag{4.8}$$

In the above equation, one now sees clearly the rotation, represented by R, and the translation, represented by $\mathbf{r_t}$. The above general equations

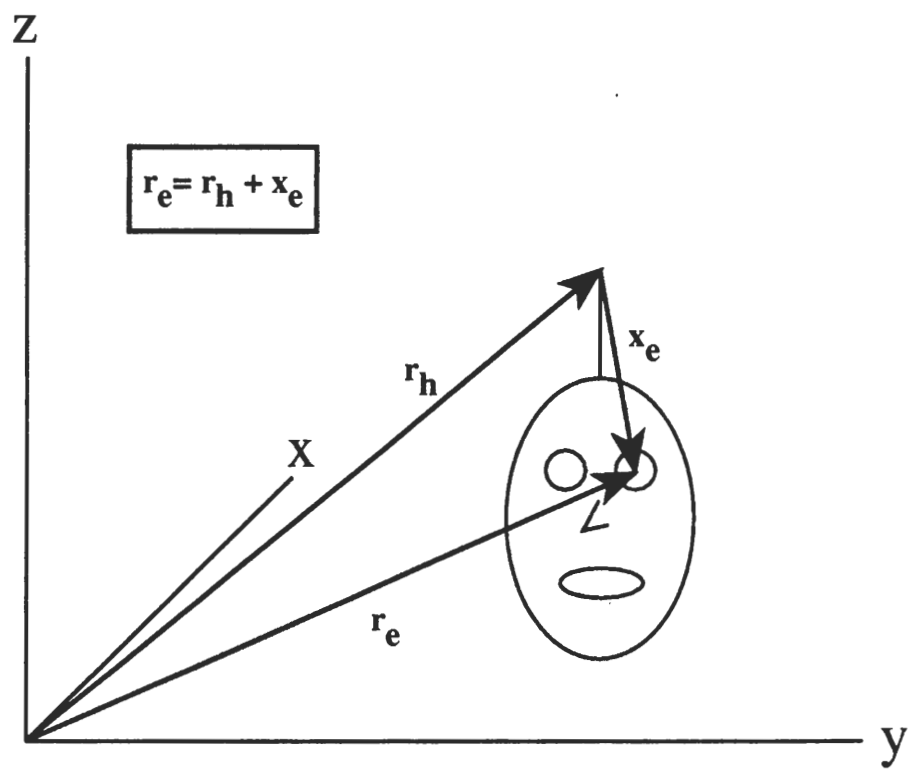

Figure 4.4: The fundamental equation

may now be applied to the case of interest. It is important here to clearly distinguish those quantities that are measured from those that are wanted.

Consider then the situation when the subject is on the biteboard. Define

$\mathbf{r_{hb}}$ = the position of the head-sparker on biteboard (measured),

$\mathbf{r_{eb}}$ = the position of the sighting-center on biteboard (measured),

$\mathbf{x_{eb}}$ = vector from sparker to sighting-center position on biteboard.

Then Eq. 4.3 becomes

$$\mathbf{r_{eb}} = \mathbf{r_{hb}} + \mathbf{x_{eb}}. \tag{4.9}$$

Since both $\mathbf{r_{eb}}$ and $\mathbf{r_{hb}}$ are measured, the vector $\mathbf{x_{eb}}$ can be found

$$\mathbf{x_{eb}} = \mathbf{r_{eb}} - \mathbf{r_{hb}}. \tag{4.10}$$

Now apply Eq. 4.3 to the standard configuration in which the head-sparker is in the biteboard position. Define

$\mathbf{r_{e0}}$ = sighting-center position in standard configuration,

$\mathbf{x_{e0}}$ = vector from sparker to sighting-center in standard configuration.

For this case the basic equation is

$$\mathbf{r_{e0}} = \mathbf{r_{hb}} + \mathbf{x_{e0}}. \tag{4.11}$$

The vector $\mathbf{x_{e0}}$ can be determined because the readings of the head-coils in both the biteboard and standard orientations are known. The biteboard readings are measured and the standard ones are known by construction or are measured. Both the horizontal and vertical readings of the large head-coil are zero in the standard orientation and the reading of the smaller head coil has the value of the non-orthogonality angle whose measurement is described later in this chapter.

All transformations will be referenced to the standard configuration. That is, all rotations will be rotations of the vector $\mathbf{x_{e0}}$ and all translations will be translations of $\mathbf{r_{hb}}$. Thus to transform from the standard configuration to the configuration on the biteboard one must perform a rotation of $\mathbf{x_{e0}}$ only since the sparker position does not change. This gives

$$\mathbf{x_{eb}} = R(\theta_{ho}, \theta_{vo}, \theta_{to})\mathbf{x_{e0}}, \tag{4.12}$$

where $R(\theta_{ho}, \theta_{vo}, \theta_{to})$ is the matrix that describes the rotation of $\mathbf{x_{e0}}$ into $\mathbf{x_{eb}}$ and the head-angles are those measured while the subject is on the biteboard during the calibration trials of a session. The value of $R(\theta_{ho}, \theta_{vo}, \theta_{to})$ can be determined from these head-angles alone. Hence all of the quantities in the above equation are measured except the vector $\mathbf{x_{e0}}$. One must solve for this vector because it is used as the reference vector. This is easily done by left-multiplying both sides Eq. 4.12 by the inverse of $R(\theta_{ho}, \theta_{vo}, \theta_{to})$ and using Eq. 4.10:

$$\mathbf{x_{e0}} = R_o^{-1}(\theta_{ho}, \theta_{vo}, \theta_{to})(\mathbf{r_{eb}} - \mathbf{r_{hb}}). \tag{4.13}$$

The above equation gives the vector from the head-sparker to the sighting-center in the standard configuration completely in terms of measured quantities.

Finally, consider once more the case of the head configuration at an arbitrary RFM burst described by Eq. 4.8. The vector $\mathbf{r_t}$ in that equation stretches from the standard head-sparker position (on biteboard) $\mathbf{r_{hb}}$, to the current arbitrary sparker position $\mathbf{r_h}$. Since both of these positions are measured $\mathbf{r_t}$ is obtained as

$$\mathbf{r_t} = \mathbf{r_h} - \mathbf{r_{hb}}.$$

The above equation along with Eq. 4.13 can be inserted into Eq. 4.8 to obtain the equation for the subject's sighting-center at an arbitrary RFM burst during a trial completely expressed in terms of measured quantities:

$$\boxed{\mathbf{r_e} = \mathbf{r_h} + R(\theta_h, \theta_v, \theta_{to}) R(\theta_{ho}, \theta_{vo}, \theta_{to})^{-1}(\mathbf{r_{eb}} - \mathbf{r_{hb}}).} \tag{4.14}$$

The vector $\mathbf{r_h}$ is the head-sparker position at the most recent sparker strobe before the current RFM burst, $(\theta_h, \theta_v, \theta_t)$ are the head-angles at the RFM burst, $(\theta_{ho}, \theta_{vo}, \theta_{to})$ are the head-angles measured when the subject's was supported on the biteboard during a calibration trial, $\mathbf{r_{eb}}$ locates the position of the subject's sighting-center during the calibration trial , and $\mathbf{r_{hb}}$ is the head-sparker position during the calibration trial. Eq. 4.14 is the working equation that is used to determine the subject's sighting-center at an arbitrary RFM burst during a trial.

It is clear from the above equation that there are two basic quantities that must be determined from raw data: (1) the TCS coordinates of the head-sparker, and (2) the rotation matrix. The equations for these quantities in terms of raw data are derived in the next two sections.

4.2 Calculation of the Sparker Position

The data needed for calculating the sparker position are (1) any set of three of the four distances (in sparker units, with corresponding scale factors) from the sparker to the microphones, (2) the 2 distances between adjacent microphones in the subset of three microphones used, and (3) the diagonal distance between the two non-adjacent microphones in the subset. The derivation presented below gives the TCS x-, y-, and z-coordinates of the sparker position in terms of the above data.

The major steps in the derivation of these equations are, (a), to find the coordinates of the sparker in the Sparker Coordinate System (SCS) and then (b) to use the matrix that transforms SCS coordinates into TCS coordinates. This matrix was obtained before the main sessions of the experiments began and the procedure for its determination will be described below. Its numerical value is given in Appendix A.

The derivation of these equations is again based on a simple idea. Since the distances from the sparker to each of three microphones is known, the sparker must simultaneously lie on three independent spheres, each sphere centered on a different microphone and of radius equal to the distance from the sparker to the microphone. The intersection of two overlapping spheres is a circle, a third sphere intersects this circle at two points. One of these points is the sparker position and is below the plane of the microphones and the other is above the plane of the microphones. Since the SCS has its positive z-axis pointing downward, the sparker location will have a positive z-coordinate in the SCS. This uniquely specifies the sparker position.

In the following derivation, microphone C is not be used because it sometimes proved unreliable whereas the others did not.

4.2.1 Finding the SCS Coordinates of the Sparker

Let d_A, d_B, and d_D be the distances from the sparker to microphones A, B, and D in millimeters respectively. See fig. 2.8. Also let s_A, s_B, and s_D be the scale factors for the same set of microphones. Then if r_A, r_B, and r_D are the corresponding distances measured in sparker units, then

$$d_A = s_A \cdot r_A, \tag{4.15}$$

$$d_B = s_B \cdot r_B, \tag{4.16}$$

$$d_D = s_D \cdot r_D. \tag{4.17}$$

These distances, now expressed in millimeters, are the radii of three distinct spheres, each centered on a different microphone. The analytic equation of a sphere whose center is at the point (x_0, y_0, z_0) and whose radius is r_0 is

$$(x - x_0)^2 + (y - y_0)^2 + (z - z_0)^2 = r_0^2, \tag{4.18}$$

where (x, y, z) is an arbitrary point on the sphere. Now, by definition of the SCS, microphone A is at the origin $(0, 0, 0)$, microphone D is at the point $(x_D, 0, 0)$, where x_D is the distance between microphones A and D (equal to *mdda*, see fig. 2.8). And letting the coordinates of microphone B be $(x_B, y_B, 0)$ the Pythagorean theorem gives, for right triangles ABE and EBD,

$$x_B^2 + y_B^2 = (mdab)^2 \tag{4.19}$$

and,

$$(mdda - x_B)^2 + y_B^2 = (mdbd)^2. \tag{4.20}$$

Eqs. 4.19 and 4.20 form two equations with two unknowns and have the following solution

$$x_B = \frac{(mdda)^2 + (mdab)^2 - (mdbd)^2}{2 \cdot (mdda)}, \tag{4.21}$$

and,

$$y_B = \left((mdab)^2 - x_B^2\right)^{\frac{1}{2}}. \tag{4.22}$$

Now, if the sparker is assumed to be at the unknown point (x_S, y_S, z_S) then this point is common to the three spheres whose equations are

$$(x_S)^2 + (y_S)^2 + (z_S)^2 = d_A^2, \tag{4.23}$$

for microphone A, and

$$(x_S - x_B)^2 + (y_S - y_B)^2 + (z_S)^2 = d_B^2, \tag{4.24}$$

for microphone B, and

$$(x_S - x_D)^2 + (y_S)^2 + (z_S)^2 = d_D^2, \tag{4.25}$$

for microphone D. This set of three equations may be solved for the three unknown coordinates, (x_S, y_S, z_S), of the sparker position in the SCS. The solution is

$$x_S = \frac{x_D^2 + d_A^2 - d_D^2}{2 \cdot x_D}, \tag{4.26}$$

$$y_S = \frac{x_B^2 + y_B^2 - \left(\frac{x_B}{x_D}\right)(x_D^2 + d_A^2 - d_D^2) + d_A^2 - d_B^2}{2 \cdot y_B}, \tag{4.27}$$

$$z_S = (d_A^2 - x_S^2 - y_S^2)^{\frac{1}{2}}. \tag{4.28}$$

where in the last equation the positive square root must be taken to ensure that the sparker position lies inside the magnetic field volume.

If the diagonal distance *mdbd* between microphones B and D is not measured, then the above equations may still be used by assuming that the microphone frame is exactly rectangular. In this case one sets $x_B = 0$, and $y_B = mdab$ in the above equations. Equations 4.26 and 4.28 are unchanged by this and Eq. 4.27 becomes

$$y_S = \frac{(mdab)^2 + d_A^2 - d_B^2}{2 \cdot mdab}. \tag{4.29}$$

4.2.2 Transforming From SCS to TCS Coordinates

The transformation of the coordinates of a point from the SCS to the coordinates of the same physical point in the TCS consists of a translation and a rotation. If (x_S, y_S, z_S) are the coordinates of the sparker in the SCS and (x, y, z) are its coordinates in the TCS, then the transformation has the following form[3]

$$x = R_{11}x_S + R_{12}y_S + R_{13}z_S + x_T, \tag{4.30}$$

$$y = R_{21}x_S + R_{22}y_S + R_{23}z_S + y_T, \tag{4.31}$$

$$z = R_{31}x_S + R_{32}y_S + R_{33}z_S + z_T. \tag{4.32}$$

These equations can be summarized in matrix form:

$$\begin{pmatrix} x \\ y \\ z \end{pmatrix} = \begin{pmatrix} R_{11} & R_{12} & R_{13} & x_T \\ R_{21} & R_{22} & R_{23} & y_T \\ R_{31} & R_{32} & R_{33} & y_T \end{pmatrix} \begin{pmatrix} x_S \\ y_S \\ z_S \\ 1 \end{pmatrix} \tag{4.33}$$

The 3×3 submatrix containing R's is the matrix that rotates the SCS coordinate axes into those of the TCS. The x_T, y_T, and z_T are the translations along the x-, y-, and z-axes respectively that take the SCS origin into the TCS origin. Matrices shall, in this document, be denoted by capital letters set in light type as below:

$$A = \begin{pmatrix} R_{11} & R_{12} & R_{13} & x_T \\ R_{21} & R_{22} & R_{23} & y_T \\ R_{31} & R_{32} & R_{33} & y_T \end{pmatrix}, \tag{4.34}$$

and three-component column vectors shall be denoted by bold-face, lower-case letters just as with vectors:

$$\mathbf{x} = \begin{pmatrix} x'_S \\ y'_S \\ z'_S \end{pmatrix}, \tag{4.35}$$

and four-component column vectors are denoted by light-type, lower-case letters:

$$y = \begin{pmatrix} x_S \\ y_S \\ z_S \\ 1 \end{pmatrix}. \tag{4.36}$$

Thus Eq. 4.33 can be written as

$$\mathbf{x} = Ay. \tag{4.37}$$

The procedure for determining the matrix A of transformation from the SCS to TCS coordinates was as follows. Sparkers were placed at N different locations on the RFM Worktable ($N = 18$, see Appendix A for the positions) and sparker data were collected for each. The TCS coordinates of each sparker was known in advance and from the sparker data the SCS coordinates of all N sparkers can be determined as described in the last section. This yields a total of N equations like Eq. 4.37:

$$\mathbf{x}_i = Ay_i, \; i = 1, ..., N. \tag{4.38}$$

Since N is larger than the twelve elements of the matrix A there are more equations than unknowns and these elements can be estimated by the method of least-squares.

The simplest way to get the least-squares solution is to build two supermatrices that summarize all N of the above equations in one matrix equation. The first supermatrix (X) is formed by making each of its columns one of the $\mathbf{x}_i$ (which is a 3×1 matrix) making it a $3 \times N$ matrix:

$$X = \begin{pmatrix} (\mathbf{x}_1)_1 & \cdot & \cdot & \cdot & (\mathbf{x}_N)_1 \\ (\mathbf{x}_1)_2 & \cdot & \cdot & \cdot & (\mathbf{x}_N)_2 \\ (\mathbf{x}_1)_3 & \cdot & \cdot & \cdot & (\mathbf{x}_N)_3 \end{pmatrix}. \tag{4.39}$$

We form the other supermatrix (Y) in the same fashion yielding a $4 \times N$ matrix:

$$Y = \begin{pmatrix} (y_1)_1 & \cdot & \cdot & \cdot & (y_N)_1 \\ (y_1)_2 & \cdot & \cdot & \cdot & (y_N)_2 \\ (y_1)_3 & \cdot & \cdot & \cdot & (y_N)_3 \\ (y_1)_4 & \cdot & \cdot & \cdot & (y_N)_4 \end{pmatrix}. \tag{4.40}$$

Thus all N equations in Eq. 4.38 are included in the following equation

$$X = AY.$$

All of the elements of both X and Y are known and when this equation is solved for A, it corresponds to the least-squares solution. The solution is

$$A = (XY^T)(YY^T)^{-1},$$

where Y^T denotes the transpose of Y. The result of this calculation for the matrix A is given in Appendix A. And so to find the TCS coordinates of a point given the SCS coordinates one uses Eq. 4.37 with the matrix given in Appendix A.

4.3 Calculation of the Rotation Matrix

In this section, the transformation that rotates the vector $\mathbf{x_{e0}}$, the vector from head-sparker to eye in the standard head-configuration, into the vector $\mathbf{x_e}$, the vector from head-sparker to eye in an arbitrary head-configuration will be derived. The data required for determining this transformation are the three head-angles in the arbitrary configuration: (1) θ_h, the horizontal head-angle, (2) θ_v, the vertical head-angle, and (3) θ_t, the torsional head-angle. It is important to note that these angles are obtained by subtracting

13,500 minarc from the raw horizontal angle to get θ_h, and subtracting 8,100 minarc from the raw vertical and torsional angles and expressing the result in radians to get θ_v and θ_t respectively. The above numbers (13500 and 8100 minarc) are the angles that would be measured by the RFM if the subject's head was in the standard configuration. This causes θ_h, θ_v, and θ_t to be zero in that configuration.

The plan of this section is as follows. The first subsection describes the information needed to completely and uniquely specify a rotation. Next follows a discussion of the Fick, and Helmholtz descriptions of eye positions (orientations) and how one may obtain the Fick coordinates if the Helmholtz coordinates are known and vice versa. In the penultimate subsection, the rotation matrix will be derived by two independent methods: the active rotation method and the passive rotation method. The final rotation matrices obtained in these derivations are identical. The reason for presenting two different derivations is that the final rotation matrix has a somewhat complicated form and that having two separate derivations should give the reader greater confidence that this complicated form is correct. The final rotation matrix obtained from these derivations depends upon the three Fick angles that describe the orientation of the head. Not all of these Fick angles are measured directly by the RMFM. Hence, in the final subsection, the relationship between the Fick angles contained in the rotation matrix and the measured RMFM angles is derived.

This section presents the heart of the data-processing method. It is the one that requires the most mathematics. The reader unfamiliar with the material on vectors and matrices in Appendix B is advised to review this appendix now.

4.3.1 Specifying a Rotation

Three independent pieces of information are required to uniquely specify a rotation of a vector or a system of coordinate axes. The first of these is **an axis of rotation**, the second is **the angle through which the vector or coordinate system is rotated** about that axis, and third is **the sense of the rotation**.

An axis of rotation is simply a direction. Since vectors are quantities that have both length and direction, an axis may be specified by giving a vector that points along this axis and that has a length of one unit (i.e., a unit

vector). Hence any unit vector uniquely defines an axis of rotation.

Specifying the sense of the rotation amounts to defining in which direction around the axis of rotation the rotation angle increases (e.g. clockwise or counterclockwise). It is customary to define the sense of rotation with the terms "left-handed" or "right-handed". In a left-handed rotation one points the thumb of the left hand along the rotation axis and the fingers of that hand then curl naturally in the direction of increasing rotation angle. All of the rotations described below will be left-handed.

4.3.2 Fick and Helmholtz Coordinate Systems

There are several different systems for describing the position (orientation) of the eye in its orbit in common use in the eye-movement literature. Some of these include the Helmholtz, Fick, and Listing systems[5]. Of these, the most important one for the purposes of the derivation given below is the Fick system. The Helmholtz system is important for the analysis of binocular data, specifically for "vergence" eye movements. Therefore, both of these systems will be briefly described below.

The reference for all of these systems is called the primary eye position. The eye is in this position when the subject looks straight ahead and is looking at a distant object. To define one of these systems, one imagines a sphere centered on the eye and having lines of latitude (corresponding to lines that measure angular distance north and south of the equator on the earth) and longitude (measuring angular distances east and west of the prime meridian) drawn on it. The lines of longitude all intersect at two points on the sphere: the north and south poles. The line joining these two points is called the pole axis. The eye position is specified by giving the angular coordinates of the intersection of the line-of-sight of the eye with the sphere and by giving the angle of rotation of the eye around this line-of-sight. The systems differ in the orientation of this axis and in the orientation of the sphere around this axis.

The Helmholtz System

In this system, the pole axis of the sphere passes through the center of both eyes and the north pole is to the right of the subject's head. The eye reaches its final position by rotating through three angles, (H_1, H_2, H_3). Starting

from the primary position, the eye first rotates about the pole axis through the angle H_1, called the first Helmholtz angle. During this rotation the eye is looking upward (if H_1 is positive) and follows the equator of the sphere. Next the eye follows the line of longitude to the right through an angle H_2 whereupon it reaches the point of intersection of the line-of-sight with the sphere. Finally it rotates around the line-of-sight through the angle H_3 (the third Helmholtz angle). See fig. 4.5. The plane that contains the line-of-sight and the pole axis is called the plane of regard and is important for studies of, for example, "vergence" eye movements.

The Fick System

In the Fick system, the pole axis is vertical and passes through one eye of the subject and the north pole is above the head. To reach its final orientation the eye first rotates about the pole axis through an angle F_1 called the first Fick angle or the longitude angle. If this angle is positive then the subject will be looking horizontally to the right during this rotation that follows the equator of the sphere. Next the eye follows a line of latitude (which eventually reaches the north pole above the head) until it reaches the intersection of the line-of-sight with the sphere in the final orientation. In this rotation, the eye moved through an angle F_2 called the second Fick angle. These two angles are similar to the "spherical polar coordinates" in elementary mathematics and the Fick system is sometimes called polar coordinates. Lastly, the eye rotates around the line-of-sight through an angle F_3 to reach its final orientation. See fig. 4.6. Note that in the descriptions of both the Fick and Helmholtz coordinates, The **order** in which the rotations are performed is specified. This is done because rotations do not commute. In what follows, this process of performing given rotations in a specified order will be referred to as a **procedure** (e.g. the Fick procedure).

Analogy of these Systems with the Eye-angles Measured by the RMFM

The vertical eye-angle measured by the RMFM is the angle between the projection of the unit vector perpendicular to the eye-coil onto the TCS xz-plane and the TCS x-axis. The horizontal angle is the angle between the projection of the unit vector perpendicular to the eye-coil onto the TCS xy-

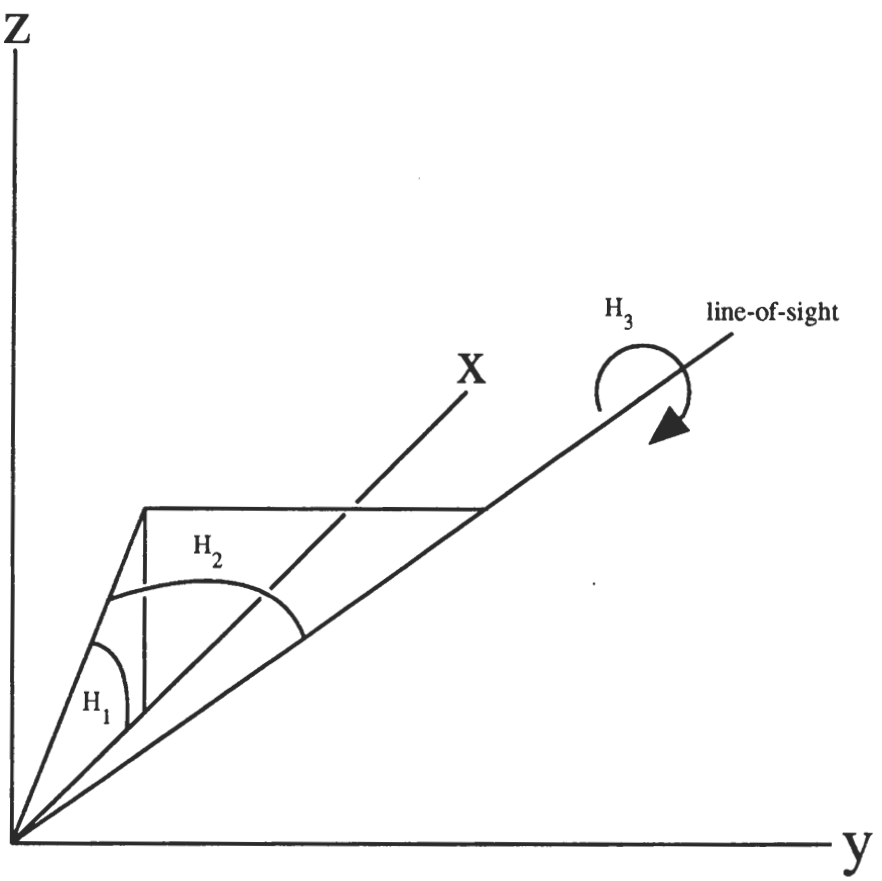

Figure 4.5: The Helmholtz system

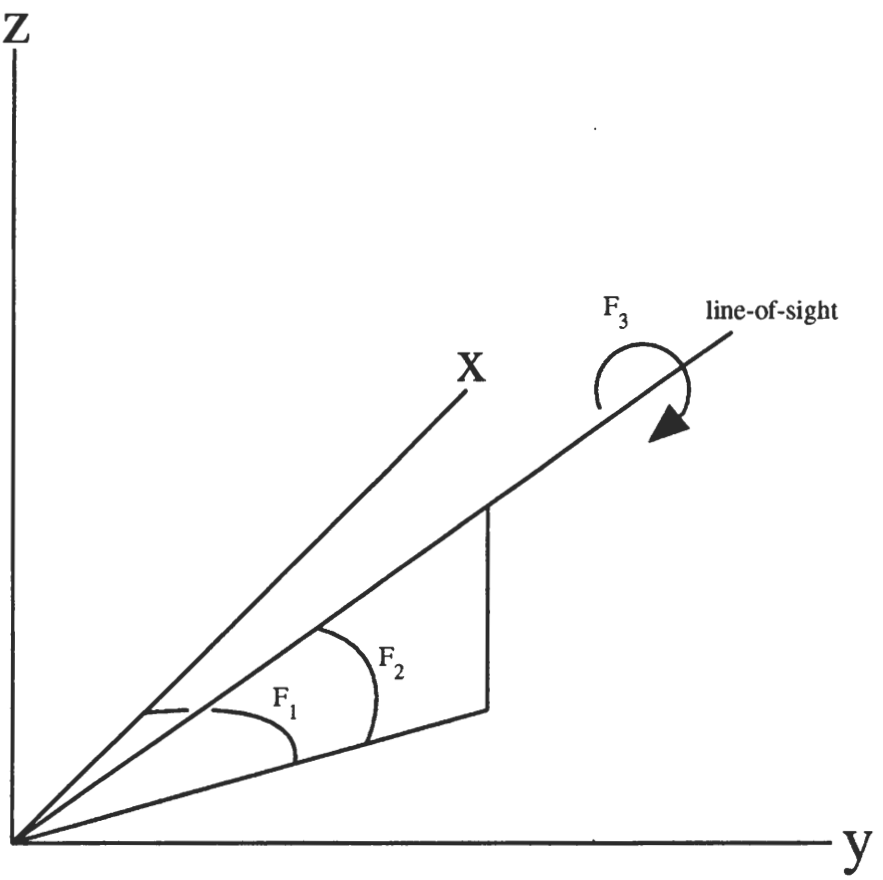

Figure 4.6: The Fick system

plane and the TCS x-axis. The angles, respectively, are analogous to angles in the Helmholtz and Fick systems described above. **They are not the same, however, because the Helmholtz and Fick systems are fixed in the body of the subject and the RMFM coordinate system is fixed in space.** The horizontal and vertical angles are identical to those in the Helmholtz and Fick systems for a subject whose head is immobilized such that the line-of-sight of the eye looking at the primary position is parallel to the TCS x-axis. This is not a disadvantage for the measurement of free-head eye-movements, however.

With the above in mind, the relationship between RMFM angles and those of the Helmholtz and Fick systems can be stated as follows. The RMFM horizontal angle is the first Fick angle, (F_1), and the vertical angle is the first Helmholtz angle, (H_1). It is very important to note that, given these two angles, the direction of the eye's line-of-sight is uniquely determined. Thus the second Fick, (F_2), and the second Helmholtz, (H_2), angles can be determined from F_1, and H_1. The equation for F_2 in terms of F_1 and H_1 are derived below.

Finding F_2 from F_1 and H_1

Figure 4.7 shows an arbitrary point in space a distance r from the origin. The direction from the origin to the point can be alternatively located by either the two Helmholtz or the two Fick angles as shown. The rectangle parallel to the yz-plane and whose upper right corner contains the point (x_o, y_o, z_o) can be considered the base of a four-sided pyramid whose apex is at the origin. The four lines connecting the origin to the corners of this rectangle form four different right triangles. Each one of these triangles contains one of the four angles, F_1, F_2, H_1, and H_2. Using these triangles, the coordinates (x_o, y_o, z_o) can be expressed in terms of either both Helmholtz angles or both Fick angles as labeled on the figure and given below.

$$x_o = r\cos(H_1)\cos(H_2) = r\cos(F_1)\cos(F_2),$$

$$y_o = r\sin(H_2) = r\sin(F_1)\cos(F_2),$$

$$z_o = r\sin(H_1)\cos(H_2) = r\sin(F_2).$$

The second equality in each of these equations yields three equations that may be solved for both F_2 and H_2 in terms of F_1 and H_1. These equations

are

$$\cos(H_1)\cos(H_2) = \cos(F_1)\cos(F_2), \tag{4.41}$$

$$\sin(H_2) = \sin(F_1)\cos(F_2), \tag{4.42}$$

$$\sin(H_1)\cos(H_2) = \sin(F_2). \tag{4.43}$$

To find F_2 in terms of F_1 and H_1 Eq. 4.42 is used to eliminate H_2. By using the identity, $\sin^2(\theta) + \cos^2(\theta) = 1$ one can find the expression for the $\cos(H_2)$:

$$\cos(H_2) = (1 - \sin^2(F_1)\cos^2(F_2))^{\frac{1}{2}}.$$

Inserting this into Eqs. 4.41 and 4.43 the following two equations are obtained.

$$\cos(F_1)\cos(F_2) = \cos(H_1)(1 - \sin^2(F_1)\cos^2(F_2))^{\frac{1}{2}},$$

and

$$\sin(F_2) = \sin(H_1)(1 - \sin^2(F_1)\cos^2(F_2))^{\frac{1}{2}}.$$

Taking the ratio of these two equations gives

$$\tan(F_2) = \tan(H_1)\cos(F_1), \tag{4.44}$$

and so finally

$$F_2 = \tan^{-1}(\tan(H_1)\cos(F_1)). \tag{4.45}$$

Using again the relation, $\sin^2(\theta) + \cos^2(\theta) = 1$, one can also derive the equations for the sine and cosine of F_2 in terms of F_1 and H_1:

$$\sin(F_2) = \frac{\tan(H_1)}{(1 + \tan^2(F_1) + \tan^2(H_1))^{\frac{1}{2}}}, \tag{4.46}$$

and

$$\cos(F_2) = \frac{\sec(F_1)}{(1 + \tan^2(F_1) + \tan^2(H_1))^{\frac{1}{2}}}. \tag{4.47}$$

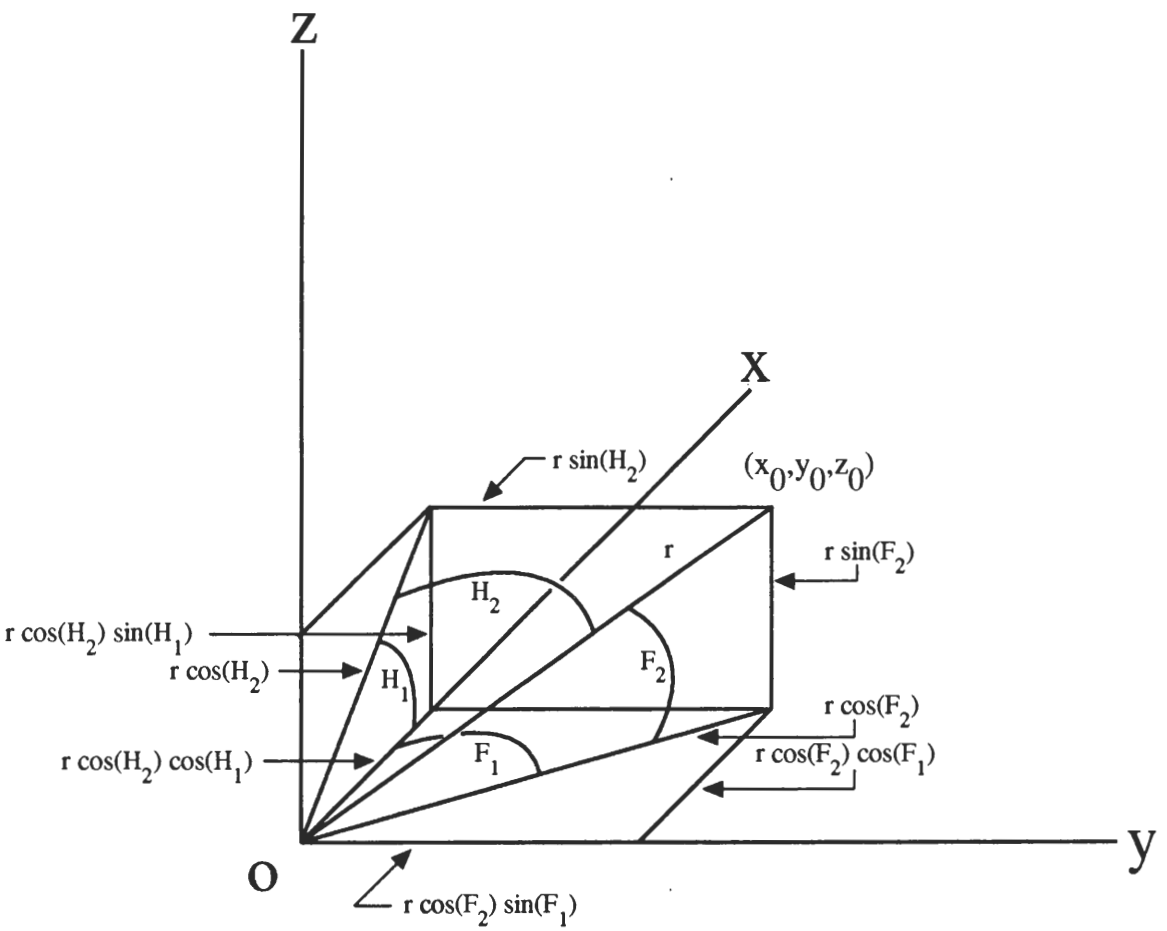

Figure 4.7: Converting between Fick and Helmholtz coordinates

4.3.3 Derivation of the Single-Axis Rotation Matrices

This subsection contains two separate derivations of the full rotation matrix for the head. The two approaches will be shown to produce identical rotation matrices thus building confidence that the final matrix is the correct one. The final matrix will depend on three angles, these angles are similar to those used in the Fick procedure for specifying eye position (orientation). These angles are different from the Fick angles in the sense that they are specified relative to a coordinate system that is fixed in space rather than in the subject's head.

The two derivations of the full rotation matrix given below represent different approaches to the same problem. The first derivation employs the rotation formula. One imagines rotating a position vector about some arbitrary axis through some arbitrary angle. Such an process, called an active rotation, would produce a new position vector in the **same** coordinate system. The rotation formula relates the coordinates of the new vector to the coordinates of the original vector and to the given parameters of the rotation. This formula is applied for each of the three Fick rotations and each application of the formula produces a matrix for each rotation, the full head-rotation matrix is obtained by multiplying the matrices for the individual rotations together in the order specified by the Fick procedure. An advantage of this approach is that the head-rotation matrix is found directly and the matrix for each individual rotation represents an actual physical rotation of the head. A disadvantage of this approach is that the axes about which the second and third rotations are performed are not, in general, along the axes of the coordinate system. This causes the final rotation matrix to be quite complex. This complicated matrix may be simplified significantly, but only after some tedious algebra.

The second approach is based on the idea of the passive rotation. In a passive rotation, the coordinate system is rotated while the physical vector remains the same. The major advantage of this method is that all rotations are performed about coordinate axes. This results in matrices that have simpler forms than in the previous derivation. One disadvantage of the method is that the full head-rotation matrix is the inverse of the passive transformation matrix. This is a very minor disadvantage, however, because the inverse of any rotation matrix is simply its transpose.

Both derivations are based on following idea. **Whatever rotations**

must be performed on the head-coils to take them from their orientation in the standard configuration to their orientation in the arbitrary configuration must also be performed on the vector x_{e0} to rotate it into the vector x_e. The rotations that must be performed in order to rotate the head-coils to an arbitrary orientation have been described just above: it is just the three rotations that comprise the Fick procedure. Hence the same rotations must be performed on the vector $\mathbf{x}_{e0}$. This is the case for both derivations.

As described above, to specify each rotation requires the specification of the unit vector that defines the axis of rotation of the vector $\mathbf{x}_{e0}$, the angle through which $\mathbf{x}_{e0}$ is rotated, and the sense of the rotation. **The sense of all rotations described below will be left-handed.**

Derivation of the Rotation Matrix Based on the Active Transformation

In this derivation, once the above information is given for all three rotations, the determination of the corresponding rotation matrix is based on the **rotation formula**. This formula, known since the eighteenth century, is derived in Appendix C and gives the actual elements of the matrix that rotates a vector in the left-handed sense through an angle θ about an axis defined by the unit vector $\hat{n}$. These three rotations will now be described.

The first rotation is performed about the TCS z-axis through the angle F_1 (the horizontal head-angle). The second rotation is performed about the axis defined by the unit vector perpendicular to the smaller head-coil through the angle F_2. Finally, the third rotation is performed about the "line-of-sight" of the head through the angle F_3.

The unit vectors associated with these rotations must all be expressed in the TCS. They are, for **rotation 1**:

$$\hat{\mathbf{n}}_1 = \mathbf{k}, \tag{4.48}$$

along the TCS z-axis and the angle of rotation is F_1. For **rotation 2**:

$$\hat{\mathbf{n}}_2 = \sin(F_1)\mathbf{i} - \cos(F_1)\mathbf{j}, \tag{4.49}$$

along the unit vector perpendicular to the smaller head-coil after the first rotation. The angle of rotation here is F_2. For **rotation 3**:

$$\hat{\mathbf{n}}_3 = \cos(F_1)\cos(F_2)\mathbf{i} + \sin(F_1)\cos(F_2)\mathbf{j} + \sin(F_2)\mathbf{k}, \tag{4.50}$$

along the "line-of-sight" of the head in its final orientation or equivalently, along the unit vector perpendicular to the large head-coil when the head is in its final orientation. The rotation angle for rotation 3 is F_3.

A 3×3 rotation matrix is associated with each of these rotations. The first rotation transforms the components of the vector $\mathbf{x_{e0}}$ into the components of the new vector ($\mathbf{x'_{e0}}$) formed by rotating $\mathbf{x_{e0}}$. This is done by multiplying the rotation matrix corresponding to the rotation by a three-component column vector whose elements are the components of $\mathbf{x_{e0}}$. This is expressed in equation form as follows

$$\mathbf{x'_{e0}} = R_1(F_1)\mathbf{x_{e0}}.$$

where $R_1(F_1)$ is the matrix representing rotation 1. The new vector $\mathbf{x'_{e0}}$ is itself rotated in rotation 2 and this is performed mathematically in the same way to get a still newer vector $\mathbf{x''_{e0}}$. In equation form

$$\mathbf{x''_{e0}} = R_2(F_1, F_2)\mathbf{x'_{e0}} = R_2(F_1, F_2)R_1(F_1)\mathbf{x_{e0}}.$$

Finally, the third rotation is performed on this newer vector and the result is the vector $\mathbf{x_e}$, the vector from head-sparker to eye when the head is in the final, arbitrary orientation

$$\mathbf{x_e} = R_3(F_1, F_2, F_3)\mathbf{x''_{e0}} = R_3(F_1, F_2, F_3)R_2(F_1, F_2)R_1(F_1)\mathbf{x_{e0}}.$$

As a point of notation, the Fick angles in above parentheses indicate the functional dependence of the various rotation matrices. Thus one can condense the above equations into the following two equations

$$\mathbf{x_e} = R(F_1, F_2, F_3)\mathbf{x_{e0}}, \tag{4.51}$$

where $R(F_1, F_2, F_3)$ is the total rotation matrix and is given by

$$R(F_1, F_2, F_3) = R_3(F_1, F_2, F_3)R_2(F_1, F_2)R_1(F_1). \tag{4.52}$$

Expressions for the individual rotation matrices will be derived below.

As developed in Appendix C, the rotation formula gives the components of a vector that has been rotated in the left-handed sense through an angle ϕ about an axis defined by the unit vector $\hat{\mathbf{n}}$. This formula is as follows

$$\mathbf{r'} = \mathbf{r}\cos(\phi) + \hat{\mathbf{n}}(\hat{\mathbf{n}}\cdot\mathbf{r})(1-\cos(\phi)) + (\mathbf{r}\times\hat{\mathbf{n}})\sin(\phi), \tag{4.53}$$

where $\mathbf{r}'$ and $\mathbf{r}$ are the rotated and original vectors respectively. The elements of the rotation matrix defined by this transformation are obtained by comparing the above equation written out in terms of components with the following equations that correspond to a rotation

$$x' = R_{11}x + R_{12}y + R_{13}z, \tag{4.54}$$

$$y' = R_{21}x + R_{22}y + R_{23}z, \tag{4.55}$$

$$z' = R_{31}x + R_{32}y + R_{33}z. \tag{4.56}$$

These equations are summarized in matrix form as follows

$$\begin{pmatrix} x' \\ y' \\ z' \end{pmatrix} = \begin{pmatrix} R_{11} & R_{12} & R_{13} \\ R_{21} & R_{22} & R_{23} \\ R_{31} & R_{32} & R_{33} \end{pmatrix} \begin{pmatrix} x \\ y \\ z \end{pmatrix}, \tag{4.57}$$

that is, the coefficients of the transformation equations form the elements of the rotation matrix.

One can write Eq. 4.53 out in terms of components by letting

$$\mathbf{r} = x\mathbf{i} + y\mathbf{j} + z\mathbf{k},$$

$$\mathbf{r}' = x'\mathbf{i} + y'\mathbf{j} + z'\mathbf{k},$$

and

$$\hat{\mathbf{n}} = n_x\mathbf{i} + n_y\mathbf{j} + n_z\mathbf{k},$$

inserting these into the equation and equating coefficients of the unit vectors $\mathbf{i}$, $\mathbf{j}$, $\mathbf{k}$. The rotation formula equations, after putting $\sin\phi = s_\phi$ and $\cos\phi = c_\phi$, then become

$$x' = (c_\phi + n_x^2(1 - c_\phi))x + (n_x n_y(1 - c_\phi) - n_z s_\phi)y + (n_x n_z(1 - c_\phi) + n_y s_\phi)z,$$

$$y' = (n_y n_x(1 - c_\phi) + n_z s_\phi)x + (c_\phi + n_y^2(1 - c_\phi))y + (n_y n_z(1 - c_\phi) - n_x s_\phi)z,$$

$$z' = (n_z n_x(1 - c_\phi) - n_y s_\phi)x + (n_z n_y(1 - c_\phi) + n_x s_\phi)y + (c_\phi + n_z^2(1 - c_\phi))z.$$

The particular values of the rotation matrix elements are found by specifying the expressions for the parameters n_x, n_y, n_z, and ϕ and are given below for each rotation.

The Matrix for Rotation 1 For rotation 1 the values of the needed parameters are

$$n_x = n_y = 0, n_z = 1, \phi = F_1.$$

inserting these into the above equations and reading the coefficients gives the following matrix for rotation 1

$$R_1(F_1) = \begin{pmatrix} \cos(F_1) & -\sin(F_1) & 0 \\ \sin(F_1) & \cos(F_1) & 0 \\ 0 & 0 & 1 \end{pmatrix}. \tag{4.58}$$

The Matrix for Rotation 2 In this rotation the parameters are

$$n_x = \sin(F_1),$$

$$n_y = -\cos(F_1),$$

$$n_z = 0,$$

and

$$\phi = F_2.$$

Hence the matrix for this rotation is

$$R_2(F_1, F_2) = \begin{pmatrix} s_1^2 + {c_1}^2 c_2 & -s_1 c_2(1 - c_2) & -c_1 s_2 \\ -s_1 c_1(1 - c_2) & c_1^2 + s_1^2 c_2 & -s_1 s_2 \\ c_1 s_2 & s_1 s_2 & c_2 \end{pmatrix}, \tag{4.59}$$

where, for brevity, the notation $s_i = \sin(F_i)$ and $c_i = \cos(F_i)$ has been introduced and where $i = 1, 2, 3$.

The Matrix for Rotation 3 The matrix for the last rotation is the most complicated, the parameters for this matrix are

$$n_x = -\cos F_1 \cos F_2,$$

$$n_y = -\sin F_1 \cos F_2,$$

$$n_z = -\sin F_2,$$

and

$$\phi = F_3.$$

And the elements of the matrix for this rotation are

$$r_{11} = \cos F_3 + (\cos F_1 \cos F_2)^2(1 - \cos F_3), \tag{4.60}$$

$$r_{12} = \sin F_1 \cos F_1 \cos^2 F_2(1 - \cos F_3) + \sin F_2 \sin F_3, \tag{4.61}$$

$$r_{13} = \cos F_1 \cos F_2 \sin F_2(1 - \cos F_3) - \sin F_1 \cos F_2 \sin F_3, \tag{4.62}$$

$$r_{21} = \sin F_1 \cos F_1 \cos^2 F_2(1 - \cos F_3) - \sin F_2 \sin F_3, \tag{4.63}$$

$$r_{22} = \cos F_3 + (\sin F_1 \cos F_2)^2(1 - \cos F_3), \tag{4.64}$$

$$r_{23} = \sin F_1 \cos F_2 \sin F_2(1 - \cos F_3) + \cos F_1 \cos F_2 \sin F_3, \tag{4.65}$$

$$r_{31} = \cos F_1 \cos F_2 \sin F_2(1 - \cos F_3) + \sin F_1 \cos F_2 \sin F_3, \tag{4.66}$$

$$r_{32} = \sin F_1 \sin F_2 \cos F_2(1 - \cos F_3) - \cos F_1 \cos F_2 \sin F_3, \tag{4.67}$$

$$r_{33} = \cos F_3 + (\sin F_2)^2(1 - \cos F_3). \tag{4.68}$$

The third matrix is then formed as follows

$$R_3(F_1, F_2, F_3) = \begin{pmatrix} r_{11} & r_{12} & r_{13} \\ r_{21} & r_{22} & r_{23} \\ r_{31} & r_{32} & r_{33} \end{pmatrix}. \tag{4.69}$$

The Final Matrix The full head-rotation matrix is obtained by multiplying the above three matrices together as given by Eq. 4.52. As is evident from the forms of these matrices, their product will be a bewilderingly complicated matrix. Through the use of various trigonometric identities, the final product matrix can be significantly simplified. The steps of this simplification will not be given here. The form of the full head-rotation matrix is given below.

$$R(F_1, F_2, F_3) = \begin{pmatrix} c_1c_2 & -s_1c_3 + c_1s_2s_3 & -s_1s_3 - c_1s_2c_3 \\ s_1c_2 & c_1c_3 + s_1s_2s_3 & c_1s_3 - s_1s_2c_3 \\ s_2 & -c_2s_3 & c_2c_3 \end{pmatrix} \tag{4.70}$$

where, again, $s_i = \sin F_i$ and $c_i = \cos F_i$ and $i = 1, 2, 3$.

Derivation of the Rotation Matrix Based on the Passive Transformation

In an active rotation, a new vector is obtained by physical rotation of the vector in a fixed coordinate system. The components of the new vector are expressed in terms of the components of the old vector and the parameters of the rotation. The mathematical equations for each type of rotation can be summarized by a rotation matrix. For experiments performed with the RFM, it is clear that the active-rotation matrix is required because the eye-to-head-sparker vector undergoes a rotation whenever the subject moves his head. It is necessary to find the new components of this vector in the TCS. **In a passive rotation of a vector, the components of a fixed vector are changed by rotation of the coordinate system.** The mathematical equations that represent this rotation express the components of the vector relative to the new coordinate system in terms of the components of the vector relative to the old coordinate system and in terms of the parameters of the rotation.

Fig. 4.8 illustrates the difference between these two types of transformations for a two dimensional vector. The active-rotation matrix is equal to the inverse of the passive-rotation matrix. This fact forms the basis for the second derivation given below: one first finds the passive-rotation matrix for the head and then finds the inverse of this matrix to obtain the active rotation-matrix. The inverse is easily found because, for all rotation matrices, the inverse is equal to its transpose.

The coordinate system being rotated here is the TCS. One imagines the three mutually perpendicular coordinate axes of the TCS to be a set of rigid rods. After rotation, this set of rods forms the coordinate axes of a new coordinate system, hence a new coordinate system is created by the rotation. Each succeeding rotation is performed relative to the coordinate system created by the previous rotation. Thus all rotations are performed about axes parallel to a coordinate axis in the newly created coordinate systems.

The rotations comprising the Fick procedure are as follows: (1) A rotation of the TCS coordinate axes about the positive TCS z-axis through the angle F_1. The new coordinate system created will be called the "primed" coordinate system. The next rotation is (2) a rotation about the negative y-axis of the primed coordinate system (creating the "double primed" system)

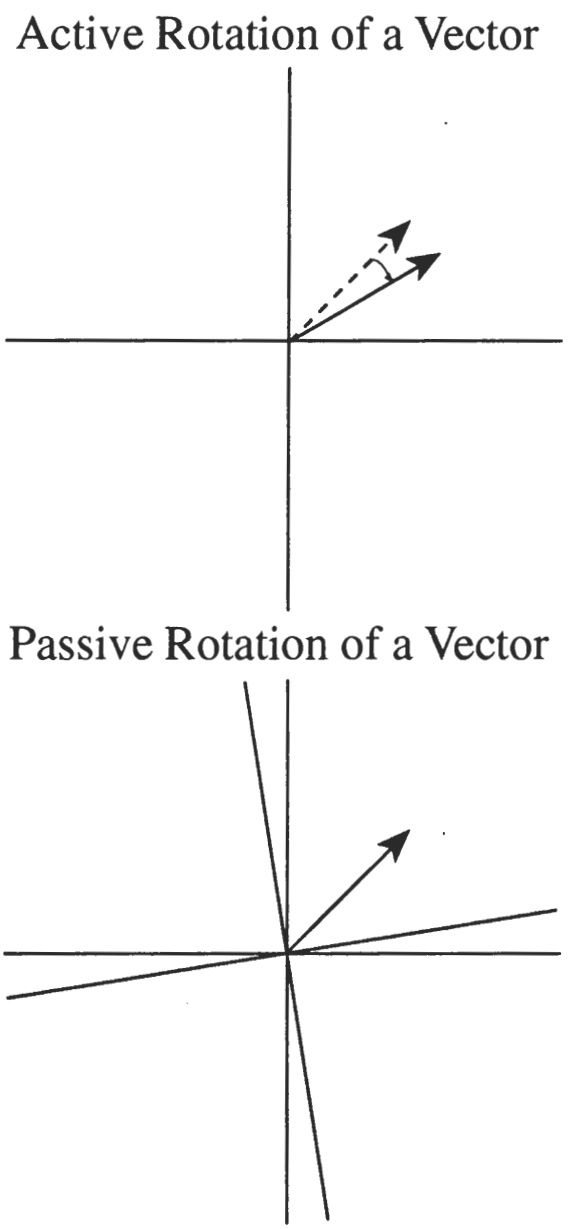

Figure 4.8: Active and passive rotations

through the angle F_2. Finally (3) a rotation is performed about the negative x-axis of the "double primed" coordinate sytem through the angle F_3. This rotation creates the final coordinate system which will be called the "triple primed" system. Figure 4.9 illustrates these rotations.

This process is represented mathematically by associating a matrix with each of the three rotations. Let $\mathbf{x}$ be an arbitrary vector whose coordinates (x, y, z) are given relative to the TCS. Then, if rotation (1) (described above) is performed on the TCS, denote by $(\mathbf{x})'$ the **same vector** except that its coordinates (x', y', z') are given relative to the "primed" system. Further let $(\mathbf{x})''$ be again the same vector except that its coordinates are given relative to the "double primed" system. Finally, let $(\mathbf{x})'''$ be the same vector whose components are given relative to the "triple primed" system.

The components of $(\mathbf{x})'$ are related to those of $(\mathbf{x})$ via the matrix $(T_1(F_1))$ that represents rotation (1):

$$(\mathbf{x})' = T_1(F_1)(\mathbf{x}). \tag{4.71}$$

The components of $(\mathbf{x})''$ are related to those of $(\mathbf{x})'$ via the matrix representing rotation (2):

$$(\mathbf{x})'' = T_2(F_2)(\mathbf{x})'. \tag{4.72}$$

And finally the components of $(\mathbf{x})'''$ are related to those of $(\mathbf{x})''$ via the matrix representing rotation (3):

$$(\mathbf{x})''' = T_3(F_3)(\mathbf{x})''. \tag{4.73}$$

Gathering these three equations together one can relate the components of $(\mathbf{x})'''$ to those of $(\mathbf{x})$ as follows

$$(\mathbf{x})''' = [T_3(F_3)T_2(F_2)T_1(F_1)]\,(\mathbf{x}). \tag{4.74}$$

The expression in square brackets is a product of three (3×3) matrices and is itself a (3×3) rotation matrix. The inverse of this matrix is the full head-rotation matrix already derived by the active rotation method and expressed in Eq. 4.70

$$R(F_1, F_2, F_3) = [T_3(F_3)T_2(F_2)T_1(F_1)]^{-1},$$

and since the inverse of any rotation matrix is simply its transpose, the following relation holds

$$R(F_1, F_2, F_3) = [T_3(F_3)T_2(F_2)T_1(F_1)]^{T}. \tag{4.75}$$

The individual passive rotation matrices are derived below.

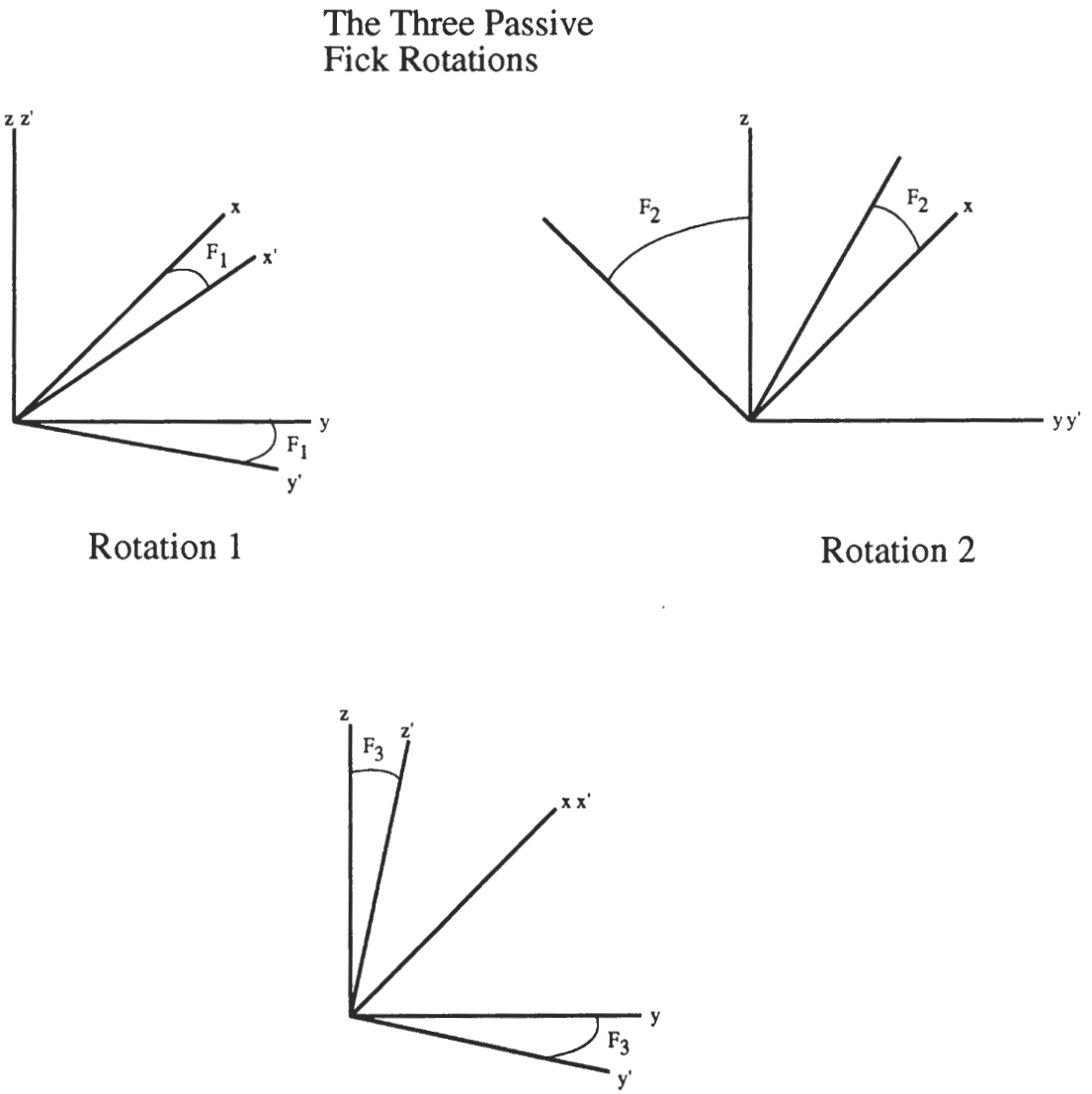

Figure 4.9: The three passive Fick rotations

Determining the Passive Rotation Matrices T_1, T_2, and T_3 The problem of determining the elements of the three passive rotation matrices defined above is equivalent to the problem of finding the relationship between the components of the same vector as expressed in two different coordinate systems. How this relationship is obtained will be illustrated for the case of the passive rotation matrix T_1.

Let $(\mathbf{x})$ be an arbitrary vector whose components are given in the TCS. Let these components be denoted by (x, y, z). Also, let $\mathbf{i}, \mathbf{j}$, and $\mathbf{k}$ be unit vectors along the TCS x-, y-, and z-axes respectively. Then $(\mathbf{x})$ may be written as

$$(\mathbf{x}) = x\mathbf{i} + y\mathbf{j} + z\mathbf{k}. \tag{4.76}$$

If $(\mathbf{x})'$ is the same vector in the "primed" system with components (x', y', z'), and if $\mathbf{i}', \mathbf{j}'$, and $\mathbf{k}'$ are the unit vectors along the x-primed-, y-primed-, and z-primed-axes respectively, then

$$(\mathbf{x})' = x'\mathbf{i}' + y'\mathbf{j}' + z'\mathbf{k}'. \tag{4.77}$$

But $(\mathbf{x})'$ and $(\mathbf{x})$ are the **same vector**, hence

$$x\mathbf{i} + y\mathbf{j} + z\mathbf{k} = x'\mathbf{i}' + y'\mathbf{j}' + z'\mathbf{k}'. \tag{4.78}$$

Taking the dot product of both sides of the above equation with the unit vector $\mathbf{i}'$, and noting that the unit vectors $\mathbf{i}', \mathbf{j}'$, and $\mathbf{k}'$ are mutually perpendicular so that $\mathbf{i} \cdot \mathbf{i} = 1$, $\mathbf{j} \cdot \mathbf{j} = 0$, and $\mathbf{k} \cdot \mathbf{k} = 0$, one obtains

$$x' = x(\mathbf{i} \cdot \mathbf{i}') + y(\mathbf{j} \cdot \mathbf{i}') + z(\mathbf{k} \cdot \mathbf{i}'). \tag{4.79}$$

Taking the dot product of both sides of Eq. 4.78 with $\mathbf{j}'$ and $\mathbf{k}'$ gives the following equations

$$y' = x(\mathbf{i} \cdot \mathbf{j}') + y(\mathbf{j} \cdot \mathbf{j}') + z(\mathbf{k} \cdot \mathbf{j}'), \tag{4.80}$$

and

$$z' = x(\mathbf{i} \cdot \mathbf{k}') + y(\mathbf{j} \cdot \mathbf{k}') + z(\mathbf{k} \cdot \mathbf{k}'). \tag{4.81}$$

The above three equations relate the components of the vector in the TCS to the components of the same vector in the primed system. The quantities in parenthesis (e.g. $(\mathbf{i} \cdot \mathbf{j}')$) are the dot products of the unit vectors in the TCS with those in the primed system. Since all of these vectors have unit

length, it follows directly from the definition of the dot product that the parenthetical quantities represent the cosines of the angles between all pairs of coordinate axes with one axis of the pair coming from the TCS and the other from the primed system. For example, the quantity $(\mathbf{i} \cdot \mathbf{j}')$ is the cosine of the angle between the x-axis of the TCS and the y-axis of the primed system. Such quantities are called **direction cosines**.

Using Eqs. 4.79, 4.80, and 4.81, it is simple to write down the form for the passive rotation matrix T_1 as follows

$$T_1 = \begin{pmatrix} \mathbf{i} \cdot \mathbf{i}' & \mathbf{j} \cdot \mathbf{i}' & \mathbf{k} \cdot \mathbf{i}' \\ \mathbf{i} \cdot \mathbf{j}' & \mathbf{j} \cdot \mathbf{j}' & \mathbf{k} \cdot \mathbf{j}' \\ \mathbf{i} \cdot \mathbf{k}' & \mathbf{j} \cdot \mathbf{k}' & \mathbf{k} \cdot \mathbf{k}' \end{pmatrix}. \tag{4.82}$$

To find the actual values of the elements of this matrix for passive rotation (1) of the Fick procedure (see fig. 4.9) consider first the x-primed-axis in relation to the x-, y-, and z-axes of the TCS. The angle between the x-primed-axis and the TCS x-axis is F_1, the angle between the x-primed-axis and the TCS y-axis is $90° - F_1$, and the angle between the x-primed-axis and the TCS z-axis is 90°. These cosines form the top row of the above matrix and recalling that $\cos(90° - \theta) = \sin(\theta)$, and that $\cos(90°) = 0$, the elements in the top row are: $\cos(F_1)$, $\sin(F_1)$, and 0.

Now consider the y-primed-axis. This axis forms angles of $90° + F_1$, F_1, and 90° with the TCS x-, y-, and z-axes respectively. Thus the elements of the second row are $-\sin(F_1)$, $\cos(F_1)$, and 0.

For the z-primed-axis, the angles are 90°, 90°, and 0° for the TCS x-, y-, and z-axes respectively. And the third row of elements are 0, 0, and 1. The final form of the above matrix is therefore

$$T_1(F_1) = \begin{pmatrix} \cos(F_1) & \sin(F_1) & 0 \\ -\sin(F_1) & \cos(F_1) & 0 \\ 0 & 0 & 1 \end{pmatrix}. \tag{4.83}$$

In exactly the same way (see fig. 4.9) one can form the other two matrices T_2, and T_3. These matrices are as follows

$$T_2(F_2) = \begin{pmatrix} \cos(F_2) & 0 & \sin(F_2) \\ 0 & 1 & 0 \\ -\sin(F_2) & 0 & \cos(F_2) \end{pmatrix}, \tag{4.84}$$

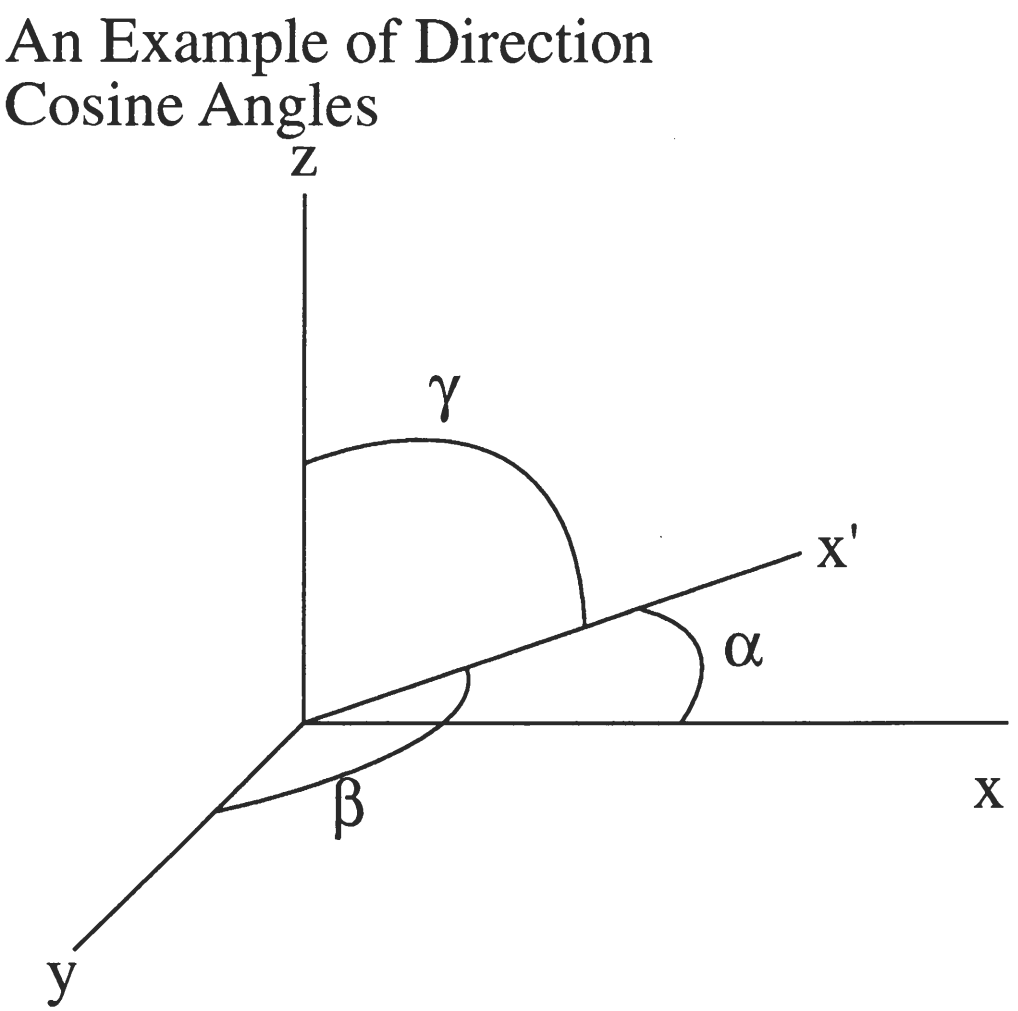

Figure 4.10: The angles the x'-axis makes with x-, y-, and z-axes

and

$$T_3(F_3) = \begin{pmatrix} 1 & 0 & 0 \\ 0 & \cos(F_3) & -\sin(F_3) \\ 0 & \sin(F_3) & \cos(F_3) \end{pmatrix}. \tag{4.85}$$

By inserting the above three matrices into Eq. 4.75, one obtains the following final head-rotation matrix

$$R(F_1, F_2, F_3) = \begin{pmatrix} c_1c_2 & -s_1c_3 + c_1s_2s_3 & -s_1s_3 - c_1s_2c_3 \\ s_1c_2 & c_1c_3 + s_1s_2s_3 & c_1s_3 - s_1s_2c_3 \\ s_2 & -c_2s_3 & c_2c_3 \end{pmatrix} \tag{4.86}$$

where $s_i = \sin(F_i)$ and $c_i = \cos(F_i)$ and $i = 1, 2, 3$. Note that this matrix is identical to that derived by the active rotation method in Eq. 4.70.

The above matrix has the following physical interpretation: It is the matrix that represents the performance of the Fick rotation procedure on the vector from the head-sparker to the sighting-center. **This matrix will never change under any circumstances**. Even if a piece of equipment such as the head-coil apparatus is replaced, this matrix will not be affected. The reason for this is that not all of the Fick angles are directly measured by the RMFM. One must find the connection between the Fick angles contained in Eq. 4.86 and the angles actually measured by the RMFM. If the head-coil apparatus is changed, these connections will change but not the matrix. This approach will minimize changes in computer programs that are based on this matrix. The rest of this section is devoted to the derivation of this connection.

Derivation of the Equations Connecting (F_1, F_2, F_3) and $(\theta_h, \theta_v, \theta_t)$

The derivation of the link between the Fick angles and the angles measured by the RMFM will be based directly on the definitions of the measured angles given in Chapter 2 and on the matrix given in Eq. 4.86. The basic procedure will be to mathematically define the form of the unit vectors normal to the head-coils in the standard head-configuration and then to perform the Fick rotation procedure on these unit vectors and finally to apply the definitions of the horizontal, vertical, and torsional angles to the rotated unit vectors.

One extra complication is introduced because the smaller head-coil is not precisely perpendicular to the large head-coil. The angle of departure from perpendicularity will be introduced as a parameter in the derivation of the

connection between the Fick angles and the measured angles. The method by which this angle was determined will be described in a subsequent paragraph.

The Head-Coil Unit Vectors in the Standard Head-Configuration Figure 4.3 shows a picture of the unit vectors normal to the large and smaller head-coils when the head-coil apparatus has the standard orientation. One can see from the figure that the unit vector normal to the large head-coil is exactly parallel to the TCS x-axis and that the other unit vector lies in a plane parallel to the TCS xy-plane but that it is not exactly perpendicular to the large-coil unit vector. The angle of departure from perpendicularity will be denoted by the symbol β. It is simple, therefore, to write down the components of these two unit vectors for this case.

The large-head-coil unit vector in this case (see fig. 4.3) is

$$\mathbf{n_L} = \begin{pmatrix} 1 \\ 0 \\ 0 \end{pmatrix}, \tag{4.87}$$

and the smaller-head-coil unit vector has the form

$$\mathbf{n_S} = \begin{pmatrix} \sin(\beta) \\ -\cos(\beta) \\ 0 \end{pmatrix}. \tag{4.88}$$

If an arbitrary rotation of the head-coil apparatus is performed, whose Fick angles are (F_1, F_2, F_3), then these two unit vectors can be obtained by applying the Fick rotation matrix given in Eq. 4.86:

$$\mathbf{n'_L} = R(F_1, F_2, F_3)\mathbf{n_L}, \tag{4.89}$$

and

$$\mathbf{n'_S} = R(F_1, F_2, F_3)\mathbf{n_S}. \tag{4.90}$$

Performing the matrix multiplication gives the following two column vectors for the unit vectors in the arbitrary configuration

$$\mathbf{n'_L} = \begin{pmatrix} c_1 c_2 \\ s_1 c_2 \\ s_2 \end{pmatrix}, \tag{4.91}$$

and

$$\mathbf{n'_S} = \begin{pmatrix} c_1c_2s_\beta + (s_1c_3 - c_1s_2s_3)c_\beta \\ s_1c_2s_\beta - (c_1c_3 + s_1s_2s_3)c_\beta \\ s_2s_\beta + c_2s_3c_\beta \end{pmatrix}. \tag{4.92}$$

where, for brevity, the following notation has been used: $c_i = \cos(F_i)$, $s_i = \sin(F_i)$, $s_\beta = \sin(\beta)$, and $c_\beta = \cos(\beta)$, and where $i = 1, 2, 3$.

The Link Between (F_1, F_2, F_3) and $(\theta_h, \theta_v, \theta_t)$ The next step will be to use the components of these unit vectors in the arbitrary head-configuration to form the expressions for the sines and cosines of the Fick angles in terms of the measured head-angles according to the definitions of the head-angles given in Chapter 2. This will be done for each of the Fick angles in turn.

The Link Between F_1 and the Measured Head-Angles From fig. 2.6 in Chapter 2, one can see that the horizontal head-angle is the angle between the projection of the unit normal vector to the large head-coil onto the TCS xy-plane and the TCS x-axis. Eq. 4.91, above, gives the components of this unit vector in terms of the three Fick angles. The vector that is the projection of $\mathbf{n'_L}$ onto the TCS xy-plane has the same components as $\mathbf{n'_L}$ except that its z-components is zero and therefore has the following form

$$\mathbf{n'_L} \text{ projected onto the TCS xy-plane} = \mathbf{n'_{LPxy}} = \begin{pmatrix} c_1c_2 \\ s_1c_2 \\ 0 \end{pmatrix}. \tag{4.93}$$

The connection to the horizontal head-angle can be made by noting that a right-triangle is formed by the x- and y-components of this projected vector with the hypotenuse of the triangle being formed by the projected vector itself. The angle between the projected vector and its TCS x-component is just the horizontal head-angle θ_h. Thus the tangent of the horizontal head-angle is the ratio of the y-component of the projected vector to the x-component of the projected vector

$$\tan(\theta_h) = \frac{(\mathbf{n'_{LPxy}})_y}{(\mathbf{n'_{LPxy}})_x} = \frac{s_1c_2}{c_1c_2} = \frac{s_1}{c_1} = \tan(F_1). \tag{4.94}$$

It follows from the above equation that the horizontal head-angle is identical to the first Fick angle (F_1) contained in Eq. 4.86. That is

$$F_1 = \theta_h, \text{ so } s_1 \equiv \sin(F_1) = \sin(\theta_h), \text{ and } c_1 \equiv \cos(F_1) = \cos(\theta_h). \tag{4.95}$$

This connection was already mentioned in the discussion of the Fick and Helmholtz systems in section 4.3.

The Link Between F_2 and the Measured Head-Angles To find the vertical head-angle, the unit vector $\mathbf{n}'_{\mathbf{L}}$ is projected onto the TCS xz-plane. This is done by setting the y-component equal to zero

$$\mathbf{n}'_{\mathbf{L}} \text{ projected onto the TCS xz-plane} = \mathbf{n}'_{\mathbf{LPxz}} = \begin{pmatrix} c_1 c_2 \\ 0 \\ s_2 \end{pmatrix}. \tag{4.96}$$

And a right-triangle similar to that for the horizontal head-angle can be constructed (see fig. 2.5) such that the tangent of θ_v is equal to the ratio of the TCS z-component to the TCS x-component of the vector $\mathbf{n}'_{\mathbf{LPxz}}$. Mathematically this is expressed as follows

$$\tan(\theta_v) = \frac{(\mathbf{n}'_{\mathbf{LPxz}})_z}{(\mathbf{n}'_{\mathbf{LPxz}})_x} = \frac{s_2}{c_1 c_2} = \frac{\tan(F_2)}{\cos(F_1)}. \tag{4.97}$$

This equation can be used to solve for the sine and cosine of F_2 in terms of θ_h and θ_v. This is needed for the Fick rotation matrix given in Eq. 4.86.

Noting that $F_1 = \theta_h$ the above equation may be rewritten as

$$\tan(F_2) = \cos(\theta_h)\tan(\theta_v). \tag{4.98}$$

and using the definition of the tangent in terms of sine and cosine the above becomes

$$\sin(F_2) = (\cos(\theta_h)\tan(\theta_v))\cos(F_2). \tag{4.99}$$

Now using $\sin^2(F_2) + \cos^2(F_2) = 1$ and Eq. 4.99 one can solve for the sine and cosine of F_2 in terms of θ_h and θ_v only. The results are

$$s_2 \equiv \sin(F_2) = \frac{\cos(\theta_h)\tan(\theta_v)}{(1 + \cos^2(\theta_h)\tan^2(\theta_v))^{\frac{1}{2}}}, \tag{4.100}$$

and

$$c_2 \equiv \cos(F_2) = \frac{1}{(1 + \cos^2(\theta_h)\tan^2(\theta_v))^{\frac{1}{2}}}. \tag{4.101}$$

These equations are part of the critical link between measured data and the matrix in Eq. 4.86. Note that F_2 depends on both θ_h and θ_v.

The Link Between F_3 and the Measured Head-Angles The torsional angle is the angle between the unit vector $\mathbf{n'_S}$ projected onto the TCS yz-plane and the negative TCS y-axis. The vector formed by projecting $\mathbf{n'_S}$ onto the TCS yz-plane is obtained by setting its x-component equal to zero

$$\mathbf{n'_S} \text{ projected onto the TCS yz-plane} = \mathbf{n'_{SPyz}} = \begin{pmatrix} 0 \\ s_1c_2s_\beta - (c_1c_3 + s_1s_2s_3)c_\beta \\ s_2s_\beta + c_2s_3c_\beta \end{pmatrix}. \tag{4.102}$$

As above, a right-triangle can be constructed such that one of the angles is the torsional head-angle. The tangent of this angle is the negative of the ratio of the z-component of $\mathbf{n'_{SPyz}}$ to the y-component of $\mathbf{n'_{SPyz}}$

$$\tan(\theta_t) \equiv t_t = -\frac{(\mathbf{n'_{SPyz}})_z}{(\mathbf{n'_{SPyz}})_y} = -\frac{s_2s_\beta + c_2s_3c_\beta}{s_1c_2s_\beta - (c_1c_3 + s_1s_2s_3)c_\beta}. \tag{4.103}$$

The equation can be rewritten as

$$t_t = -\frac{s_2t_\beta(t_3^2+1) + c_2t_3}{s_1c_2t_\beta(t_3^2+1) - (c_1 + s_1s_2t_3)}, \tag{4.104}$$

where $t_\beta = \tan(\beta)$.

The procedure for finding the sine and cosine of F_3 in terms of measured angles is similar to that for the vertical angle. Eq. 4.104 contains factors such as s_1, c_1, s_2, and c_2, all of which have already been found in terms of measured angles so these factors can be taken as known. Also, the of the angle β are known (its determination will be described below) and since θ_t is measured, $\tan(\theta_t)$ is also known. Thus Eq. 4.104 yields a quadratic equation for $t_3 = \tan(F_3)$ that can be solved entirely in terms of measured angles. The result is

$$t_3 = \frac{-ab - c[a^2 + b^2 - c^2]^{\frac{1}{2}}}{a^2 - c^2}, \tag{4.105}$$

where the second minus sign in the numerator indicates that the negative root of the quadratic equation has been used. This is due to the fact that when the torsion angle is zero, the third Fick angle (F_3) must be **negative**. The factors a, b, and c are given by

$$a = s_1s_2t_t - c_2, \tag{4.106}$$

$$b = c_1 t_t, \tag{4.107}$$

$$c = (s_2 + s_1 c_2 t_t)^{\frac{1}{2}} t_\beta. \tag{4.108}$$

Then Eq. 4.105 can be used along with the identity $\sin^2(F_3) + \cos^2(F_3) = 1$ to find s_3 and c_3 in terms of measured angles. The results are

$$s_3 = \frac{t_3}{(1 + t_3^2)^{\frac{1}{2}}}, \tag{4.109}$$

and

$$c_3 = \frac{1}{(1 + t_3^2)^{\frac{1}{2}}}. \tag{4.110}$$

These equations give s_3 and c_3 entirely in terms of measured angles because t_3 is expressed this way via Eqs. 4.105 - 4.108.

Determination of the Non-Orthogonality Angle β The angle β was determined by making simultaneous measurements of the horizontal and vertical angles of the large head-coil and the torsional and **horizontal** angles of the smaller head-coil. Since the measurement of the first three of these angles serves to uniquely determine the orientation of the head-coil apparatus, the measurement of the horizontal angle of the smaller head-coil constitutes an independent measurement of the non-orthogonality angle β.

The horizontal angle for the smaller head-coil is defined in exactly the same way as for the large head-coil. The expression for the tangent of this measured angle in terms of the Fick angles and the non-orthogonality angle is

$$\tan(\theta_{th}) \equiv t_{th} = \frac{s_1 c_2 t_\beta - (c_1 c_3 + s_1 s_2 s_3)}{c_1 c_2 t_\beta + (s_1 c_3 - c_1 s_2 s_3)}. \tag{4.111}$$

From the measurements of θ_h and θ_v, the quantities s_1, c_1, s_2, and c_2 can be determined. Using these and the measurements of θ_t and θ_{th} in Eqs. 4.104 and 4.111 along with the identity $\sin^2(F_3) + \cos^2(F_3) = 1$ yields a system of three equations for the three unknowns: s_3, c_3, and t_β. Recall that s_3 and c_3 cannot be determined unless the angle β is known.

The experimental procedure for determining the non-orthogonality angle was as follows. The head-coil apparatus was mounted on a fixed object and the four angles described above were measured by the RMFM in five trials with each trial having a duration of 2 seconds. Some care was observed to

mount the apparatus in an orientation similar to its orientation when worn by a subject and such that θ_h and θ_v were nearly zero (i.e. raw angle readings of 13,500 and 8,100 minarc respectively). A direct measurement, without the need for calculation, would have been possible if the apparatus had been mounted such that θ_h, θ_v, and θ_t were all zero. This would have placed an undue burden on the experimenter to orient the head-coil apparatus so exactly. Also, given the above algorithm for determining the angle β, the apparatus could have been placed in any orientation.

The angle readings were averaged over each trial and standard deviations of the data were computed. The trial whose data was selected for use in the equations for determining the non-orthogonality angle were those in which the standard deviations were the smallest. The final data were as follows (angle units in minarc): $\theta_h = 13548.69 - 13500$, $\theta_v = 8178.77$, $\theta_{th} = 8113.92 - 8100$, and $\theta_t = 7482.92 - 8100$. The final value for the non-orthogonality angle was

$$\beta = 0.80517^\circ = 48.487 \text{ minarc.} \tag{4.112}$$

Thus the two coils in the head-coil apparatus were mounted perpendicularly to within 1degree of arc. This is remarkable since no special care was taken to make them perpendicular at the time the apparatus was constructed.

Chapter 5

Summary of the Data Processing Method

In this chapter the entire algorithm will be summarized in a way suitable for encoding in a computer program. The presentation is organized into three parts (1) Inputs, (2) Outputs, and (3) Processing. The algorithm presented refers to one eye only.

5.1 Inputs

The required inputs are as follows.

1. **TCS coordinates of target** - $\mathbf{r}_{tar} = (r_{tar1}, r_{tar2}, r_{tar3})$ are the TCS coordinates of the target, measured in millimeters.

2. **TCS coordinates of eye while subject is on the biteboard** - $\mathbf{r}_{eb} = (x_{eb}, y_{eb}, z_{eb})$ are the TCS coordinates of the sighting-center of subject while on biteboard, measured in millimeters.

3. **Head-Sparker data from mirror-trial** - $d_{aoi}, d_{boi}, d_{coi}, d_{doi}$, the distances from sparker to microphone in sparker units where $i = 1, ..., N_{sso}$ and N_{sso} is the number of sparker strobes in the mirror trial for the appropriate eye. The a, b, c, d subscripts denote the particular microphone.

4. **Head-Coil data from mirror-trial** - $hdh_{oj}, hdv_{oj}, toz_{oj}$, the horizontal, vertical, and torsional angles measured during the mirror trial for the appropriate eye, measured in minarc. The index j run from 1 to N_{cso}, the number of RFM bursts during the trial.

5. **Eye-Coil data from mirror-trial** - (lsh_{oj}, lsv_{oj}), or (rsh_{oj}, rsv_{oj}) are the horizontal and vertical eye-coil readings for the left or right eye respectively taken from the appropriate mirror trial and measured in minarc.

The subscript j runs over the same range as in 4.

6. **Trial number** - n, number of the trial to be processed.

7. **Head-Sparker data from trial** n - $d_{ani}, d_{bni}, d_{cni}, d_{dni}$, the same data as in 3 but for trial n. The subscript i runs from 1 to N_{ssn}, the number of sparker strobes during trial n.

8. **Head-Coil data from trial** n - $hdh_{nj}, hdv_{nj}, toz_{nj}$, the same data as in 4 but for trial n. The subscript j runs from 1 to N_{cso}, the number of RFM bursts during trial n.

9. **Eye-Coil data from trial** n - (lsh_{nj}, lsv_{nj}), or (rsh_{nj}, rsv_{nj}) are the same data as in 5 but for trial n. The subscript j runs over the same range as in 9.

10. **Instrument characteristic quantities** - distances between microphones

$$mdab = 1762 \text{ mm},$$

$$mdbc = 1760 \text{ mm},$$

$$mdcd = 1763 \text{ mm},$$

$$mdda = 1764 \text{ mm},$$

$$mdbd = 2490 \text{ mm},$$

$$mdac = 2494.392107 \text{ mm},$$

Scale factors for each microphone

$$s_a = 0.097302 \text{ mm/sparker unit},$$

$$s_b = 0.097187 \text{ mm/sparker unit},$$

$$s_c = 0.097731 \text{ mm/sparker unit},$$

$$s_d = 0.096076 \text{ mm/sparker unit}.$$

The SCS to TCS transformation matrix A, given in Appendix A. The elements in the 3×3 submatrix are dimensionless and element in the fourth column are measured in mm. Reference angles: horizontal reference angle

$$href = 13500 \text{ minarc},$$

vertical reference angle

$$vref = 8100 \text{ minarc},$$

and torsional reference angle

$$tref = 8100 \text{ minarc.}$$

And finally, the non-orthogonality angle

$$\beta = 0.80517° = 48.487 \text{ minarc.}$$

5.2 Outputs

The quantities to be computed and output are horizontal and vertical gaze errors and table gaze positions at each RFM burst of trial n. The horizontal and vertical gaze errors are the differences between the horizontal and vertical gaze angles (as determined from eye-coil data) and the horizontal and vertical gaze angles as determined by a straight line from sighting-center to target. The table gaze position is the TCS x- and y-coordinates of the intersection of the subject's line-of-sight with a plane that is parallel to the table xy-plane and contains the target point.

1. **Horizontal gaze errors** - geh_j, the horizontal gaze error with respect to the target at the j^{th} RFM burst of trial n. The subscript j runs from 1 to N_{csn}.

2. **Vertical gaze errors** - gev_j, the vertical gaze error with respect to the target at the j^{th} RFM burst of trial n.

3. **Table gaze position x-coordinate** - gpx_j, the TCS x-coordinate of the table gaze position at the j^{th} RFM burst.

4. **Table gaze position y-coordinate** - gpy_j, the TCS y-coordinate of the table gaze position at the j^{th} RFM burst.

5. **sighting-center** - $\mathbf{r}_{ej} = (x_{ej}, y_{ej}, z_{ej})$, the TCS coordinates of the sighting-center of the subject at the j^{th} RFM burst of trial n.

Other quantities can also be computed once the sighting-center is calculated. The equations for horizontal and vertical gaze errors and for table gaze positions presented later in this chapter are derived in Appendix A.

5.3 Processing

The major steps that must be performed to compute the outputs given the inputs are described below.

5.3.1 Compute mirror-trial averages and initial head-sparker position

Compute average mirror-trial sparker readings

Compute average sparker readings for the mirror-trial as follows for each microphone. For microphone A,

$$d_{aoa} = \frac{1}{N_{sso}} \sum_{i=1}^{N_{sso}} d_{aoi}, \tag{5.1}$$

for microphone B,

$$d_{boa} = \frac{1}{N_{sso}} \sum_{i=1}^{N_{sso}} d_{boi}, \tag{5.2}$$

for microphone C,

$$d_{coa} = \frac{1}{N_{sso}} \sum_{i=1}^{N_{sso}} d_{coi}, \tag{5.3}$$

and for microphone D,

$$d_{doa} = \frac{1}{N_{sso}} \sum_{i=1}^{N_{sso}} d_{doi}. \tag{5.4}$$

All of these quantities are measured in sparker units.

Compute average residual eye-coil angles

Compute mirror-trial averages for the horizontal and vertical eye-angles in the mirror-trial. This must be done for the appropriate eye.

Left-eye horizontal angle average

$$lsh_{oa} = \frac{1}{N_{cso}} \sum_{j=1}^{N_{cso}} lsh_{oj}, \tag{5.5}$$

left-eye vertical angle average

$$lsv_{oa} = \frac{1}{N_{cso}} \sum_{j=1}^{N_{cso}} lsv_{oj}, \tag{5.6}$$

right-eye horizontal average

$$rsh_{oa} = \frac{1}{N_{cso}} \sum_{j=1}^{N_{cso}} rsh_{oj}, \tag{5.7}$$

right-eye vertical average

$$rsv_{oa} = \frac{1}{N_{cso}} \sum_{j=1}^{N_{cso}} rsv_{oj}. \tag{5.8}$$

Compute average initial head-coil angles

Compute the average horizontal, vertical, and torsional head coil readings for the mirror-trial as follows.

Horizontal angle average

$$hdh_{oa} = \frac{1}{N_{cso}} \sum_{j=1}^{N_{cso}} hdh_{oj}, \tag{5.9}$$

vertical angle average

$$hdv_{oa} = \frac{1}{N_{cso}} \sum_{j=1}^{N_{cso}} hdv_{oj}, \tag{5.10}$$

and torsional angle average

$$toz_{oa} = \frac{1}{N_{cso}} \sum_{j=1}^{N_{cso}} toz_{oj}. \tag{5.11}$$

Compute head-sparker position with subject on the biteboard

Compute head-sparker position in the SCS

Convert average sparker readings to millimeter units To perform the conversion, multiply the raw readings by the appropriate scale factor. Microphone C is not used here because it sometimes proved unreliable.

For microphones A, B, and D respectively

$$r_{aoa} = s_a d_{aoa}, \tag{5.12}$$

$$r_{boa} = s_b d_{boa}, \tag{5.13}$$

$$r_{doa} = s_d d_{doa}. \tag{5.14}$$

Get the SCS coordinates Since *mdbd* has now been measured, the assumption that the frame on which the microphones are mounted is exactly rectangular need not be made. Thus compute the SCS coordinates of the head-sparker using the following equations.

First compute, once and for all, the coordinates of microphone B in the STS xy-plane.

$$x_B = \frac{(mdda)^2 + (mdab)^2 - (mdbd)^2}{2 \cdot mdda} \tag{5.15}$$

and

$$y_B = ((mdab)^2 - x_B^2)^{\frac{1}{2}}. \tag{5.16}$$

Using these equations and setting $x_D = mdda$, the STS coordinates of the sparker are found as follows:

SCS x-coordinate:

$$x_{so} = \frac{x_D^2 + r_{aoa}^2 - r_{doa}^2}{2 \cdot x_D}, \tag{5.17}$$

SCS y-coordinate:

$$y_{so} = \frac{x_B^2 + y_B^2 - (\frac{x_B}{x_D})(x_D^2 + r_{aoa}^2 - r_{doa}^2) + r_{aoa}^2 - r_{boa}^2}{2 \cdot y_B}, \tag{5.18}$$

SCS z-coordinate:

$$z_{so} = (r_{aoa}^2 - x_{so}^2 - y_{so}^2)^{\frac{1}{2}}. \tag{5.19}$$

Get the TCS coordinates Compute the TCS coordinates of the head-sparker on biteboard from the SCS coordinates by first forming the four component column vector

$$r_{so} = \begin{pmatrix} x_{so} \\ y_{so} \\ z_{so} \\ 1 \end{pmatrix}, \tag{5.20}$$

and left multiplying it by the transformation matrix A given in Appendix A.

$$\mathbf{r}_{hb} = A r_{so.} \tag{5.21}$$

Where

$$\mathbf{r}_{hb} = \begin{pmatrix} x_{hb} \\ y_{hb} \\ z_{hb} \end{pmatrix}. \tag{5.22}$$

5.3.2 Compute the Vector from Head-Sparker to Eye with the Head in the Standard Configuration

Compute the vector from head-sparker to eye when the subject is on the biteboard

Compute the components of this vector as follows

$$xeb_1 = x_{eb} - x_{hb}, \tag{5.23}$$

$$xeb_2 = y_{eb} - y_{hb}, \tag{5.24}$$

$$xeb_3 = z_{eb} - z_{hb}. \tag{5.25}$$

Compute the transpose of the rotation matrix from the standard orientation to the biteboard orientation

Compute the rotation matrix from the standard orientation to the biteboard orientation Using the horizontal, vertical, and torsional head angle averages converted to radians as follows

$$hdv0a = hdv_{oa} \cdot (\frac{\pi}{60 \cdot 180}), \tag{5.26}$$

$$hdh0a = hdh_{oa} \cdot (\frac{\pi}{60 \cdot 180}), \tag{5.27}$$

$$toz0a = toz_{oa} \cdot (\frac{\pi}{60 \cdot 180}), \tag{5.28}$$

compute the 3×3 rotation matrix (denoted by $R(hdv0a, hdh0a, toz0a)$) by the method described in Chapter 4.

Compute the transpose of this matrix Compute the transpose as follows

$$\left[R^T(hdv0a, hdh0a, toz0a)\right]_{ij} = [R(hdv0a, hdh0a, toz0a)]_{ji}. \tag{5.29}$$

Get the components of the vector from the head-sparker to the eye with the head in the standard configuration

Compute the components of this vector by left-multiplying the vector from head-sparker to eye with the subject on the biteboard (**xeb**) with the above matrix

$$xe0_i = \sum_{j=1}^{3} \left[R^T(hdv0a, hdh0a, toz0a)\right]_{ij} xeb_j. \tag{5.30}$$

5.3.3 Compute Sighting-centers, Gaze Errors, and Table Gaze Positions at each RFM burst of Trial n

Compute the current sighting-center (sparker strobe i of trial n)

Compute the head-sparker position at sparker strobe i of trial n Calculate the vector from the TCS origin to the current head-sparker position by using Eqs. 5.12 to 5.22 starting with d_{ani}, d_{bni}, and d_{dni} instead of d_{aoa}, d_{boa}, and d_{doa}. The TCS x-, y-, and z-coordinates of the final vector are denoted by rh_{1i}, rh_{2i}, and rh_{3i} respectively.

It is very important to note that the i subscript here is the index of the sparker strobe. These strobes are synchronized with RFM bursts but occur only once every eight bursts (RFM burst occur 488 times per second and sparker strobes only 61 times per second). Thus, for now, one must include an eight-fold repetition of the above vector to provide a sparker position at each RFM burst. Some sort of interpolation must done to improve this however.

Compute the rotation matrix at RFM burst j of trial n Calculate this matrix by first converting the measured head angles to radians

$$hdvn_j = hdv_{nj} \cdot (\frac{\pi}{60 \cdot 180}), \tag{5.31}$$

$$hdhn_j = hdh_{nj} \cdot (\frac{\pi}{60 \cdot 180}), \tag{5.32}$$

$$tozn_j = toz_{nj} \cdot (\frac{\pi}{60 \cdot 180}), \tag{5.33}$$

and then computing the matrix $R(hdvn_j, hdhn_j, tozn_j)$ as described in Chapter 4.

Compute the sighting-center at RFM burst (RFM burst) j of trial n Compute the TCS coordinates of the eye at RFM burst j of trial n by using the following equations

$$re_{kj} = rh_{kj} + \sum_{m=1}^{3} [R(hdvn_j, hdhn_j, tozn_j)]_{km} \cdot xe0_m. \tag{5.34}$$

Where $k = 1, 2, 3$ for the TCS x-, y-, and z-coordinates of the sighting-center and j denotes the RFM burst (RFM burst). The quantity rh_{kj} is the sparker position computed at the most recent sparker strobe before RFM burst j.

Compute the gaze errors at RFM burst j

Compute the horizontal gaze error at RFM burst j

Compute the horizontal angle of the line from sighting-center to target Compute as follows.

$$losh_j = (\frac{180 \cdot 60}{\pi}) \cdot \arctan(\frac{r_{tar2} - re_{2j}}{r_{tar1} - re_{1j}}), \tag{5.35}$$

where $losh_j$ is measured in minarc.

Compute measured horizontal gaze angle For the left eye

$$gah_j = lsh_{nj} - lsh_{oa}, \tag{5.36}$$

and for the right eye

$$gah_j = rsh_{nj} - rsh_{oa}. \tag{5.37}$$

Compute the horizontal gaze error at RFM burst j As follows

$$geh_j = gah_j - losh_j. \tag{5.38}$$

Compute the vertical gaze error at RFM burst j

Compute the vertical angle of the line from sighting-center to target Compute as follows.

$$losv_j = (\frac{180 \cdot 60}{\pi}) \cdot \arctan(\frac{r_{tar3} - re_{3j}}{r_{tar1} - re_{1j}}), \tag{5.39}$$

where $losv_j$ is measured in minarc.

Compute measured vertical gaze angle As follows

$$gev_j = gav_j - losv_j. \tag{5.40}$$

Compute table gaze positions

Compute the TCS x-coordinate of the table gaze position Use the following equation

$$gpx_j = re_{1j} + \frac{r_{tar3} - re_{3j}}{\tan((\frac{\pi}{180 \cdot 60}) \cdot gav_j)}. \tag{5.41}$$

Compute the TCS y-coordinate of the table gaze position Use the following equation

$$gpy_j = re_{2j} + \frac{\tan((\frac{\pi}{180 \cdot 60}) \cdot gah_j)}{\tan((\frac{\pi}{180 \cdot 60}) \cdot gav_j)} \cdot (r_{tar3} - re_{3j}). \tag{5.42}$$

Chapter 6

The Real-Time Line-of-Sight of the Subject

6.1 Definition of the Line-of-sight

A quantity of major importance in the study of eye movements is the real-time line-of-sight of a subject. There are several different ways to define this quantity[?]. Intuitively one could imagine that the line-of-sight should be the line that connects a point at the center of the fovea with a point on a target that is currently being fixated by the subject. Unfortunately, there is no way to determine such a line using the data collected in the Table Experiments as the foveal position is not measured. Thus one must develop an operational definition of the line-of-sight which is at once plausible (in the sense of the definition given above) and also satisfies the criterion that it can be determined using available Table Experiment data. One needs only to define the line-of-sight under a given set of circumstances for it to be defined in all other cases since the line-of-sight is assumed to be fixed relative to the eye.

The definition stated below shall be adopted in this document. It is based on the assumption, stated in Chapter 4, that, while the subject fixated his pupil during the mirror trial, his line-of-sight was parallel to the TCS x-axis. Furthermore, it will be assumed that during this activity, the subject's gaze was very nearly in the "primary position". This assumption will be important for the derivation of the subject's Helmholtz coordinates. **During the mirror trial of a session while the subject is fixating his pupil, the line-of-sight of the subject will be defined as the line that is parallel to the TCS x-axis and passes through the biteboard sighting-center**

position. The line-of-sight at later times is determined by the rotations and translations of the subject's eye. The unit vector that is directed along this line in the direction of the positive TCS x-axis can be computed from Table Experiment data.

At a later RFM burst, therefore, one can (given the instantaneous sighting-center coordinates and the eye-coil data) determine the unit vector directed along the line-of-sight defined above. The derivation of the equation for the line-of-sight unit vector in terms of sighting-center coordinates and eye-coil data forms the subject of this chapter. As described earlier, the sighting-center coordinates will be assumed known in all of the derivations presented below.

6.2 Obtaining the TCS coordinates of the Line-of-sight Vector

Before proceeding to the derivation of the TCS coordinates of the line-of-sight unit vector, it is important to describe the relationship between the placement of the sensor-coil on the subject's eye and the line-of-sight defined above. During the mirror calibration trial, when the subject fixates his pupil in the mirror, the line-of-sight is (by the definition above) parallel to the TCS x-axis. If the sensor-coil on the eye had been perfectly placed on the eyeball, the unit vector normal to this coil would be parallel to the line-of-sight and hence to the TCS x-axis. In this hypothetical situation, this normal vector would point directly towards magnetic north. The raw horizontal and vertical readings produced by the RMFM in that case would be $13,500$ minarc on the horizontal meridian and $8,100$ minarc on the vertical meridian.

In practice, however, the placment of the sensor-coil is never perfect and varies from session to session. It is, indeed, the purpose of the mirror calibration trial to determine the horizontal and vertical offsets of the *physical sensor coil* from a *logical sensor coil* whose unit normal vector is always exactly parallel to the subject's line-of-sight. Thus all of the equations in the previous chapters that include eye-coil angle variables are expressed in terms of the horizontal and vertical angles of this logical eye-coil. These angles are referenced to magnetic north, i.e. when the logical sensor-coil's normal vector points toward magnetic north, both its horizontal and vertical readings

are defined to be zero. All future references to the "eye-coil" shall mean the logical sensor coil.

The relationship between the raw measured horizontal and vertical angles of the physical eye-coil and their counterparts for the logical eye-coil are as follows

$$\theta_h = C(\theta_h^{(raw)} - \theta_h^{(offset)} - 13500), \tag{6.1}$$

$$\theta_v = C(\theta_v^{(raw)} - \theta_v^{(offset)} - 8100). \tag{6.2}$$

where θ_h, and θ_v are the horizontal and vertical angles of the logical eye-coil respectivley and are expressed in radians. The angles $\theta_h^{(raw)}$ and $\theta_h^{(raw)}$ are the raw horizontal and vertical angles of the physical eye-coil as measured by the RMFM, and $\theta_h^{(offset)}$ and $\theta_v^{(offset)}$ are the horizontal and vertical offset angles between the logical and physical eye-coil that were measured in the the mirror calibration trial and are expressed in minutes of arc (minarc). The symbol C represents the factor converting minarc into radians. More details about how these angles were determined can be found in Chapter 3.

6.2.1 Derivation of the Line-of-sight Vector

To begin the derivation, consider the coordinate system shown in fig. 6.1. The coordinate axes of this system are parallel to those of the TCS and its origin is located at the position of the subject's sighting center at RFM burst k (the time of this RFM burst will be denoted by t_k). The line-of-sight of the subject at this RFM burst is also shown in the figure and is denoted by the symbol **u**. The problem is to express the components of this *unit* vector in terms of the angles θ_h and θ_v.

Determining the components of **u** can be achieved by considering the triangles **AOB** and **BOC** shown in the figure and by using the condition that **u** is a unit vector:

$$u_x^2 + u_y^2 + u_z^2 = 1. \tag{6.3}$$

Triangle **AOB** is a right triangle. Its legs have lengths u_x and u_z. By considering this triangle it is easy to see that the components u_x and u_z of **u** are related by

$$u_z = u_x \tan\theta_v. \tag{6.4}$$

Now consider the right triangle **BOC** which lies in the xy-plane. The lengths of its legs are u_x and u_y. These lengths are related by the horizontal angle

$$u_y = u_x \tan\theta_h. \tag{6.5}$$

By inserting Eqs. 6.4 and 6.5 into Eq. 6.3 the following equation containing only u_x is obtained

$$u_x^2 + u_x^2 \tan^2\theta_h + u_x^2 \tan^2\theta_v = 1.$$

solving for u_x gives

$$u_x = \frac{1}{(1 + \tan^2\theta_h + \tan^2\theta_v)^{\frac{1}{2}}} \equiv \frac{1}{D(\theta_h, \theta_v)}. \tag{6.6}$$

Inserting Eq. 6.6 for u_x back into the equations for u_y and u_z gives

$$u_y = \frac{\tan\theta_h}{D(\theta_h, \theta_v)},$$

and

$$u_z = \frac{\tan\theta_v}{D(\theta_h, \theta_v)}.$$

Hence the line-of-sight unit vector $\mathbf{u}$ at an arbitrary RFM burst can be written, in TCS coordinates, as

$$\mathbf{u} = \frac{1}{D(\theta_h, \theta_v)} \left[\mathbf{i}_{\mathbf{TCS}} + \mathbf{j}_{\mathbf{TCS}} \tan\theta_h + \mathbf{k}_{\mathbf{TCS}} \tan\theta_v\right]. \tag{6.7}$$

Where $\mathbf{i}_{\mathbf{TCS}}$, $\mathbf{j}_{\mathbf{TCS}}$, and $\mathbf{k}_{\mathbf{TCS}}$ are the unit vectors along the x-, y-, and z-axes of the TCS respectively.

6.2.2 The Instantaneous Line-of-sight Velocity Along a Saccade

The path of a saccade executed by the eye of a subject can be represented as a trace drawn by the intersection of the instantaneous line-of-sight with a sphere centered on the eye. It is of some interest in the analysis of the data collected in the Table Experiments to determine the speed of the line-of-sight

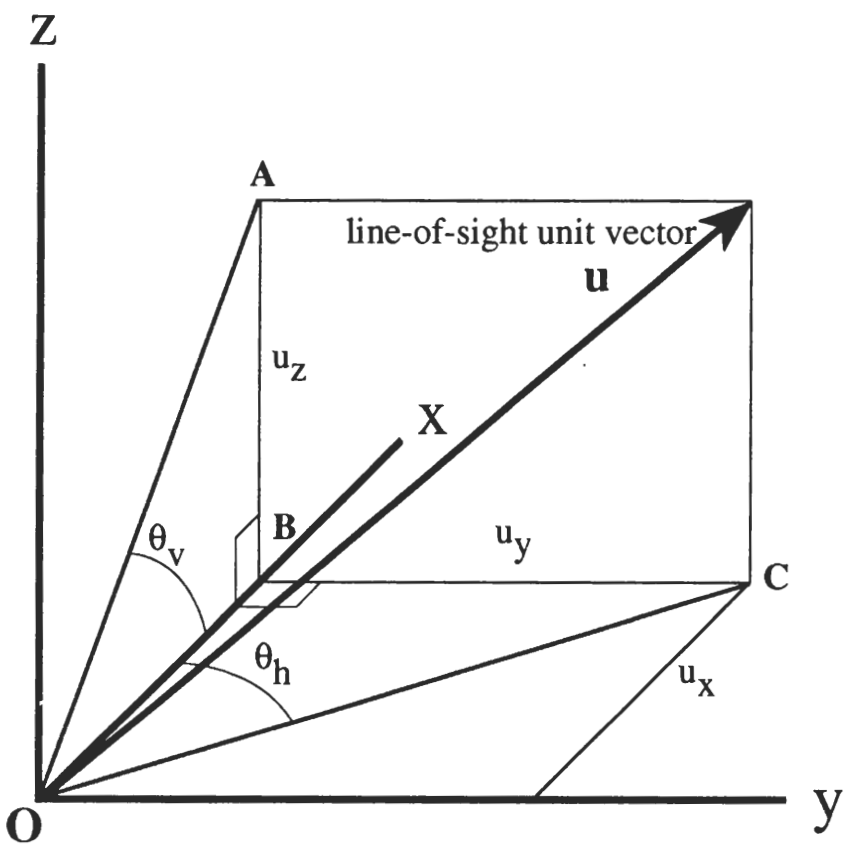

Figure 6.1: Finding the TCS components of the line-of-sight unit vector

as it travels along this trace. Note that this quantity will be referenced to the lab frame and not to the subject's head.

To compute this quantity, let δt be the time between succesive RFM bursts expressed in seconds and let $\mathbf{u}_k$ be the line-of-sight unit vector at RFM burst k and $\mathbf{u}_{k+1}$ be the line-of-sight unit vector at burst $k+1$. The angle through which the line-of-sight rotates during the time δt is thus

$$\delta\theta = \cos^{-1}(\mathbf{u}_k \cdot \mathbf{u}_{k+1}). \tag{6.8}$$

which is expressed in radians and the instantaneous speed along the saccade path is, therefore,

$$v_{los} = \frac{\delta\theta}{\delta t} = \frac{\cos^{-1}(\mathbf{u}_k \cdot \mathbf{u}_{k+1})}{\delta t}. \tag{6.9}$$

This (angular) speed is measured in radians per second.

Chapter 7

Gaze Errors and Table Gaze Positions

Once one has determined the instantaneous line-of-sight of the subject, it is important, in eye-movement research, to analyze the relative position of this line with respect to a given target. In many eye-movement experiments, the subject is asked to direct his gaze toward various objects in his visual field. In the Table Experiments subjects were instructed to tap various lighted LED-tipped rods located on the RFM Worktable (see Chapter 3). In these experiments, determining the position of the instantaneous line-of-sight relative to the targets is critical to the analysis. Two such types of quantities were considered in the analysis of Table Experiments: (1) Instantaneous Gaze Errors, and (2) Instantaneous Table Gaze Positions.

The definition of the horizontal and vertical gaze errors is based on the idea that, given the coordinates of the instantaneous sighting-center position and given the target position coordinates, one can determine the line in space that is directed from the subject's sighting-center to the target at that instant. Such a line represents the line-of-sight the subject would have if he was fixating precisely the mathematical point that represents the position of the target. This line can be described by its vertical and horizontal angles in the TCS. The actual line-of-sight can also be determined as described in Chapter 6 and its vertical and horizontal angles can be determined (in fact, these are directly measured). **The instantaneous horizontal gaze error is defined as the difference between the horizontal angle of the actual line-of-sight and the horizontal angle of the line-of-sight that a subject would have if he were fixating the exact point at which the target is located, the instantaneous vertical gaze error is the difference between the vertical angles of these two lines.**

Instantaneous gaze errors therefore provide a measure of the offset of the instantaneous line-of-sight relative to a given target. Such gaze errors are generally presented as time traces over the timespan of a trial. Alternatively, two-dimensional gaze error can be defined as the angle between the line-of-sight unit vector and the unit vector that points from the sighting-center to the target.

Instantaneous table gaze positions are defined as the point of intersection of the instantaneous line-of-sight with a plane that is parallel to and at a given height above the RFM Worktable surface. The totality of table gaze position points over all of the RFM bursts of a trial are presented as curves superimposed on the RFM Worktable surface as would be seen from a vantage point directly over the worktable surface. By also superimposing the positions of the targets on this picture, one can determine such things as fixation positions and times of fixation.

This chapter contains two sections. The first section presents the derivation of the algorithm for determining the instantaneous gaze errors and the second contains the derivation of the algorithm for determining table gaze positions.

7.1 Horizontal and Vertical Gaze Errors

The calculation of the horizontal or vertical gaze error at a given RFM burst divides (as the above definition implies) into the calculation of the horizontal or vertical angle of the instantaneous line-of-sight followed by subtraction of the directly measured instantaneous horizontal or vertical angle of the subject's line-of-sight. Thus it will be sufficient to derive expressions for the horizontal and vertical angles of the line passing through the position of the target and the instantaneous position of the subject's sighting center. In the derivation below, the TCS coordinates of both the target and the sighting center are assumed known.

The TCS target coordinates were measured before the main sessions of the Table Experiments began. They were determined by measuring the heights of the LED-tipped rods and also measuring the height of the low sparker rod and using the definition of the TCS.

Consider fig. 7.1, the coordinate axes shown in this figure are parallel to the corresponding TCS axes and the origin is located at the instantaneous

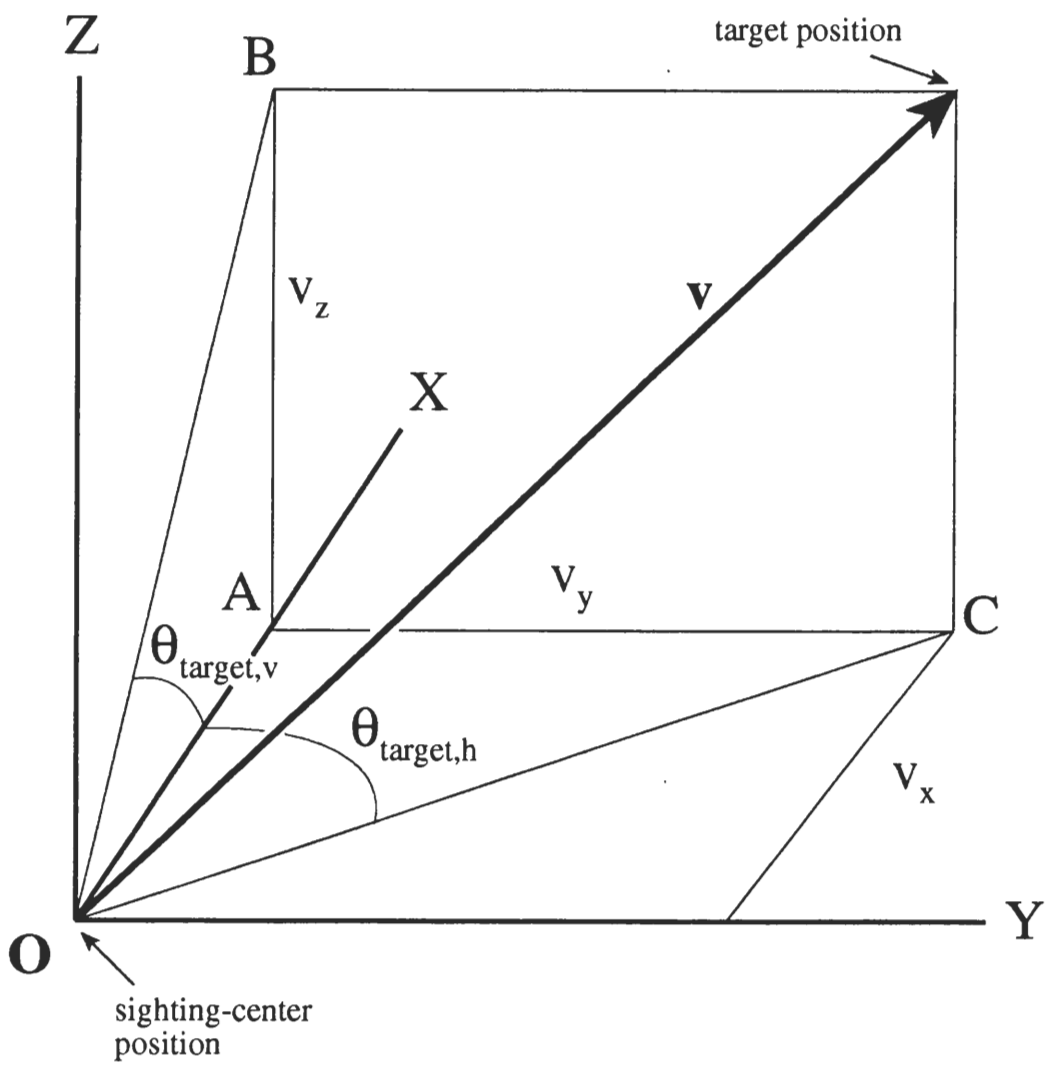

Figure 7.1: Horizontal and vertical angles of the line from eye to target

position of the subject's sighting-center at RFM burst k (time t_k). The vectors locating the sighting-center and the target in the TCS are denoted by $\mathbf{r}_{sc}(t_k)$ and $\mathbf{r}_{\text{target}}(t_k)$, respectively. It will be convenient to write out the TCS components of these vectors:

$$\mathbf{r}_{sc}(t_k) = x_{sc}(t_k)\mathbf{i}_{\mathbf{TCS}} + y_{sc}(t_k)\mathbf{j}_{\mathbf{TCS}} + z_{sc}(t_k)\mathbf{k}_{\mathbf{TCS}} \tag{7.1}$$

$$\mathbf{r}_{\text{target}} = x_{\text{target}}\mathbf{i}_{\mathbf{TCS}} + y_{\text{target}}\mathbf{j}_{\mathbf{TCS}} + z_{\text{target}}\mathbf{k}_{\mathbf{TCS}}. \tag{7.2}$$

Now let $\mathbf{v}(t_k)$ denote the vector whose tail is at the sighting-center position and whose tip is at the target position:

$$\mathbf{v}(t_k) = \mathbf{r}_{\text{target}} - \mathbf{r}_{sc}(t_k) \equiv v_x(t_k)\mathbf{i}_{\mathbf{TCS}} + v_y(t_k)\mathbf{j}_{\mathbf{TCS}} + v_z(t_k)\mathbf{k}_{\mathbf{TCS}} \tag{7.3}$$

so

$$v_x(t_k) = x_{\text{target}} - x_{sc}(t_k), \tag{7.4}$$

$$v_y(t_k) = y_{\text{target}} - y_{sc}(t_k), \tag{7.5}$$

$$v_z(t_k) = z_{\text{target}} - z_{sc}(t_k). \tag{7.6}$$

Now consider the right triangle **AOC** in fig. 3.1. By definition of the tangent:

$$\tan(\theta_{tar,h}) = \frac{v_y(t_k)}{v_x(t_k)} = \frac{y_{\text{target}} - y_{sc}(t_k)}{x_{\text{target}} - x_{sc}(t_k)}, \tag{7.7}$$

and by considering the right triangle **AOB** in fig. 3.1, the angle $\theta_{tar,v}$ can be expressed in terms of the components of $\mathbf{v}(t_k)$ by

$$\tan(\theta_{tar,v}) = \frac{v_z(t_k)}{v_x(t_k)} = \frac{z_{\text{target}} - z_{sc}(t_k)}{x_{\text{target}} - x_{sc}(t_k)}. \tag{7.8}$$

Thus the angles $\theta_{tar,h}$ and $\theta_{tar,v}$ are given by

$$\theta_{tar,h} = \tan^{-1}\left(\frac{y_{\text{target}} - y_{sc}(t_k)}{x_{\text{target}} - x_{sc}(t_k)}\right) \tag{7.9}$$

and

$$\theta_{tar,v} = \tan^{-1}\left(\frac{z_{\text{target}} - z_{sc}(t_k)}{x_{\text{target}} - x_{sc}(t_k)}\right). \tag{7.10}$$

The two-dimensional gaze error, θ_{2d}, which is the angle between the instantaneous line-of-sight, $\mathbf{u}$, and the target vector, $\mathbf{v}$, is given by

$$\theta_{2d} = \cos^{-1}\left(\frac{\mathbf{u}\cdot\mathbf{v}}{|\mathbf{v}|}\right), \tag{7.11}$$

and is expressed here in radians. This quantity gives only the absolute error.

7.2 Table Gaze Positions

The table gaze position at a given RFM burst is the intersection of the subject's line-of-sight, as defined above, with a specified reference plane which is parallel to the surface of the RFM Worktable and which lies a given distance above the TCS xy-plane (which is itself parallel to the RFM Worktable surface. See figure 7.2. The collection of these points at all RFM bursts of a trial describes a curve on this imaginary plane and is an indication of the where the subject is fixating during the trial.

Figure 7.2 depicts the line-of-sight of a subject at an arbitrary RFM burst. At such a burst, the subject is not necessarily fixating a target, and this is so indicated in the figure. Denote the location of the sighting-center of the subject's eye in this situation by **E**, and its TCS coordinates are $(x_{sc}(t_k), y_{sc}(t_k), z_{sc}(t_k))$, where t_k is the time-tag of the given RFM burst. Assume further that the reference plane is a distance a above the TCS xy-plane (if the reference plane is below the TCS xy-plane, then a will be a negative number). The line passing through **E** that is parallel to the TCS z-axis intersects the reference plane at a point that will be denoted by **A**. The table taze position is labeled as **B** and **C** is the point of intersection of the orthographic projection of the line-of-sight (onto a plane which contains **A** and is parallel to the TCS xz-plane) and lying in the reference plane.

Thus the line **EC** is the parallel to the orthographic projection of the line-of-sight onto the TCS xz-plane and the line **AB** is parallel to the orthographic projection of the line-of-sight onto the TCS xy-plane. From the definitions of the horizontal and vertical angles given in Chapter 2, the angle **CAB** is the horizontal eye angle θ_h and the angle **ACE** is the *negative* of the vertical eye angle θ_v. Now, if the TCS coordinates of the table gaze position are denoted by (x_T, y_T, z_T), then the coordinates of the other two labeled points in fig. 7.2 are

$$\mathbf{A} = (x_{sc}, y_{sc}, a),$$

and

$$\mathbf{C} = (x_T, y_{sc}, a).$$

The length of line **AC** is, therefore, $x_T - x_{sc}$, the length of **BC** is $y_T - y_{sc}$, and the length of **AE** is $z_{sc} - a$. So, considering the triangles **ABC** and **ACE**, the horizontal and vertical eye angles are related to the coordinates

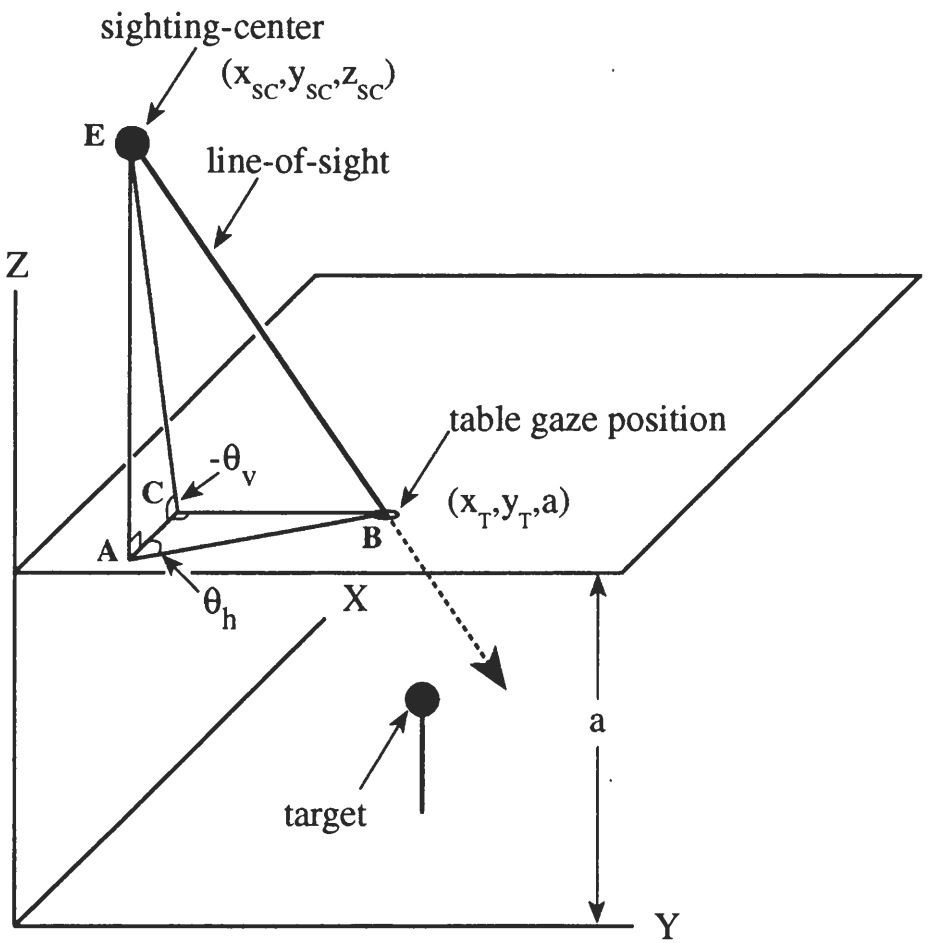

Figure 7.2: Finding the table gaze position

of the line-of-sight and the table gaze position as follows:

$$\tan(\theta_h) = \frac{y_T - y_{sc}(t_k)}{x_T - x_{sc}(t_k)} \tag{7.12}$$

and

$$-\tan(\theta_v) = \frac{z_{sc}(t_k) - a}{x_T - x_{sc}(t_k)}. \tag{7.13}$$

These two equations may be solved for the x and y TCS coordinates of the table gaze positions giving

$$x_T = x_{sc} - (z_{sc} - a)\left(\frac{1}{\tan(\theta_v)}\right), \tag{7.14}$$

and

$$y_T = y_{sc} - (z_{sc} - a)\left(\frac{\tan(\theta_h)}{\tan(\theta_v)}\right). \tag{7.15}$$

Chapter 8

Target and Ocular Vergence

8.1 The Instantaneous Helmholtz Coordinate System of the Subject

One intuitive goal in processing the RFM data is to determine "where the subject is looking" in real-time. It seems reasonable that such a quantity depends on the directions of the lines-of-sight of *both eyes* at a given instant of time. One quantity, designed to answer this question, will be defined later in this work. As discussed earlier, the most useful coordinate system for analyzing quantities that depend on the lines-of-sight of both eyes is the Helmholtz system. In this section, the definition of, and the supporting equations for, the origin and axes of a subject's Helmholtz coordinate system will be given in terms of the TCS. Since the TCS is a space-fixed coordinate system and the Helmholtz system is attached to the subject, these quantities will vary as the subject moves.

Briefly, (see Vol. I), given that the head and eyes of the subject are fixed, the axes of the Helmholtz system are defined by the sighting centers of the two eyes (the line joining these two points is called the *baseline*) and by a direction which shall, in this document, be called the "primary direction". The "primary direction" is roughly defined as the direction of the lines-of-sight of the eyes when the subject sits or stands upright in a comfortable position and fixates a distant object. In this situation the lines-of-sight are, very nearly, parallel. Once the Helmholtz axes are determined in the TCS for a subject at any instant of time, they may be determined at any later time if the new configuration of the head is known because the Helmholtz axes are fixed with respect to the head. The definition of these initial axes in terms of quantities measured by the RFM posed some difficulties that bear

some discussion.

Recall that the plane that contains the baseline and the lines-of-sight of the two eyes is called the *plane of regard.* At a given instant during the time a subject moves around the RFM Worktable looking at objects, there arises the mathematical difficulty that there is no plane that contains the baseline and **both** lines-of-sight. It is true that these three lines are nearly coplanar most of the time but such a situation is useless in developing a mathematical definition. One possibility is to arbitrarity choose one eye and then define the Helmholtz axes in terms of the baseline and the line-of-sight of the chosen eye. If this definition is used there remains the difficulty that the line-of-sight of this eye must be directed along the "primary direction". Even under these circumstances, there is no guarantee that the baseline and such a line-of-sight will be perpendicular as would be needed for defining mutually orthogonal Helmholtz axes.

The definition given below optimizes the constraints imposed by the difficulties described above and is consistent with earlier assumptions. That is, it is based on the assumption that when the subject's head is supported on a biteboard during the calibration trials at the beginning of a session, the line-of-sight of the subject's eye is parallel to the TCS x-axis. This assumption is made regardless of which eye is the focus of the particular calibration trial. **An additional assumption, made here to facilitate the development of a suitable definition of the subject's Helmholtz axes, is that, when the subject fixates his pupil in the mirror, the line-of-sight (and hence the TCS x-axis unit vector) is directed along the "primary direction". It is further assumed that the line-of-sight and the baseline are very nearly perpendicular in this situation.** The second assumption allows the definition of one of the Helmholtz axes to be defined as the component of the TCS x-axis unit vector that is orthogonal to the baseline and that lies in the plane that contains both the baseline and the line-of-sight. This vector component will be both perpendicular to the baseline and will, very nearly, point along the "primary direction".

Given the above motivation, the axes of the subject's Helmholtz coordinate system while the subject's head is supported on the biteboard during the mirror trials of a session are defined as follows. The Helmholtz y-axis unit vector is a vector that lies along the line joining the sighting centers of the two eyes and points from the subject's left eye to his right eye (see Fig. 8.1). Letting $\mathbf{r}_{ebR}$ be the vector that locates the sighting center of the sub-

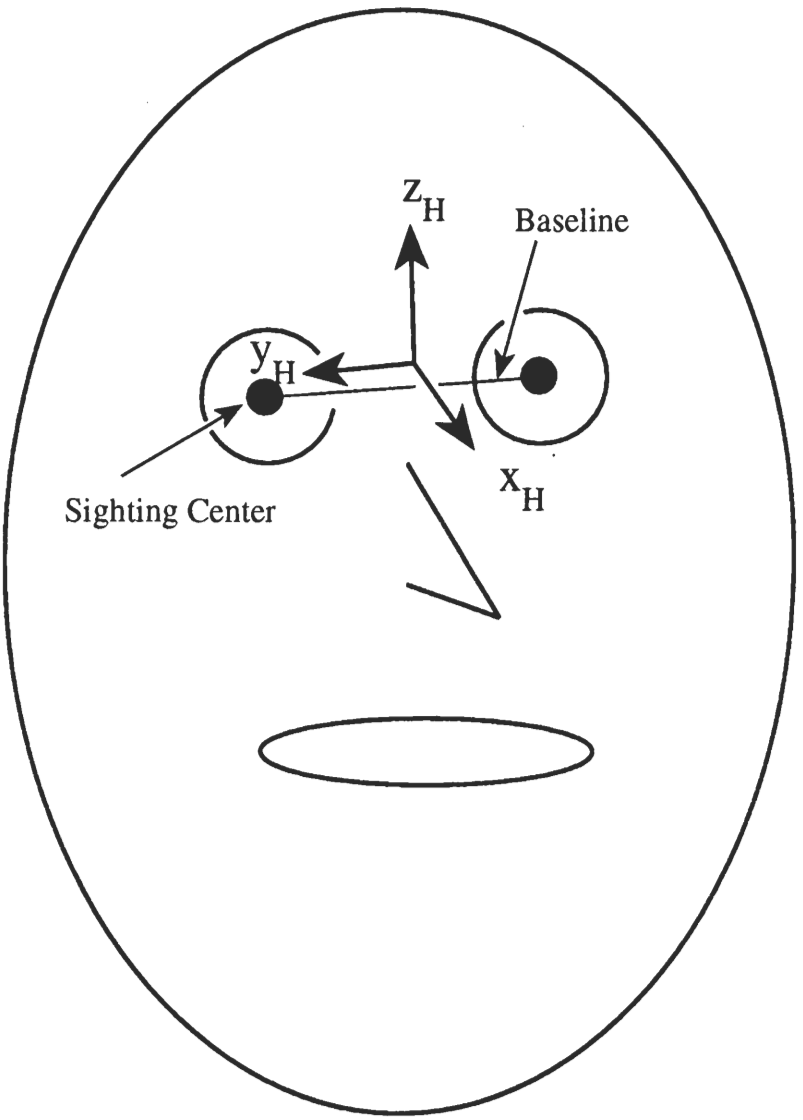

Figure 8.1: The helmholtz coordinate axes

ject's right eye while on the biteboard and letting $\mathbf{r}_{ebL}$ be the corresponding vector for the left eye, the y-axis unit vector is given by

$$\hat{\mathbf{y}}_{\mathbf{H0}} = \frac{\mathbf{r}_{ebR} - \mathbf{r}_{ebL}}{|\mathbf{r}_{ebR} - \mathbf{r}_{ebL}|}. \tag{8.1}$$

The Helmholtz x-axis unit vector is obtained by Gram-Schmidt orthogonalization of this vector and the TCS x-axis unit vector, $\hat{i}_{TCS}$:

$$\hat{\mathbf{x}}_{\mathbf{H0}} = \frac{\hat{\mathbf{i}}_{\mathbf{TCS}} - (\hat{\mathbf{i}}_{\mathbf{TCS}} \cdot \hat{\mathbf{y}}_{\mathbf{H0}})\hat{\mathbf{y}}_{\mathbf{H0}}}{\left|\hat{\mathbf{i}}_{\mathbf{TCS}} - (\hat{\mathbf{i}}_{\mathbf{TCS}} \cdot \hat{\mathbf{y}}_{\mathbf{H0}})\hat{\mathbf{y}}_{\mathbf{H0}}\right|}. \tag{8.2}$$

And finally the z-axis unit vector is obtained from the cross product of these two vectors

$$\hat{\mathbf{z}}_{\mathbf{H0}} = \hat{\mathbf{y}}_{\mathbf{H0}} \times \hat{\mathbf{x}}_{\mathbf{H0}}, \tag{8.3}$$

where the conventional right-hand-rule is used to determine the direction of this cross product. These equations give the x-, y-, and z-axes of the Helmholtz system relative to the TCS in the situation in which the subject's head is supported on a biteboard during the mirror trials of a session.

When the subject is free to move around inside the RFM chamber during subsequent trials, the Helmholtz axes move with his head. Hence, at an arbitrary burst of the RFM, the Helmholtz coordinate axes undergo the same rotations as the subject's head. Thus the instantaneous Helmholtz axes are given by

$$\hat{\mathbf{x}}_{\mathbf{H}} = R(\theta_h, \theta_v, \theta_t) R_o^{-1}(\theta_{ho}, \theta_{vo}, \theta_{to}) \hat{\mathbf{x}}_{\mathbf{H0}}, \tag{8.4}$$

$$\hat{\mathbf{y}}_{\mathbf{H}} = R(\theta_h, \theta_v, \theta_t) R_o^{-1}(\theta_{ho}, \theta_{vo}, \theta_{to}) \hat{\mathbf{y}}_{\mathbf{H0}}, \tag{8.5}$$

$$\hat{\mathbf{z}}_{\mathbf{H}} = R(\theta_h, \theta_v, \theta_t) R_o^{-1}(\theta_{ho}, \theta_{vo}, \theta_{to}) \hat{\mathbf{z}}_{\mathbf{H0}}. \tag{8.6}$$

Where $(\theta_h, \theta_v, \theta_t)$ are the head-coil angles recorded at the RFM burst and $(\theta_{ho}, \theta_{vo}, \theta_{to})$ are the head-coil angles recorded during the mirror calibration trials.

8.2 Target Vergence

In many eye movement experiments, one interesting analysis quantity is the target vergence. **Target vergence, θ_{tv}, is defined as the angle subtended at a given target by the sighting centers of the two eyes of**

the subject. The target vergence is independent of the directions of the lines-of-sight of the eyes and is usually used for comparison with some measure of where the subject is fixating or for comparison with some other eye movement behavior. Calculating the instantaneous target vergence is quite easy and can be performed directly in TCS coordinates.

Denoting by $\mathbf{r_{eL}}$ and $\mathbf{r_{eR}}$ the vectors that locate the sighting centers of the left and right eyes in the TCS at an arbitrary RFM burst respectively, and denoting by $\mathbf{r_{tar}}$ the vector that locates the target in the TCS, the vector whose tail lies at the target and whose tip lies at the sighting center of the subject's left eye is given by

$$\mathbf{x_L} = \mathbf{r_{eL}} - \mathbf{r_{tar}}, \tag{8.7}$$

and the corresponding vector for the right eye is

$$\mathbf{x_R} = \mathbf{r_{eR}} - \mathbf{r_{tar}}. \tag{8.8}$$

The plane defined by the two sighting centers and the target contains both of the above vectors. The scalar product of these vectors is, by definition of this product

$$\mathbf{x_L} \cdot \mathbf{x_R} = |\mathbf{x_L}||\mathbf{x_R}| \cos(\theta_{tv}). \tag{8.9}$$

Hence the target vergence angle is given by

$$\theta_{tv} = \cos^{-1}\left(\frac{(\mathbf{r_{eL}} - \mathbf{r_{tar}}) \cdot (\mathbf{r_{eR}} - \mathbf{r_{tar}})}{|\mathbf{r_{eL}} - \mathbf{r_{tar}}||\mathbf{r_{eR}} - \mathbf{r_{tar}}|}\right). \tag{8.10}$$

See Fig. 8.2.

8.3 Ocular Vergence

The ocular vergence of a subject is a measure of whether a subject is fixating an object that is nearby or far away. **The horizontal ocular vergence is defined to be the difference between the azimuths (H_2, or the second helmholtz angles) of the left and right eyes. The vertical ocular vergence is the angle between the planes of regard of the left and right eyes or equivalently, the difference between the elevations (H_1, or the first helmholtz angles) of the left and right eyes.** At each

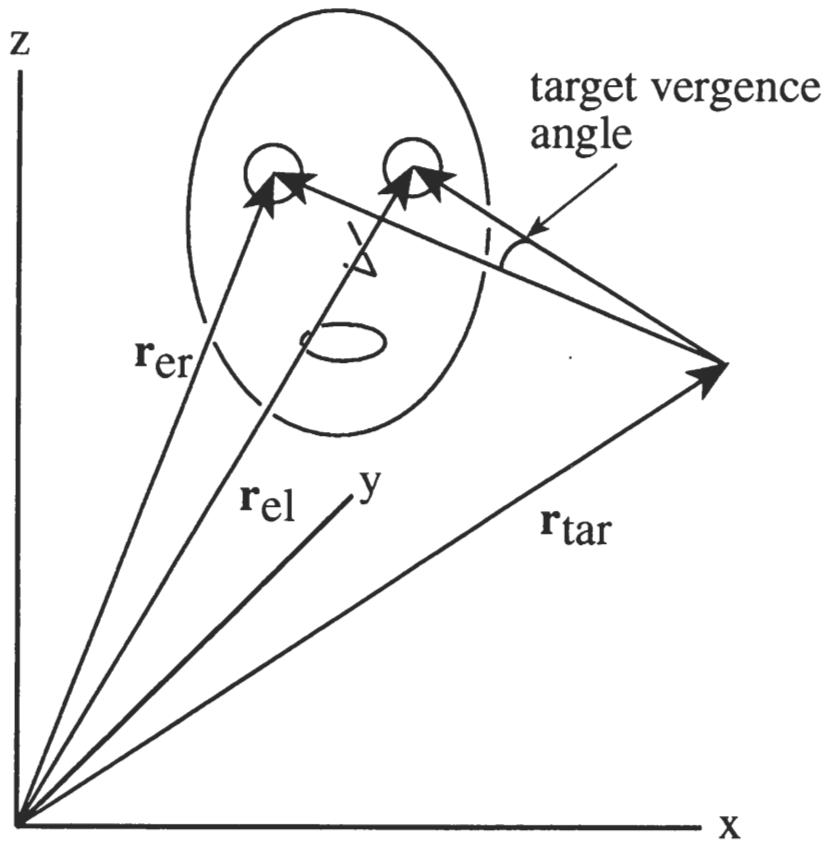

Figure 8.2: Definition of the target vergence angle

RFM burst, there exists a set of helmholtz axes and a line-of-sight unit vector for each eye. The components of each of the unit vectors along the instantaneous helmholtz axes as well as the line-of-sight unit vector for each eye is known in terms of the (static) TCS basis. Thus, it is a simple matter to find the components of the lines-of-sight unit vectors in the helmholtz system and once these are known, the helmholtz angles of each can be computed. The two pairs of helmholtz angles, (H_{1L} and H_{2L} for left eye and H_{1R} and H_{2R} for right eye) can then be used to determine the instantaneous horizontal and vertical ocular vergence of the subject. The derivations of these quantities are presented below.

8.3.1 Determining the Helmholtz Angles of the Line-of-sight unit vector

The expression for the TCS components of the instantaneous line-of-sight unit vector for a given eye was derived earlier and is given by Eq. 6.7. The components of the helmholtz unit vectors in the TCS are given in Eqs. 8.4, 8.5, and 8.6. So, if the line-of-sight vector in TCS coordinates is denoted by $\mathbf{u}$, and the helmholtz unit vectors are denoted by $\hat{\mathbf{x}}_\mathbf{H}$, $\hat{\mathbf{y}}_\mathbf{H}$, and $\hat{\mathbf{z}}_\mathbf{H}$, then the *helmholtz* components of $\mathbf{u}$ are given at time t by

$$u_x^{(H)}(t) = \mathbf{u} \cdot \hat{\mathbf{x}}_\mathbf{H}(t), u_y^{(H)}(t) = \mathbf{u} \cdot \hat{\mathbf{y}}_\mathbf{H}(t), \text{and } u_z^{(H)}(t) = \mathbf{u} \cdot \hat{\mathbf{z}}_\mathbf{H}(t). \quad (8.11)$$

These components $u_x^{(H)}(t)$, $u_y^{(H)}(t)$, and $u_z^{(H)}(t)$ can also be expressed in terms of the helmholtz *angles* of $\mathbf{u}$ by examining fig. 4.7 in Chapter 4. These expressions are

$$u_x^{(H)}(t) = \cos H_1 \cos H_2, \quad (8.12)$$

$$u_y^{(H)}(t) = \sin H_2, \quad (8.13)$$

and

$$u_z^{(H)}(t) = \sin H_1 \cos H_2. \quad (8.14)$$

Note that the value of r in fig. 4.7 is unity here because $\mathbf{u}$ is a unit vector.

Eqs. 8.12, 8.13, and 8.14 can be inverted to obtain H_1 and H_2 in terms of $u_x^{(H)}(t)$, $u_y^{(H)}(t)$, and $u_z^{(H)}(t)$ as follows. Adding the first and third of these equations eliminates H_1 so that

$$\cos H_2 = \left[(u_x^{(H)}(t))^2 + (u_z^{(H)}(t))^2\right]^{\frac{1}{2}}. \quad (8.15)$$

Thus the helmholtz angles can be written in terms of $u_x^{(H)}(t)$, $u_y^{(H)}(t)$, and $u_z^{(H)}(t)$ as

$$H_1(t) = \tan^{-1}\left(\frac{u_z^{(H)}(t)}{u_x^{(H)}(t)}\right), \tag{8.16}$$

and

$$H_2(t) = \tan^{-1}\left(\frac{u_y^{(H)}(t)}{\left[(u_x^{(H)}(t))^2 + (u_z^{(H)}(t))^2\right]^{\frac{1}{2}}}\right). \tag{8.17}$$

Note well that the above equations apply to a single eye only.

8.3.2 Instantaneous Vertical and Horizontal Ocular Vergence

Using the definition for the vertical ocular vergence as the elevation (H_{1R}) of the right eye minus the elevation (H_{1L})of the left eye stated at the beginning of this section and the equations for the helmholtz angles given above, the instantaneous vertical ocular vergence is given by

$$V_v(t) = H_{1R} - H_{1L} = \tan^{-1}\left(\frac{u_z^{(HR)}(t)}{u_x^{(HR)}(t)}\right) - \tan^{-1}\left(\frac{u_z^{(HL)}(t)}{u_x^{(HL)}(t)}\right). \tag{8.18}$$

The instantaneous horizontal ocular vergence is given by the azimuth (H_{2R}) of the right eye minus the azimuth (H_{2L}) of the left eye:

$$V_h(t) = \tan^{-1}\left(\frac{u_y^{(HR)}(t)}{\left[(u_x^{(HR)}(t))^2 + (u_z^{(HR)}(t))^2\right]^{\frac{1}{2}}}\right) - \tan^{-1}\left(\frac{u_y^{(HL)}(t)}{\left[(u_x^{(HL)}(t))^2 + (u_z^{(HL)}(t))^2\right]^{\frac{1}{2}}}\right). \tag{8.19}$$

8.4 The Instantaneous Cyclopean View

In an attempt to determine "where the subject is looking" in real time, it is useful to define a single point in space which corresponds roughly to the center of the "circle of least confusion" of a focused pencil of light rays in geometrical optics. In this section, such a point is defined and the equations required for its computation are presented.

At a given instant of time, the lines-of-sight of the two eyes define two lines in space. In practice, these lines almost never intersect but they (usually) narrowly miss one another. It seems reasonable that a point midway between the closest approach of the two lines could serve as a figure-of-merit in estimating "where the subject is looking" at a given instant. Thus **the instantaneous "binocular gaze point" is defined as the midpoint of the line joining the pair of points, each of which is on a different line-of-sight, whose distance from each other is smaller than for any other pair of points**. The line joining these two points is perpendicular to *both lines-of-sight* simultaneously as will be shown below.

Once this point is determined, an instantaneous "cyclopean view" unit vector can be defined as a unit vector that is directed from the midpoint of the subject's baseline to the instantaneous "binocular gaze point". The equations for the computation of the components of this unit vector will also be presented in this section.

8.4.1 The Instantaneous "Binocular Gaze Point"

According to the above definition, the "binocular gaze point" is the midpoint of the shortest line connecting a pair of points, one point lying on the line-of-sight of the right eye and the other on the line-of-sight of the left eye. The derivation of the TCS coordinates of this point will be presented in several stages. First, the each of the lines in space corresponding to the instantaneous lines-of-sight of each eye will be expressed in terms of a single parameter. This can be done because a line is one-dimensional. Hence, an arbitrary point on the line-of-sight of, say, the left eye will correspond to a unique value of a parameter (which will be denoted by s_l). There will be a similar parameter for the line-of-sight of the right eye (s_r). Once these parametrizations are defined, the Euclidean distance between any two points, one lying on the left-eye line-of-sight and one lying on the right-eye line-of-sight, can be cast as a function of two variables $d(s_r, s_l)$. The values of s_r and s_l for which this distance function is minimized is then determined by the methods of elementary calculus.

Parametrization of the line-of-sight

Since the TCS coordinates of both the sighting-center of the eye, ($\mathbf{r_e}$), and the line-of-sight unit vector, ($\mathbf{u}$), are assumed calculated, the parametrization of the line-of-sight can be simply obtained. Figure 4.3 shows the sighting-center of a given eye along with the line-of-sight. The vector $\mathbf{r}$ locates an arbitrary point lying on the line-of-sight and a distance s from the sighting-center. The vector that stretches from the sighting-center to the arbitrary point is $s\mathbf{u}$ so $\mathbf{r}$ is simply the vector sum of $\mathbf{r_e}$ and $s\mathbf{u}$. Therefore the parametric relationship between an arbitrary point on the line-of-sight and its distance s from the sighting-center is

$$\mathbf{r}(s) = \mathbf{r_e} + s\mathbf{u}. \tag{8.20}$$

Hence, at any instant of time there is such a relationship for each eye

$$\begin{aligned} \mathbf{r_R}(s_R) &= \mathbf{r_{eR}} + s_R\mathbf{u_R} \\ \mathbf{r_L}(s_L) &= \mathbf{r_{eL}} + s_L\mathbf{u_L} \end{aligned} \tag{8.21}$$

Finding the line-of-closest approach

Picking two arbitrary points, each lying on a different line-of-sight, corresponds to a unique ordered-pair of values (s_R, s_L). As long as the distances are restricted to *positive* values, situations in which the subject looks out the back of his head are excluded. No such restriction will be assumed here, however. The euclidean distance between two such point is given by

$$d(s_R, s_L) = |\mathbf{r_R}(s_R) - \mathbf{r_L}(s_L)|\,. \tag{8.22}$$

It will be more convenient, for calculational purposes, to work with the square of this distance. Since it is always positive, minimizing the square of d will minimize d as well. So define the distance-squared function

$$D(s_R, s_L) \equiv d^2(s_R, s_L) = |\mathbf{r_R}(s_R) - \mathbf{r_L}(s_L)|^2 = (\mathbf{r_R}(s_R) - \mathbf{r_L}(s_L)) \cdot (\mathbf{r_R}(s_R) - \mathbf{r_L}(s_L)) \tag{8.23}$$

To find the values $s_R^{(m)}$ and $s_L^{(m)}$ such that $D(s_R^{(m)}, s_L^{(m)})$ is a minimum, the following conditions must be met

$$\frac{\partial D}{\partial s_R} = \frac{\partial D}{\partial s_L} = 0. \tag{8.24}$$

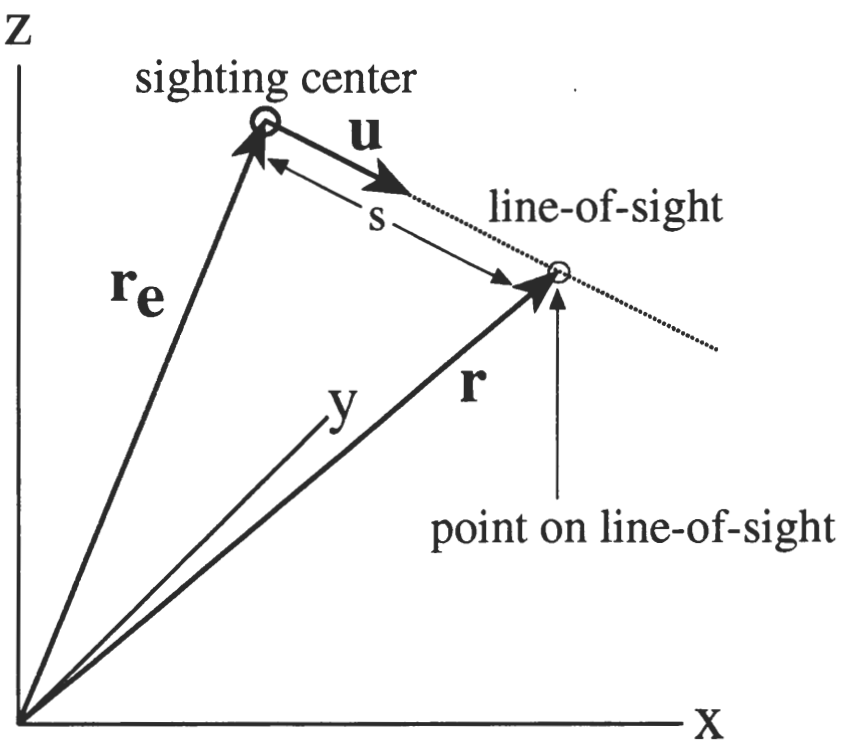

Figure 8.3: Parametrization of the line-of-sight

Using Eq. 8.23 these derivatives become

$$\frac{\partial D}{\partial s_R} = 2\left(\frac{\partial \mathbf{r_R}(s_R)}{\partial s_R}\right) \cdot (\mathbf{r_R}(s_R) - \mathbf{r_L}(s_L)) \tag{8.25}$$

and

$$\frac{\partial D}{\partial s_L} = -2\left(\frac{\partial \mathbf{r_L}(s_L)}{\partial s_L}\right) \cdot (\mathbf{r_R}(s_R) - \mathbf{r_L}(s_L)). \tag{8.26}$$

From Eqs. 8.21 the derivatives in the last equalities of the above equations can be written as

$$\frac{\partial \mathbf{r_R}(s_R)}{\partial s_R} = \mathbf{u_R}, \tag{8.27}$$

and

$$\frac{\partial \mathbf{r_L}(s_L)}{\partial s_L} = \mathbf{u_L}. \tag{8.28}$$

Thus, the minimization conditions satisfied by $s_R^{(m)}$ and $s_L^{(m)}$ become

$$\mathbf{u_R} \cdot (\mathbf{r_R}(s_R^{(m)}) - \mathbf{r_L}(s_L^{(m)})) = 0 \tag{8.29}$$

and

$$\mathbf{u_L} \cdot (\mathbf{r_R}(s_R^{(m)}) - \mathbf{r_L}(s_L^{(m)})) = 0. \tag{8.30}$$

Since $\mathbf{r_R}(s_R^{(m)})$ and $\mathbf{r_L}(s_L^{(m)})$ are vectors that locate the pair of points on the lines-of-sight that are closest to each other, the vector $\mathbf{r_R}(s_R^{(m)}) - \mathbf{r_L}(s_L^{(m)})$ is the vector along the line that joins these points. The above equations demand that this line be perpendicular to both lines of sight simultaneously, see fig. 8.4.

Solving for $s_R^{(m)}$ and $s_L^{(m)}$

Equations 8.29 and 8.30 provide a system of two equations in two unknowns for the values of $s_R^{(m)}$ and $s_L^{(m)}$. The solutions are

$$s_R^{(m)} = \frac{(\mathbf{b} \cdot \mathbf{u_L})(\mathbf{u_R} \cdot \mathbf{u_L}) - (\mathbf{b} \cdot \mathbf{u_R})}{1 - (\mathbf{u_R} \cdot \mathbf{u_L})^2} \tag{8.31}$$

and

$$s_L^{(m)} = -\frac{(\mathbf{b} \cdot \mathbf{u_R})(\mathbf{u_R} \cdot \mathbf{u_L}) - (\mathbf{b} \cdot \mathbf{u_L})}{1 - (\mathbf{u_R} \cdot \mathbf{u_L})^2}. \tag{8.32}$$

Where

$$\mathbf{b} = \mathbf{r_{eR}} - \mathbf{r_{eL}} \tag{8.33}$$

is a vector lying along the subject's baseline. The vectors

$$\begin{aligned} \mathbf{r_R}(s_R^{(m)}) &= \mathbf{r_{eR}} + s_R^{(m)}\mathbf{u_R} \\ \mathbf{r_L}(s_L^{(m)}) &= \mathbf{r_{eL}} + s_L^{(m)}\mathbf{u_L} \end{aligned} \tag{8.34}$$

locate the points on the lines-of-sight shown in fig. 8.4.

Finding the "Binocular Gaze Point"

The midpoint of the line joining the points located by the vectors in Eqs. 8.34 is the "binocular gaze point" and is given by the average of these two vectors

$$\mathbf{r_{BGP}} = \frac{1}{2}(\mathbf{r_R}(s_R^{(m)}) + \mathbf{r_L}(s_L^{(m)})). \tag{8.35}$$

Substituting the expressions for $\mathbf{r_R}(s_R^{(m)})$ and $\mathbf{r_L}(s_L^{(m)})$ into the above equation gives, after some rearrangement

$$\mathbf{r_{BGP}} = \mathbf{r_{CYC}} + \frac{1}{2}(s_R^{(m)}\mathbf{u_R} + s_L^{(m)}\mathbf{u_L}). \tag{8.36}$$

Where $\mathbf{r_{CYC}}$ is the midpoint of the subject's baseline

$$\mathbf{r_{CYC}} = \frac{1}{2}(\mathbf{r_{eR}} + \mathbf{r_{eL}}). \tag{8.37}$$

The "cyclopean direction"

The vector that begins at the midpoint of the subject's baseline and ends at the "binocular gaze point" can be termed the "cyclopean direction". This vector provides a rough, intuitive measure of "where the subject is looking" at each instant of time. The expression for the "cyclopean direction" can instantly be found from Eq. 8.36

$$\mathbf{x_{CYC}} = \mathbf{r_{BGP}} - \mathbf{r_{CYC}} = \frac{1}{2}(s_R^{(m)}\mathbf{u_R} + s_L^{(m)}\mathbf{u_L}). \tag{8.38}$$

The *unit* vector along this direction is given by

$$\mathbf{u_{CYC}} = \frac{\mathbf{x_{CYC}}}{|\mathbf{x_{CYC}}|}. \tag{8.39}$$

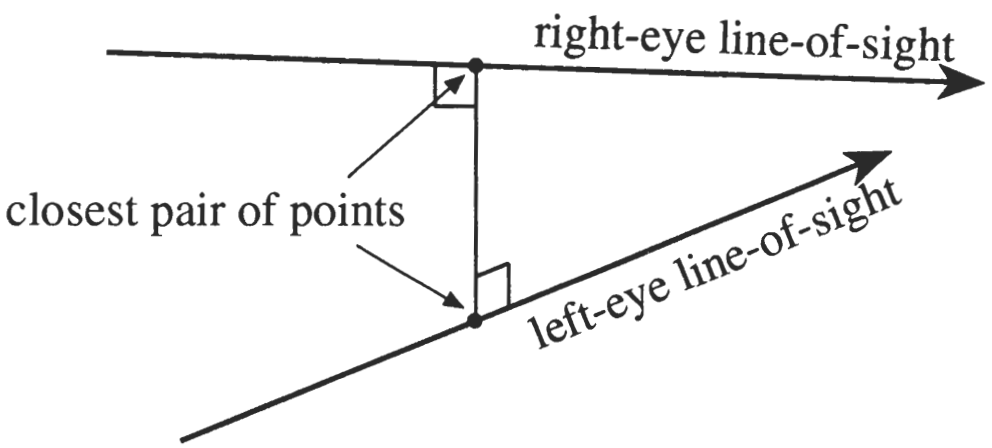

Figure 8.4: Closest approach line is orthogonal to both lines-of-sight

Bibliography

[1] Rubens S. R. (1945) Cube-surface coil for producing a uniform magnetic-field, *Rev. Scient. Instrum.*, **16**, 243-245

[2] Collewijn H. (1977) Eye and head movements in freely moving rabbits, *J. Physiol., Lond.* **266**, 471-498

[3] Beyer W. H. (1991) In *Standard Mathematical Tables of Formulae*, 29 ed., (edited by Beyer, W. H.) 159, CRC Press, Boca Raton

[4] Ferman L., Collewijn H., Jansen T. C., and Van den Berg A. V. (1987) Human gaze stability in the horizontal, vertical, and torsional directions during voluntary head movements, evaluated with a three-dimensional scleral induction coil technique, *Vision Res.*, **27**, pp. 811-828

[5] Hallett P. E. (1986) Eye movements, In *Handbook of Perception and Human Performance, Vol. 1 - Sensory Processes and Perception*, John Wiley, New York

[6] Park R. S. and Park G.E. (1933) The center of ocular rotation in the horizontal plane, *Am. J. Physiol.*, **104**, pp. 545-552

[7] Alpern M. (1962) in Davson H. (Ed.), *The Eye.* (pp. 7-26). Academic: New York.

Appendix A

Determination of the Sighting-Center with Subject on the Biteboard

This appendix contains a description of the method used to obtain the sighting-center of the eye while the subject is on the biteboard. As noted in Chapter 4, this determination is critical for determining the position of the eye in real time. The details of the SCS to TCS transformation, described in the same chapter, will also be given here.

A.1 Determining the Sighting-Center of the Eye

The concept of a point in the human eye that is fixed in relation to the head and that lies along the line-of-sight is founded in previous work [see ref.], at least for horizontal movements of the eye in its orbit. In that work this point was found to be approximately 13.5 mm behind the front surface of the subject's cornea along the line-of-sight.

The method used in the Table Experiments for obtaining the sighting-center was simple and direct. An apparatus was constructed that attached to the biteboard and consisted of a cylindrical tube having sighting holes in its ends. The tube was mounted on an apparatus that contained instruments for moving the tube in three dimensions with high precision and such that the axis of the tube was parallel to the plane of the RFM Worktable (i.e. parallel to the xy-plane of the TCS). When the subject sighted through the tube at an LED located behind an aperture at the far end of the table, this